THE MEMBRANE LIPID COMPOSITION REGULATES TALIN MEDIATED INTEGRIN ACTIVATION

BY

XIN YE

DISSERTATION

Submitted in partial fulfillment of the requirements
for the degree of Doctor of Philosophy in Biochemistry
in the Graduate College of the
University of Illinois at Urbana-Champaign, 2016

Urbana, Illinois

Doctoral Committee:

Professor Stephen Sligar, Chair
Professor James Morrissey
Professor Emad Tajkhorshid
Associate Professor Rutilio Fratti

ABSTRACT

Integrins are a family of transmembrane receptors that mediate cell-cell and cell-extra cellular matrix (ECM) interaction and signaling. Inside-out activation of integrin receptors often requires the binding of the cytoplasmic domain of the subunits by talin. This interaction leads to separation of the integrin and transmembrane domain and significant conformational changes in the extracellular domains, resulting in a dramatic increase in integrins affinity for ligands. Membrane bilayers containing anionic lipids are indispensable for proper talin - integrin interaction, yet the detail picture of the interplay between protein and membrane has remained elusive.

This thesis describe a series of fluorescence based assay for measuring talin-membrane interactions with bilayers of controlled composition using Nanodiscs technology. Results show that recruitment of talin head domain (THD) to the membrane surface is governed by electrostatics in the absence of other adapter proteins. In addition, distance measurements reveal that anionic lipids stimulate a conformational change in the talin head domain allowing interaction of the F3 domain with the phospholipid bilayer. The magnitude of this conformational change is regulated by the identity of the phospholipid headgroup, with phosphatidylinositides promoting the largest change. This emphasizes the importance of PIP2 in converting talin to a conformation optimized for interactions with integrin cytoplasmic tails. Moreover, a phenylalanine-rich region in F2 serves as a hidden hydrophobic anchor was initially indicated by computational simulation and later observed experimentally. It inserts into membrane after initial electrostatic contact providing a stabilizing force

for membrane bound talin. Insertion of these phenylalanine may be critical for triggering the F3 conformational change described above.

In the cytosol, talin adopts an auto-inhibited conformation, that C-terminal rod binds the N-terminal head domain, preventing talin interactions with the membrane surface and the integrin cytoplasmic domain. A Fluorescence Resonance Energy Transfer (FRET) based binding assay reveals that R9 and R12R13 segments of the talin rod domain inhibit the binding of the talin head to anionic lipid bilayers. In contrast, the binding of talin to bilayers containing PIP2 is insensitive to the presence of the inhibitor domains thereby directly implicating PIP2 as an effective activator of talin. The interaction of PIP2 with talin head for activation was located at F2F3 domain.

The Nanodisc technology also offer an ideal platform for assembling unclustered integrin transmembrane and cytoplasmic domain in lipid bilayer. Measurements of the THD binding to integrin inserted Nanodiscs reveal that integrin provides most binding free energy of talin-membrane recruitment. The conformational change of THD F3, which is critical for optimal talin-integrin interactions, remains sensitive to lipid headgroup identity in the presence of integrin tail and PIP2 promotes the largest change. Further investigation also demonstrates that, with integrin inserted Nanodiscs, talin self-inhibitory rod domains impede THD binding to PS membrane in different degrees. PIP2 membrane renders THD insensitive to inhibition by talin R9 and R12R13. Results also implicates that talin R9 sterically blocks THD binding integrin on F3 domain and R12R13 may hinder the membrane interaction on F2 domain.

Thus, this thesis work shows that PIP2 plays a central role in the regulation of the auto-inhibited form of talin and stimulates recruitment of talin to the membrane and integrin, which is essential for integrin inside-out activation.

To my family and friends, for their love and support.

ACKNOWLEDGMENTS

This thesis would not exist without the contributions of many people, both directly and indirectly. I would like to first and foremost thank my doctoral advisor Prof. Stephen Sligar for his inspiration, encouragement, and generous support on my graduate career. His teaching and example have not only give me scientific guidance, but also sharpened me to become an enthusiastic researcher, effective communicator and better scientist. His passion and critical eye will continue to inspire me throughout my career.

I also need to specially thanks Dr. Mark McLean, who is my mentor as well as a good friend in the Sligar research group. I joined the laboratory with no prior experience in biophysics and membrane protein, and he patiently taught and trained me more that he realizes. His perceptive advices and extensive research experience have played an undisputed role in helping the project going forward.

I would also like to thanks my dissertation committee members, Prof. James Morrissey, Prof. Emad Tajkhorshid, and Prof. Rutilio Fratti, who have given me insightful suggestions and critics during the past few years.

I own many thanks to all of the past and current members of the Sligar Laboratory. I was very fortunate to be a part of this stimulating group. Dr. Ilia Denisov taught me fundamental P450 knowledge and gave me tremendous help when I first started. Dr. Yelena Grinkova has always been my "Wikipedia" of molecular biology methods. Abhi has been a kind big brother to all the junior lab members and gave many helpful suggestions to me. I also enjoy getting lost on the Internet with Mike, who is always able to bring laughter and

make the time in lab more enjoyable. Ivan is a wonderful and supportive peer who is always a pleasant to chat and drink with. Ruchia is my saver when I forget my keys in lab and prevent me from sleeping on the street many times. I also thank Aretta for her excellent work on organizing the lab and lovely gossips. I would also like to thank the other members: Dr. Yogan Khatri, Dr. Michael Marty, Katie Baker, Erin Wildeman, Monika Waclaw, Matthew Wilkins, and Wangsoo Lee for their major and minor helps and the fun time we shared.

I have had the privilege to work with a number of wonderful collaborators. I thank Dr. Mark Arcario and Prof. Emad Tajkhorshid for providing the excellent computational simulation on talin binding to anionic lipid bilayers, which was directly mentioned several times in this dissertation and greatly facilitate the talin research project. I thank Dr. Feng Ye and Prof. Mark Ginsberg at University of California, San Diego for the generous gifts of talin constructs and helpful discussions. Working with them was very educational, exciting and rewarding.

My graduate education was partly funded by the Guangzhou Elite Student Fellowship. I thank the Guangzhou government for their generous support and this amazing opportunity to pursue a scientific career.

Finally, I would like to thank my family for their love and support. My parents offered a lot of encouragement, caring, and have been scholarly role models who inspired me to continue my graduate study. My parents in law have played a critical role in every stage of my graduate education. Last but not least, my lovely and wonderful wife has been with me every step along the journey. From applying graduate school to finding next place to go, she has been my constant companion and greatest comfort even when we are thousands mile apart. Thank you!

TABLE OF CONTENTS

LIST OF ABBREVIATIONS

ABS	Actin binding site
DMPA	1,2-dimyristoyl-sn-glycero-3-phosphate
DMPC	1,2-dimyristoyl-sn-glycero-3-phosphocholine
DMPG	1,2-dimyristoyl-sn-glycero-3-phospho– (1'-rac-glycerol)
DMPS	1,2-dimyristoyl-sn-glycero-3-phospho-L-serine
DTT	Dithiothreitol
ECM	Extra cellular matrix
E.coli	*Escherichia coli*
FAK	Focal adhesion kinase
FAP	F3 Association Patch
FERM	Band 4.1/ezrin/radixin/moesin
FRET	Fluorescence resonance energy transfer
GPCR	G protein-coupled receptors
HMMM	Highly Mobile Membrane Mimetic
IBS	Integrin binding site
IMC	Inner membrane clasp
IPTG	Isopropyl-β-D- thiogalactopyranoside
Kd	Dissociation constant
LB	Lysogeny broth
MBP	Maltose binding protein

MD	Molecular dynamic
MOP	Membrane orientation patch
MSP	Membrane scaffold protein
Ni-NTA	Nickel-nitrilotriacetic acid
NMR	Nuclear magnetic resonance
OD	Optical density
OMC	Outer membrane clasp
PCR	Polymerase chain reaction
PH	Pleckstrin homology
PI4P	Porcine brain L--phosphatidylinositol-4-phosphate
PIP2	Porcine brain L--phosphatidylinositol-4,5-bisphosphate
PKC	Protein Kinase C
PTB	Phosphate tyrosine binding
RIAM	Rap1-interacting adapter molecule
PMSF	Phenylmethylsulfonyl fluoride
RPM	Round per minute
SPR	Surface plasmon resonance
TBE	Tris/Borate/EDTA
TCEP	Tris (2-carboxyethyl) phosphine
THD	Talin head domain
UA	UniblueA

CHAPTER 1

INTRODUCTION

1.1 Overview

In multicellular organisms, tissues with diverse characteristics arise from the specific interactions between cells and extracellular matrix (ECM). Cell shape change, cell adhesion, and cell migration are tightly controlled by the communication of intracellular cytoskeleton and ECM substrates in response to physiological and pathological signals. Integrins, identified almost three decades ago [1], are considered to be the major mediators for such cellular reactions. Hence, they play a key role in many cell events, such as development regulation, immunity, and hemostasis.

Integrins are a family of heterodimeric membrane receptors that consist of one α- subunit and one β-subunit, which each comprise a huge ectodomain, a single transmembrane domain and a commonly small cytosolic tail [2, 3]. The affinities of ECM ligands, such as collagen, laminin, and fibronectin, to integrins are regulated by the cellular pathway named inside-out signaling resulting in integrin activation. It governs changes of cell adhesion, polarity of migrating cells, and the assembly of the ECM, thereby controlling platelet aggregation, leukocyte transmigration, and tumor cell metastasis [4]. Due to the prospective therapeutic and extensive biological significance of integrin activation, it has been and is being studied intensely.

Talin [5, 6, 7, 8, 9], together with other many other protein, such as vinculin [10, 11, 12], filamin [13, 14], kindlin [15, 16, 17], are known critical players for the linkage of integrin and

cytoskeleton, which are able to simultaneously and directly bind to both integrin cytosolic tails and actin. The rich protein-protein interplays within integrin-actin networks coalesce to construct the distinct structures of focal adhesion site that serve as dynamic hubs of adhesive and signaling activities [18, 19]. Protein-lipid interactions at the cytoplasmic face of integrin are key elements in the activation mechanism yet largely uncharacterized despite the well-known lack of efficient integrin activation in the absence of membrane [20].

The major obstacle that hampered detail interrogation of protein-lipid interactions is due to the fact that many of the common experimental techniques are not able to provide precisely controlled composition of lipid bilayer. In addition, result interpretation of in vitro experiments, such as unilamellar vesicles, using mixed lipid, particularly with regard to anionic phospholipids, suffer with strong tendency for lipid clustering and phase separation [21].

This thesis describes an innovative experimental study of the critical question in integrin signaling, the effect of membrane lipid bilayer on inside-out integrin activation. By using an novel experimental membrane mimetic known as Nanodiscs to deconvolute the multiple interactions occurring at the phospholipid membrane of known composition on purified targets, an unprecedented level of structural details on the role of specific lipid-protein interaction in talin mediated activation of integrin is provided.

1.2 Talin Cellular Distribution and Structure

As one of the most abundance proteins at cell adhesion sites, talin was identified around three decades ago [22]. The talin gene and its orthologs are ubiquitously expressed from single cell protists to vertebrates [23]. There are two isoforms of talin in mammalian cells. Talin 1, being highly enriched in the heart and scared in the brain, can be traced in most parts of body. In contrast, talin 2 is rare in the skeletal muscle, liver and lung but

mostly abundant in the brain [24]. Even though talin 1 and talin 2 isoforms share a 74% DNA sequence similarity, they do not functionally compensate for each other. It has been shown that talin 1 level do not enhance to compensate the loss of talin 2 in deficient mice model [25]. During epithelial embryogenesis and in muscle or heart specific knockout models, talin 2 levels remain steady and do not compensate for the inactivated talin1 [26, 27, 25]. By using various model organisms[24, 28, 29, 30] and tissue-specific knock down or knock out of talin[26, 31, 32], the pivot role of talin in cell adhesion and integrin activation has been well demonstrated.

Talin monomer is a 270 kDa cytoplasmic protein with 2541 amino acids. It is composed of a globular N-terminal talin head domain (THD) of 433 amino acids and a much larger C-terminal rod domain. The THD can be subsequently divided into four subdomains, F0, F1, F2, and F3. F1-F3 is homologous to the domain found in band 4.1/ezrin/radixin/moesin family of proteins (FERM domain). Additional ubiquitin-like F0 closely packs against F1 domain [33] and form an atypical linear conformation as opposed to traditional cloverleaf arrangement in most other FERM domain proteins [34]. Moreover, there is a 30 amino acids insert with F1 subdomain that is no visualized in the X-ray crystallography structure of THD due to stability enhancement [34, 35]. Many functions of talin are exerted by F3 domain as it binds to integrins [36], layilin [37], and phosphatidylinositol-4 phosphate 5 kinase gamma 90 (PIPKγ90) [38, 39, 40]. Focal adhesion kinase (FAK) is another implicated talin F2F3 binding partner [41, 42], although the biophysical evidence for such interaction is missing. Early study show that the unstructured insert in F1 has a tendency to form helix upon binding membrane and F2 domain provides anchor to lipid bilayer, which may facilitate F3 domain positioning to a preferable orientation for integrin engagement [43, 33, 44]. A large unstructured region connects the talin head to the talin rod, and its fully extended form may span about 20nm long [45].

Talin rod domain, which is a compilation of 62 amphipathic α-helixes that organized

into 13 4-helix or 5-helix bundles. The C-terminus of rod domain is implicated as the dimerization domain. Talin rod domain is a hub of various protein interaction sites for integrin [46], RIAM [47, 48, 49], vinculin [50] as well as a C-terminal dimerization subdomain [50]. Also, three actin binding sites can be found in talin, one within THD and two at talin rod domain. Structural study reveals that the dimerization sequence (2496-2529) is essential for the talin's C-terminus actin binding [51]. Although biophysical evidence and structural detail of the crosslinking among the three sites and actin remodeling regulation remain unclear, a recent study suggests a model that initial force acting vie talin C-terminal actin binding site (ABS) and vinculin binding promote and lock talin into an actin-binding configuration which stabilizes focal adhesions [10]. Different species and even specific tissues may possess different overall organizations of talin, dimer versus monomer. At low concentration at physiological ion strength, purified talin from chicken gizzard stays in monomeric state with a filamentous and extended configuration. Lower ionic strength could induces a globular overall conformation of full-length chicken talin monomer [52, 53]. In contrast, talin extracted from human platelets predominately shows as an antiparallel homodimer [54].

1.3 The Interplays of Membrane, Integrin, and Talin

The heterodimeric integrin associate α-subunit and β-subunit via an interaction between the transmembrane helices within the phospholipid bilayer [55, 56]. Studies of platelet αIIbβ3 integrin transmembrane domain reveal that β3 integrin subunit forms a long helix, whereas the αIIb integrin subunit adopts a shorter helix that allows a backbone reversal and packs Phe992-Phe993 against the transmembrane helix. For α integrin subunits, the conserved C-terminal Gly-Phe-Phe residues are embedded in membrane and ends the short transmembrane helix which is perpendicular to the membrane surface. The β integrin transmembrane domain is tilted by about 25°to the plane of membrane to accommodate the

corresponding hydrophobic residues to α Phe residues as well as the interactions of closely packed glycine residues termed as the outer membrane clasp (OMC) [57, 58, 59]. The electrostatic interaction between Arg995 in αIIb integrin and Asp723 in β3 integrin is essential to stabilize the association of $\alpha\beta$ integrin dimer and main low affinity integrin state. Mutations that disrupt this electrostatic interactions lead to integrin tail separation and activation [60, 61, 62, 63, 64].

Talin is unique for its abilities to bind and activate integrins among the identified integrin tail binding proteins. Binding of THD to numbers of β integrin cytoplasmic tails have been described although the reported affinities are widely dispersed [7, 36, 65, 66, 67, 68]. Measured by solution nuclear magnetic resonance (NMR), the dissociation constants (Kd) of talin F3 domain to β tails is in the μM range with highest affinity for β1D followed by β7, β3 and β1A cytoplasmic tails [36, 43, 69]. As one example, The dissociation constant of talin F3 binding to integrin β3 tail is 273 μM measured by NMR. On the other hand, dissociation constants estimated by surface plasmon resonance (SPR) are significantly lower, 91 nM and 12.5 nM for talin F2F3 binding to β3 and β2 cytoplasmic tails [8]. Moreover, the dissociation constant of talin F2F3 for β1 is 67 nM estimated by pulldown assays [70]. The dispersedly distributed affinities described above may arise from diverse measuring technologies, different talin fragments, sequence variation of talins and β integrin tails, and sample preparation. In the presence of phospholipids, the binding affinity of talin to β3 tail noticeably increases [71, 72] indicating that membrane plays a critical role during the talin mediated integrin activation. Conversely, the relatively low affinity of talin for integrin β cytoplasmic tails could be explained by the hypothesis that the weak interaction proved a biological control mechanism of integrin activation, so that, during cell adhesion or migration processes, the activation state of integrin can be readily inte-converted. In some other scenarios, such as those major integrins regulating platelet (αIIbβ3) and leukocyte (β2 and β7) functions, speedy transition between inactivated and activated states is required. Furthermore, the

ubiquitous expressed integrin $\beta 1$ is found in a partially active form [2, 73]. Therefore, for cases like $\beta 2$, $\beta 3$, and $\beta 7$, the tighter association of the THD to integrin tails may be needed to ensure efficient and timely integrin activation. It should be noted that same integrin tail could exhibit different affinities to the two talin isoforms. For example, talin 1 has been reported to bind integrin $\beta 1$A and $\beta 3$ stronger than the talin 2. Whereas, in myotendinous junctions, it may be necessary to tightly couple talin 2 with muscle specific $\beta 1$D integrin for resisting the high mechanical stress of muscle contration [43, 74, 69]. On the other hand, the association of talin and the α cytoplasmic tail of the platelet integrin αIIb$\beta 3$ has been found yet further study is needed to elucidate the functional significance of such interaction [75, 76, 77].

THD F3 domain possesses the major integrin binding sites which are able to recognize two regions in integrin β cytoplasmic tail: a conserved peptide sequence NPxY/F motif [7, 78] and the membrane proximal region where a salt bridge is form between integrin α subunit and β subunit to maintain the rest state [9, 64, 79]. In current popular model of talin mediated integrin activation, the membrane proximal interaction of talin disrupt the α/β integrin inner membrane salt bridge thereby leading to the unlocking of the integrin cytoplasmic tail complex. This mechanism is initially demonstrated for integrin αIIbβ and has been also shown for other integrin heterodimers [80, 81, 82]. The unlocking motion of cytoplasmic face of integrin transmits into the membrane causing separation of α/β transmembrane helixes and eventually induces integrin extracellular domain conformational changes [56, 58, 55, 83]. Recently, it has been shown that talin binding to membrane and integrin $\beta 3$ cytoplasmic tail is able to change the β integrin transmembrane domain topology, which requires the presence of anionic lipid bilayer and membrane binding residues on talin. This research provides additional information on transmission of activation signal across the membrane and reach the integrin extracellular domain [84]. Yet, the detail topology of the transmembrane helixes, especially the interplay and dissociation of α and β subunits, still remain unclear [85]. A

secondary integrin binding site is found on talin rod domain, termed as IBS-2, in addition to the talin head integrin binding site, which is known as IBS-1. The 1974–2293 amino acids fragment within talin rod domain was shown binding to integrin $\beta 3$ and $\beta 1$ cytoplasmic tails with similar affinities as THD, although no implication of integrin activating regulation has been identified in IBS-2 region [76, 86].

While the affinity modulation of integrin is believed to be primarily triggered by the binding of talin and dissociation of integrin α/β subunits, the clustering of integrins is also induced by talin to modulate integrin avidity. The formation of integrin-rich clusters or microdomains in the plasma membrane results from the lateral movement of integrins. It has been shown that clusters of integrin possess high avidity for ligands allowing for multivalent adhesive linkages. Previous research suggests that, in Chinese hamster ovary cells, the formation of integrin-abundant clusters is correlated with the agonist stimulation or exogenous THD expression. Conversely, ligand binding to integrin in the clusters could later induce extracellular domain conformational change to a higher affinity state [87, 88, 89, 90]. Above hypothesis is in a good agreement with the data from *Drosophila* integrin that regulating clustering is the major function of talin rather than modulating integrin affinity to ligands [28, 91]. Another key role of talin in *Drosophila* is to connect ECM bound integrins to cytoskeleton and transduce mechanical forces. Studies of integrin $\alpha \mathrm{L}\beta 2$ implicate that the clustering of integrin participates in its function [86, 92, 93, 94]. Intercellular Adhesion Molecule 1 binds to T-lymphocytes where $\alpha \mathrm{L}\beta 2$ integrin enriched clusters can be found on the membrane but not to dendritic cells which do not have the densely packed integrin microdomains. Stabilizing $\alpha \mathrm{L}\beta 2$ integrin clusters in high affinity state by talin also has been reported [95].

On immobilized ECM ligands, integrin activation and clustering depends on the release of THD from talin rod domain, and it supports the idea that integrin clustering after affinity modulation strengthen the linkage to the actin cytoskeleton. Talin recruitment was not found

precede to the formation of integrin enriched clusters in *Drosophila* [96]. On the other hand, talin plays a pivot role in the clustering of integrins in myotendinous junctions, supported by the mice model with skeletal muscle specific talin 1 and talin 2 knocked out. [25]. The mechanism of affinity and avidity modulation is vastly different, responding cells may require overlapping these processes, and talin is involved with both signaling events. Certain cells, tissues or developmental stage may utilize specific pathways to achieve integrin activation [25, 27].

1.4 Talin Auto-Inhibition and Its Regulation

In resting state cells, talin is auto-inhibited and restricted from binding to integrin [97, 98, 99] and membrane [100], and the distribution of talin is randomly diffused in cytosol [101]. It has been shown that talin rod domain structurally masks the THD and inhibits the interactions of the THD, the plasma membrane, and integrin. Auto-inhibited talin crystal structure (pdb 4F7G) offers a detailed view of the interface of the THD F3 domain and talin rod at the atomic level. In addition with the NMR binding data, a mechanism based on steric clash and electrostatic interaction is proposed to explain the event of relieving the auto-inhibited talin, named as "push-pull" mechanism. The membrane association to talin head F2F3 domain is prevented by talin rod domain forming complex with talin F2F3. Anionic phosphatidylserine lipid headgroups on membrane repel the negatively charges on talin rod domain surface, while the enriched PIP2 with higher concentration of negatively charge in focal adhesion would be able to attract the positively charged talin F2F3 domain, at the same time, create a repulsion force to talin rod domain [99]. This push-pull motion is likely to misalign the interface of talin rod and F3 domains, so that, overcome the auto-inhibition and allow THD docking onto membrane for subsequent interactions with integrin tails.

A recent study proposes a structure of cytoplasmic talin in a compact "donut" shape like homodimer with the THD filling the central "hole" and talin rod forming the ring. It is based on the data combination of small angle X-ray scattering, electron microscopy, NMR, and the known X-ray structures of talin fragments [102]. Large conformational change of talin domains may be needed to allow optimal bindings of integrin and vinculin. Multiple vinculin binding sites have been identified within talin rod domain [50, 103], and need mechanical forces from actin cytoskeleton to allow the access of vinculin [104, 10]. Yet, detail molecular mechanism and spatiotemporal of how vinculin participates talin mediated integrin activation remain elusive.

Furthermore, Rap1A, Rap1-interacting adapter molecule (RIAM), Protein Kinase C (PKC), calpain have been reported to promote the localization of talin to membrane and activate auto-inhibited talin [89, 105, 47, 48, 106, 35]. It has been shown that several RIAM molecules would competes with vinculin for ABSs, indicating RIAM may responsible for the initial recruitment for talin to the focal adhesion site and a possible turnover mechanism that a later replacement by vinculin would happen to facilitate focal adhesion formation [49]. The calcium dependent protease, calpain, is able to cleave the peptide bond between talin Q433 and Q434 [107], thereby liberating THD to bind cell membrane and integrin cytoplasmic tail with a significantly higher affinity compared to fulllength talin [106] and resulting in integrin activation. The other calpain cleavage site in talin, K2493-K2494 in the rod domain, has been linked to regulate the focal adhesion turnover [35, 45]. However, cleavage of talin by calpain is not strictly required for talin activation and consequent integrin activation, and evidences have been provided by the RIAM induced $\beta 3$ integrin [89] and ionophore-mediated $\alpha \mathrm{L} \beta 2$ integrin activation [108] in the absence of proteolysis of full-length talin by calpain. Thus, further investigation are needed to probe precise mechanism and hierarchy of how Rap1A, RIAM, PKC, and calpain are recruited and expose IBS in THD.

The affinity of talin rod domain for integrin $\beta 3$ cytoplasmic tail is reported as 34.5 nM

[109], which is tighter than published affinity value of THD [106]. Based on the previous observation, two inhibitory mechanisms may be involved in talin-integrin activation: firstly, as described above, talin rod R9 domain (1654–2344 residues) structurally covers integrin β tail binding site of talin FERM domain; Secondly, C-terminal talin rod segment (2300–2541 residues) inhibits IBS-2 (1974–2293 residues) binding to β cytoplasmic tail. THD activates integrin by interacting with its cytoplasmic tail, and talin rod domain plays a vital role in recruitment of other focal adhesion molecules [94]. Another proposed model is that IBS-1 is responsible for integrin activation while IBS-2 is required for maintain integrin talin linkage, then freeing talin head to bind other protein partners, for example PIPKγ90 [93].

1.5 Crosstalk between Talin and Other Integrin Partners

In addition to talin auto-inhibition, cells also employ many other mechanisms to regulate the dynamics of talin mediated integrin activation, such as coactivator kindlins [16, 110, 111], negative regulator filamin [14, 112], ICAP-1 [113], lipid binding [71, 114], and β cytoplasmic tail phosphorylation [74, 115].

Over the past few years, ample evidences suggest that kindlins also play a key roles in integrin activation and signaling [116, 117, 118, 119]. Much less structural information is characterized for kindlins, comparing to talin, partially due its difficult expression. The highly conserved sequences of three discovered kindlins show that they are also FERM domain containing protein with the atypical linear arrangement similar to talin [120]. Additional ubiquitin-like F0 domain and a large unstructured loop in F1 are also found in kindlin head domain [121]. One unique feature in kindlin, unlike talin, is that kindlin F2 domain implants a Pleckstrin homology (PH) domain [122, 123, 124] which specifically targets phosphatidylinositol lipids. Kindlin interacts with the membrane-distal NPxY motif in the β integrin tail with a highly similar manner as THD binding to the membrane-proximal NPxY

motif [111, 125]. Although, in purified systems, it is sufficient to activate membrane-inserted αIIbβ3 by talin binding [5], knock out, knock down, or integrin binding defective mutations of kindlin, either in mice [126, 127, 128] or human [129, 130, 131, 132], profoundly affect integrin mediated cellular responses.

For optimal integrin activation, talin and kindlins need to work in cooperation. *In vitro* studies have shown that THD, kindlin, and integrin β tail form a ternary complex [111, 125], yet interaction with adjacent integrins or the sequential binding of these components are not well understood [133]. There is no proof for direct interaction between talin and kindlin. Previous studies also suggest that binding of kindlin to integrin neither facilitates talin recruitment to inner membrane nor assists talin-integrin binding, which led to the hypothesis that kindlin affects subsequent events after talin binding to integrin [119, 134]. Kindlin, by binding to the distal NPxY motif in the integrin β tail and negatively charged membrane, might stabilize the integrin tail separation caused by talin binding. It has been shown that binding of kindlin F0 domain, F1 loop and the PH inserted in F2 domain to anionic phospholipids is essential for fully co-activation of integrin αIIbβ3 [121, 122, 124, 135]. The alternative mechanism, for kindlin talin cooperation, is that kindlin binding to integrin could recruits additional activators or dislodge inhibitors that regulate the talin mediated integrin activation. Consistent with this, ICAP-1 [113] and filamin [14], which are the known integrin activation inhibitory protein, are structurally predicted to overlap the kindlin binding site in β integrin tail, indicating that the binding of kindlin would displace these inhibitors.

On the other hand, talin also competes with ICAP-1 and filamin [136, 137, 138], which have tighter affinity for integrin β talin comparing to talin. Competition from these proteins at talin integrin binding site would further suppress integrin activation. In agreement with this, deficiency of filamin expression [14]and presence of migfilin, which binds to filamin and masks the integrin binding site on filamin [138, 139], enhance integrin activation. 14-3-3 proteins are able to bind Thr758 phosphorylated β2 integrin tails and inhibit the binding

of filamin to β integrin [140, 141]. ICAP-1 is another well-investigated integrin inhibitor. With a phosphate tyrosine binding (PTB) domain within ICAP-1, it binds to the membrane distal NPxY motif, which interacts with kindlin, and also inhibits the binding of talin to integrin [142]. The solved crystal structure of ICAP-1 integrin β1 complex [113] shows that ICAP-1 is not perturbing the interface of talin and integrin, indicating that ICAP-1 is not inhibiting talin mediated integrin activation via direct competition. In addition, expression of Krev interaction trapped 1 (KRIT1) can displace ICAP-1 from integrin and enhance talin mediated integrin activation [113].

Interestingly, the actin binding protein α-actinin has been shown to both positively and negatively regulates talin binding to integrin, which may due to the overlapping binding sites on β integrin cytoplasmic tail [143]. The binding competition between talin and α-actinin is consistent with a recent study that αIIbβ3 integrin activation in platelet is suppressed by α-actinin binding [144]. Conversely, α-actinin has been reported to facilitate talin binding to integrin β1 tail. Although α-actinin is regarded as the regulator of talin mediated integrin activation, the explanation of the opposite effect on different integrin tail still remains unclear. Other protein could also modulate integrin talin interaction by directly binding to talin FERM domain. Overexpression of PIPKγ has been shown to suppress talin mediated integrin by competing the talin F3 PTB domain. Furthermore, SHARPIN (SHANK-associated RH domain-interacting protein), an inhibitor of integrin activation that binds to integrin α tail, impedes talin and kindlin via an unidentified mechanism [142, 145]. The tyrosine residues in the NPxY motif of integrin β tail can be phosphorylated by SRC family kinase (SFK) and inhibit talin binding by favoring other binding partners, for example Dok1, which preferentially attaches to phosphorylated β-tail [74, 115]. 30 phosphorylation sites in talin have been identified by mass spectrometry [146]. Studies established that serines and threonines on talin can be phosphorylated by PKC [147, 148], calyculin [149], and Cyclin-dependent kinase 5 (CdK5) [150]. The phosphorylation on talin is also linked to the intracellular turnover by

Smurf1 ubiquitination [150]. However, it is not clear that whether the phosphorylation of talin is involved in integrin related events. PKC mediated THD phosphorylation in thrombin activated platelets is relevant with talin redistribution but independent of integrin binding [151]. An early report implicates that talin phosphorylation by PKC may be related to focal adhesion disassembly [152]. Thus, talin integrin interaction and integrin activation can be modulated by various protein-protein interaction or post-translation modification.

CHAPTER 2

RECRUITMENT OF TALIN BY ANIONIC BILAYER

2.1 Introduction

The protein-protein interactions of talin mediated integrin activation have been a heated research field in recent years. lately, several studies have directed their attention toward the functions of the membrane composition, particularly anionic lipids, during the structural mechanism of integrin inside-out signaling [43, 20, 153]. The solved crystal structure of talin FERM domain revealed an atypical extended linear arrangement with a bipolar charge distribution on the protein surface [34]. The positively charged regions are primarily located on the F2 and F3 domains. The asymmetry arrangement of charge on talin is vital for its recruitment to the inner membrane surface [44, 154].

The positively charged patch residing on the F2 domain have been termed as the membrane orientation patch (MOP). It plays a key role in steering the THD toward negatively charged membrane surface as well as position the talin F3 for efficient integrin interaction [44]. Four positively charged residues, K256, K272, K274, and R277 on talin 1, make up the MOP, and reverse charge mutations of these four residues have been shown to diminish talin binding to anionic lipid vesicles in pull down assays. Intriguingly, single charge reversal at any of these positions in the MOP remarkably impairs the ability of THD activating inte-

Reproduced in part with permission from Ye Xin, McLean A. Mark, and Sligar G. Stephen. Conformational equilibrium of talin is regulated by anionic lipids. *Biochimica et Biophysica Acta-Biomembranes*, 1858(8), 1833–1840, 2016. The published version may be found online at http://doi.org/10.1016/j.bbamem.2016.05.005.

grins [43]. These results suggest that the role of MOP in integrin activation extends beyond providing a membrane-binding site and the exact details of this role are not well understood.

The F3 residues, K322 and K324, involved in the membrane interactions have been named as the F3 Association Patch (FAP). Early study demonstrated that K324 is critical for integrin activation due to the potential formation of a salt bridge with D723 in $\beta 3$ integrin, which would disrupt the inner membrane clasp (IMC) of integrin α/β subunits [71, 98, 56]. It has been also shown that the unstructured loop in talin F1 domain contains a high proportion of positively charged residues, and these residues are located in the region that has a strong propensity to from an α-helix revealed by NMR. Based on the above data, Goult *et al.* suggest a "fly-casting" model of talin F0F1 interacting with membrane. Upon contacting with negatively charged lipid phospholipids, the favored helical state of the F1 loop draws the talin FERM domain towards the membrane [33].

The affinity of talin for inner membrane surface seems to be largely modulated by the overall membrane charge. In vesicle cosedimentation assays, talin 1 F2F3 domain binds to negatively charged phosphatidylserine (PS) vesicle but remains in unbound fraction in the presence of neutral phosphatidylcholine (PC) vesicle [43]. Moore *et al.* measured the dissociation constants (Kds) of talin-membrane interaction at sub-micromolar level by using SPR and immobilizing phospholipid bilayers on a hydrophobically modified BIacore L1 SPR chip [72]. However, many *in vitro* membrane experiments with mixed phospholipids are often hampered by the strong tendency of lipid clustering and phase separation [155, 156], making it difficult to interrogate protein–membrane interaction with imprecise control of lipid composition in them membrane.

Nanodiscs, pioneered in Sligar laboratory, provide a powerful tool to resemble a native membrane environment with controlled lipid compositions. Nanodiscs are nanoscale discoidal lipid bilayers stabilized by two membrane scaffold proteins (MSP), which is derived from ApoAI protein. The N-terminal globular domain is truncated, and the protein is en-

gineered for optimal expression in *Escherichia Coli* (*E. Coli*). The self-assembly process of Nanodiscs is initial by removing detergent from the cholate solubilized phospholipids and MSPs. Measurement of atomic force microscopy and small angle X-ray scattering characterized a diameter of 10 nm and a thickness of 5-6 nm of Nanosics[157, 158]. Monodisperse and homogeneous Nanodiscs can often be obtained by titrating lipids to find optimal lipid to MSP ratios. Furthermore, larger size of Nanodiscs, up to 17 nm diameters, can be reproduced by adding extra copies of a 22 amino acid helix to increase MSP length or fusing two MSP sequences together [158, 159]. Incorporation of membrane proteins into the Nanodiscs is usually achieved by mixing detergent solubilized membrane protein with lipid and MSP before detergent removal [160, 161, 162].

Nanodiscs display a number of potential advantages over other membrane mimetic techniques. Firstly, Nanodiscs offer a native membrane in a soluble and detergent-free environment to avoid detrimental effect of detergents on membrane protein, which may lead to improper folding or alter function mechanism. Previous studies have demonstrated that detergents could alter substrate binding of cytochrome P450 3A4 (CYP3A4), and epidermal growth factor receptor shows enhanced stability in Nanodiscs compared to detergent micelles [161, 163]. Secondly, Nanodiscs can be used to isolate specific oligomeric states of membrane protein by adjusting the stoichiometry of protein to MSP with large excess MSP in the process of Nanodiscs assembly, such as the investigation of various oligomerization states affecting rhodopsin activity [164]. In addition, both sides of the Nanodiscs-embedded membrane are accessible, which is extremely useful for studying transmembrane signaling, such as integrin bidirectional signaling [5]. This is a key advantages of the Nanodisc technology over vesicle preparations which has no mean of knowing the fraction of receptors that are presenting the extracellular domain on the surface of the vesicle as oppose to being pointed inside. Thirdly, the lipid composition of Nanodiscs bilayer can be finely tuned by mixing desired phospholipids during self-assembly, thus provide a controlled membrane system to

investigate protein-lipid interaction. For instances, Nanodiscs were used to probe how lipid membrane content changes can modulate the redox potentials of membrane-embedded cytochromes P450s and show the lipid composition can regulate the interactions between G proteins and G protein-coupled receptors (GPCR) [165, 166]. Finally, the MSP provides a convenient site for various of tag modification, allowing easy interfacing with monitoring and hybridization technologies. MSP sequence has been previously engineered with polyhistidine, FLAG, and other genetically programmed tags. A single cysteine residue mutation in MSP also provides a way for chemically modification with various thiol-reactive labels, thus the Nanodisc could be easily modified for various system and analysis techniques due to such wide range of tagging strategies. One excellent example would be the detail investigation of strategies for anchoring Nanodiscs to SPR surface when the popular Nickel-nitrilotriacetic acid (Ni-NTA) attachment was not ideal [167].

This chapter describes the first comprehensive study in order to elucidate the mechanism of talin interactions with native like membrane bilayers. To investigate influences of the lipid headgroups on THD/bilayer interactions, a solution assay has been developed based on fluorescence resonance energy transfer and using Nanodisc to provide precisely controlled membrane bilayer. The dissociation constants of full-length or subdomains of THD to various anionic membrane surfaces were measured by this novel binding assay. The initial interpretation was that higher percentage of negatively charged phospholipids leads to tighter association of THD/Nanodisc complex. Further study and analysis suggest an additional preference of lipid headgroup identity that contributes to the optimal THD-membrane recruitment.

2.2 Experimental Methods

2.2.1 Materials

1,2-dimyristoyl-sn-glycero-3-phosphate (DMPA), 1,2-dimyristoyl-sn-glycero-3-phosphocholine (DMPC), 1,2-dimyristoyl-sn-glycero-3-phospho-(1'-rac-glycerol) (DMPG), 1,2-dimyristoyl-sn-glycero-3-phospho-L-serine (DMPS), porcine brain L-α-phosphatidylinositol-4-phosphate (PI4P), and porcine brain L-α-phosphatidylinositol-4,5-bisphosphate (PIP2) were purchased from Avanti Polar Lipids (Alabaster, AL). *Escherichia coli* (*E.coli*) BL21 DE3 and *E.coli* BL21 DE3 gold were purchased from Stratagene (San Diego, CA). Competent cells of NEB Turbo *E.coli* were obtained from New England Biolabs (Ipswich, MA). Tetramethylrhodamine-5 (and -6) C2 maleimide (TAMRA) was obtained from Anaspec (Fremont, CA). iProof polymerase kit was purchased from BioRad (Hercules, CA). Uniblue A (UA), Amberlite XAD-2 beads, and sodium cholate obtained from Sigma-Aldrich (St. Louis, MO). pET30A-THD for expression of talin 1 head domain was a generous gift from Dr. Mark Ginsberg in University of California at San Diego (San Diego, CA).

2.2.2 Cloning and mutagenesis of THD

To reproduce pure pET30A-THD plasmid, it was transformed into NEB Turbo competent cells following manufacturer's protocol. Three colonies on kanamycin Luria broth (LB) agar plate after overnight growth at 37°C were selected and seeded into 5 mL LB liquid medium with kanamycin. Plasmids from overnight grown culture were exacted with QIAprep Spin Miniprep Kit (QIAGEN, Valencia, CA) following manufacturer's protocol. The DNA product was electrophoresed in a 1% agarose, 1x Tris/Borate/EDTA (TBE) gel and visualized under ultraviolet light by ethidium bromide.THD I398C mutant were generate by using pET30A-THD as the template plasmid for the polymerase chain reaction (PCR). Primers

were designed using the SerialCloner software package and purchased from Integrated DNA Technologies (Coralville, IA). An EcoRV restricted digestion site was eliminated with silent mutation for subsequent screening (I398C Forward: 5'-GCC GGC TAC ATC GAT TGC ATC CTG AAG AAG -3'; I398C Reverse: 5'- CTT CTT CAG GAT GCA ATC GAT GTA GCC GGC-3'). The PCR mixture was constituted, according to manufacturer's recommendation, and incubated at 98°C for 5 minutes, followed by 18 cycles of melting at 98 °C for 1 minute, annealing at 55 °C for 45 seconds, and extending at 72 °C for 3 minutes 30 seconds. Additional final extension step at 72 °C for 10 minutes was integrated in PCR to reduce partial amplified sequences. The PCR products were then digested by DpnI to specifically eradicate template plasmid. Purified pET30-THD-I398C plasmids were prepared by transforming digested products into NEB Turbo competent cells, and then isolated from overnight culture as described above. Positive clones were screened by digesting with EcoRV restricted enzyme at 37 °C for 1 hour and electrophoresis. Plasmid samples with no effect from EcoRV digestion were sent for DNA sequencing by ACGT (Northbrook, IL) using a T7 promoter primer.

In order to generate expression construct of talin head F0F1 and F2F3 domain into the pET30A backbone, NdeI and XhoI digestion sites were engineered onto the 5' and 3' ends of each gene sequence (THD Forward: 5'- CG CG CG CAT ATG ATG GTT GCA CTT TCA CTG AAG -3'; F1 Reverse: 5'- CTC GAG CCT CCG CAG CAG CAG CGT CTC AT AT AT -3'; F2 Forward: 5'- CGC GCG CAT ATG AAG TTC TTT TAC TCA GAC CAG -3'; THD Reverse: 5'- GTG CTC GAG CTG CAG GAC TGT TGA CTT TTT -3'). iProof polymerase, again, was used for PCR to amplified the THD F0F1 and F2F3 sequences using pET30A-THD-I398C as plasmid template. The reaction setup was adapted from the previous PCR parameters with 1 minute extension time due to the shorter target DNA sequence. The PCR products were electrophoresed and purified by QIAquick Gel Extraction Kit (QIAGEN, Valencia, CA) to eliminate template DNA. The XhoI and NdeI

digested fragments of THD were subsequently cloned into pET30A with same sticky ends. The ligations were exerted at an ratio of 3 to 1 for inserts versus vectors with T4 ligase. The recombinant plasmid was transformed into NEB Turbo *E. coli* competent cells and then incubated on kanamycin LB agar plate at 37 °C overnight and extracted as previously described. The positive clones were confirmed by sequence analysis. Additional mutagenesis PCR was performed to introduce N123C (F1 N123C Forward: 5'- GCC CGC ATT GGC ATC ACG TGC CAT GAT GAA TAT TC -3'; F1 N123C Reverse: 5'- GAA TAT TCA TGG CAC GTG ATG CCA ATG CGG GC -3') into THD F0F1 domain using pET30A-F0F1 as reaction template. Detail protocol can be referred to the THD I398C mutagenesis section.

2.2.3 Expression and purification of THD

All cloned expression constructs of THD were transformed into the expression host, *E. coli* BL21 (DE3) gold. Single colony of an expression strain was isolated by spreading cell culture on LB kanamycin agar plate for overnight at 37 °C incubation, and inoculated into 50 mL LB kanamycin liquid media. The starting culture was shake at 250 round per minute (RPM) 37 °C till optical density (OD) at 600 nm reached 0.6 to 0.8. 10 mL of starting culture were seeded into 1 L of LB media containing 50 μg/L kanamycin in a 4 L flask and incubated at 37 °C with shaking at 250 RPM. To induce expression of protein, isopropyl-β-D-thiogalactopyranoside (IPTG) was added to a final concentration of 1 mM when OD 600 nm reached 0.8, and the cells were continued to grow at 37 °C and 230 RPM for an additional 4 to 6 hours. Cells were collected by centrifugation at 8,000 RPM for 10 minutes at 4 °C. The pellet of bacterial was stored at -80 °C for subsequent use.

For purification, the *E. coli* pellets containing THD protein were suspended in loading buffer (20 mM Tris buffer at pH 7.4 with 500 mM NaCl and 20 mM Imidazole) at the ratio of 5 mL buffer to 1 g pellet. DNAse and phenylmethylsulfonyl fluoride (PMSF) were added to final concentrations of 20 μg/mL, and 0.5 mM, respectively. The mixture was

gently stirred at 4 °C for 45 minutes or until no chunk of cell pellet can be observed. The cell suspension was sonicated for 5 rounds of 1 minute using a duty cycle of 50% and a power setting at 6 (Branson sonifier 450) on ice with 5-minute intervals to allow DNA digestion. The cell debris and membrane were removed by ultracentrifugation (BECKMAN L8-M Ultracentrifuge) at 30,000 RPM 4 °C for 45 minutes. Cell supernatant was immediately loaded onto a column (2.5 × 10 cm) with 35 mL Ni (II) chelating Sepharose fast flow (GE Healthcare Life Science, Pittsburgh, PA) equilibrated with loading buffer. The loading flow rate is 1 mL/ min, and the flow through of cell supernatant was collected for later analysis. Then the column was washed by washing buffer (20mM Tris buffer at pH 7.4 with 500 mM NaCl and 50 mM Imidazole) with 10 times bed volumes. The THD proteins were eluted with elution buffer (20mM Tris buffer at pH 7.4 with 500 mM NaCl and 300 mM Imidazole) in fractions of 4 mL. 10 μL of each fractions were mixed with 150 μL of Coomassie Plus (Bradford) Assay Reagent (Thermo Fisher Scientific, Waltham, MA) and incubated for 3 min at room temperature. Elution fractions that turned bright blue were pooled together and dialysis against 8,000,000 volumes of labeling buffer (20 mM Tris, 150 mM KCl at pH 7.0). The final products and purification process were exanimated by sodium dodecyl sulfate polyacrylamide gel electrophoresis (SDS-PAGE). The concentrations of protein were determined by ultraviolet spectroscopy (HP/Agilent 8453 UV-Vis Spectrophotometer) and calculated using $\varepsilon_{280\ \mathrm{nm}} = 42\ \mathrm{mM}^{-1}$ for full-length THD, $\varepsilon_{280\ \mathrm{nm}} = 18\ \mathrm{mM}^{-1}$ for THD F0F1 domain, and $\varepsilon_{280\ \mathrm{nm}} = 23.4\ \mathrm{mM}^{-1}$ for THD F2F3 domain.

2.2.4 Preparation of Uniblue A labeled THD

The concentrations of THD I398C, THD F0F1 N123C, and THD F2F3 I398C were adjusted to around 100 μM by centrifugation with Amicon Ultra 15 mL centrifugal filter (EMD Millipore, Billerica, MA) in order to prevent protein aggregation during labeling. Four equivalents of tris (2-carboxyethyl) phosphine (TCEP) pH 7.4 were added to the protein stock

in 20 mM Tris pH 7.0, 150 mM NaCl. After 10-minute incubation at room temperature, two equivalents of UA dissolved in DMSO were mixed with the sample dropwise and continue incubation at room temperature. 100 μL aliquots were collected every 15 minutes and purified by 2 mL of Sephadex G25 column (GE Healthcare Life Science, Pittsburgh, PA) to remove excess dye. The absorbance at 280 nm and 595 nm were measured to calculate the dye to protein ratio using below equation.

$$E = \frac{Abs_{595nm}/\varepsilon_{595nm}}{\left(Abs_{280nm} - Abs_{595nm} * 1.45\right)/\varepsilon_{280nm}} \tag{2.1}$$

Here E represents labeling efficiency; $\varepsilon_{280\ \mathrm{nm}}$ equals extinction coefficient for THD, THD F0F1, or THD F2F3; $\varepsilon_{595\ \mathrm{nm}}$ extinction coefficient for UA, which is 11 mM^{-1}; The correction factor for 280 nm from UA dye is 1.45.

The reaction was allowed to proceed until the labeling efficiency was larger than 95% after which the reaction was blocked by addition of dithiothreitol (DTT) to a final concentration of 10 mM. The usual reaction time to achieve complete labeling is around 45 minutes at room temperature. Free dye was removed by loading the labeling mixture into a G25 column equilibrated in 20 mM HEPES pH 7.2, 4 mM KH_2PO_4, 125 mM KCl, 14 mM NaCl, 1 mM $MgCl_2$, 0.02 mM EGTA. The first blue fraction was captured for further labeling efficiency calculation. The final dye to protein ratios were larger than 95%.

2.2.5 Preparation of TAMRA labeled MSP

MSP variant MSP1 D37C, which is a version of MSP1D1 with a cysteine engineered in 73 position for thiol-reactive labeling, was expressed and purified as previously described [157, 158]. MSP stock was prepared at a concentration around 100 μM and incubated with two equivalents TCEP in 20 mM Tris, pH 7.4, 150 mM NaCl, 10 mM Sodium Cholate for 10 minutes to inhibit potential formation of disulfide bounds. In the mean time, the sample was

stirred and purged with pure argon gas to remove oxygen. 10-fold molar excess of TAMRA dissolved in DMSO was added dropwise to the protein. The labeling reactions were allowed to incubated at room temperature for 4 hours, followed by overnight incubation at 4 °C. The removal of excess dye was initiated by adding equivalent volume of Amberlite XAD hydrophobic beads and followed by passage over a Sephadex G25 column equilibrated in 20 mM Tris, pH 7.4, 150 mM NaCl. The labeling efficiency (E) was calculated using $\varepsilon_{280\ \mathrm{nm}} =$ 21.4 mM^{-1} for MSP, and $\varepsilon_{557\ \mathrm{nm}} = 60\ \mathrm{mM}^{-1}$ for TAMRA with equation showed as below.

$$E = \frac{Abs_{557nm}/\varepsilon_{557nm}}{\left(Abs_{280nm} - Abs_{557nm} * 0.34\right)/\varepsilon_{280nm}} \tag{2.2}$$

An $\mathrm{Abs}_{280\ \mathrm{nm}}$ correction factor of 0.34 was used to subtract the absorbance of the dye at 280 nm. Final dye to protein ratios were larger than 60%.

2.2.6 Assembly of Nanodiscs

The TAMRA labeled MSP stock was prepared at a concentration around 100 μM. Phospholipid mixtures were dissolved in chloroform, dried under gentle stream of pure nitrogen gas in disposable glass culture tubes, and placed in a vacuum desiccator at least 4 hours or overnight to eliminate any residual chloroform. Dried lipids were then suspended in 100 mM sodium cholate to a final lipid concentration of 50 mM. Samples were sonicated in warm water (45 °C) for 15 minutes to facilitate solubilization. The final lipid solution should be clear. TAMRA labeled MSP were added to achieve a 100:1 lipid to MSP ratio. The reconstitution mixtures were incubated at 25 °C for 20-30 minutes followed by the addition of 0.8 g Amberlite XAD hydrophobic beads for each mL of solution to remove the detergent and initiate Nanodisc self-assembly. The samples were vigorously shaken at room temperature for at least 4 hours or overnight. Amberlite beads were removed, and the Nanodiscs were purified by passing over an Superdex 200 increase size exclusion column (GE Healthcare Life

Science, Pittsburgh, PA) equilibrated in 20 mM HEPES pH 7.2, 4 mM KH_2PO_4, 125 mM KCl, 14 mM NaCl, 1mM $MgCl_2$, 0.02 mM EGTA at flow rate 0.75 mL/minute. Only the middle fractions of Nanodisc were collected, and the final concentrations were between 10 and 20 μM. The final products were stored at 4 °C dark room up to 4 weeks.

2.2.7 FRET based THD binding assay

The FRET based THD binding assay was adopted from that of Bayburt *et al.* [164]. Fluorescence quenching experiments were performed in a Hitachi 3010 fluorometer attached with a circulating water bath for temperature control at 20 °C. All experiments were exerted with an excitation wavelength of 557 nm, an emission wavelength of 580 nm, 5 nm bandwidth for excitation, 10 nm bandwidth for emission. Typically, total 5 μM of UA labeled THD was titrated stepwise into 100 nM TAMRA labeled Nanodiscs solutions in 20 mM HEPES pH 7.2, 4 mM KH_2PO_4, 125 mM KCl, 14 mM NaCl, 1 mM $MgCl_2$, 0.02 mM EGTA to mimic cytoplasmic environment. At each THD addition, samples were thoroughly mixed and allowed to equilibrate until the fluorescence signal were stabilized, commonly after 3-5 minutes. The stable fluorescence intensities were recorded and the FRET efficiencies were calculated using the equation below:

$$F = 1 - \frac{F}{F_0} \tag{2.3}$$

F_0 is the starting fluorescence intensity of TAMRA labeled Nanodiscs in the absence of UA labeled THD and F represents fluorescence level at each titration point; E is the symbol for FRET efficiency.

Titration data was imported into Matlab software (the Mathworks, Natick, MA) and fit to a single binding site model in Curve Fitting Toolbox using the following equation:

$$F = \frac{F_{max}\left[(x + ND + K_d) - \sqrt{(x + ND + K_d)^2 - 4 * ND * x}\right]}{2 * ND} \tag{2.4}$$

F is the measured FRET efficiency, F_{max} is the FRET efficiency of the bound complex, x is the total THD concentration, ND is twice the Nanodisc concentration assuming one THD bound to each leaflets of Nanodisc. Statistical fitting of the data is then used to derive F_{max} and dissociation constant.

2.3 Results and Discussion

2.3.1 THD expression and purification

The desired THD DNA segments were cloned into pET30A backbone between restricted digesting site NdeI and XhoI with a C-terminal ployhistidine tag to generate expression vectors. *E.coli* was chosen as the expression strain because it is an excellent bacterial system for molecular cloning and high-level overexpression of exogenous eukaryotic protein. In *E.coli* BL21 Gold (DE3) transformed with THD expression vectors, maximum expression level of THD or its variants was measured in the cell lysate at 4 hours after 1 mM IPTG induction. In typical expression condition, 1 L cell culture yields around 5 g of bacterial pellet. Figure 2.1 lane 2 is the total cell lyse on SDS-PAGE showing the most dominant protein expressed in cell is THD.

One step purification of THD protein over a Ni^{2+} chelating Sepharose fast flow column effectively produce a homogeneous final product. The initial loading flow rate was adjusted to 1 mL/min allowing effective protein/resin binding. 20 mM imidazole was used during loading to prevent non-specific binding of non-target protein (Figure 2.1 lane 4 and 5). In the purification, 500 mM NaCl provides a high ion strength allowing potential self-aggregated protein to disassociate. Then the protein bound Ni^{2+} resin was washed with 50 mM imidazole

buffer to further reduce impurities. The purified protein was eluted with 500 mM imidazole and analysis by SDS-PAGE (Figure 2.1) and Superdex 200 increase size exclusion column (Figure 2.2). Analysis of both methods revealed that the purity of THD protein is sufficient for subsequent FRET based THD binding assay.

2.3.2 Nanodisc assembly and characterization

MSP1D1 D37C was labeled with 10-fold molar excess TAMRA-maleimide, which is specifically thiol-reactive under pH 7.5. Addition of 4 equivalents of TECP prior to labeling dye allowed reducing the possible disulfide bonds existed among MSPs. 10 mM sodium cholate were also mixed with MSPs to inhibit protein aggregation. Samples were flushed with and kept in argon during labeling to exclude oxygen and prevent disulfide bond formation. Maximal labeling efficiency was detected after 4-hour room temperature incubation followed by 4 °C overnight. The mixture of MSP and dye can be easily purified by adding equal volume of Amberlite hydrophobic beads and passing over a Sepharose G25 size exclusion column. The first red color fraction was collected and analysis by UV-vis spectroscopy. In the typical spectrum of purified labeled MSP (data not shown), the small peak in front of the main 557 nm TAMRA peak represents the absorbance of TAMRA dimmer. Adding extra cholate promotes the dissociation of the dimmer and increases the TAMRA absorbance at 557nm.

Due to the inconsistent reported extinction coefficiencies of TAMRA, the concentration of labeled MSP and labeling efficiency were roughly calculated. Therefore, a pilot lipid titration was performed to determine optimal lipid:MSP ratio for Nanodiscs assembly. Figure 2.3 shows that 125:1 of DMPC to TAMRA labeled MSP ratio, instead of 80:1 in unlabeled MSP, allows ideal formation of Nanodiscs and leads to most symmetrical chromatography peak without severe over lipidation. Then arrays of various phospholipids were used for Nanodiscs. 0, 10, 30, and 50% of PS, PA and PG as well as 2.5%, 5% and 10% PIP2

Nanodiscs were prepare. Figure 2.4 shows the chromatography spectra of DMPS Nanodiscs in Superdex 200 increase column. One interesting observation is that higher anionic lipid composition slightly shortens the retention time of Nanodiscs in size exclusion column. It may be explained by the repulsion between anionic lipid surface and slightly negatively charged column matrix composed by cross-linked agarose and dextran in running pH condition.

2.3.3 THD binds to anionic lipid bilayers

It has been shown that talin interacts with anionic bilayers. A study of vesicle cosedimentation assay revealed that THD preferably associate with PS containing liposomes but neutral PC vesicles [43]. Moore *et al.* reported a sub-micromolar dissociation constant range of THD binding to phospholipid bilayers measured by steady state SPR [72]. However, it is still not clear that whether there is a preference for a specific negatively charged lipid headgroup. Also the functional role of the headgroup identity remains elusive.

Here, Nanodiscs were used to precisely control the phospholipid composition to elucidate the mechanism of talin interactions with the membrane surface. The precise dissociation constants of talin binding to negatively charged phospholipids were measured by the FRET based binding assay. Figure 2.5 demonstrates a molecular model of talin docking on the surface of a 10 nm Nanodiscs to provide sufficient contact interface. In this system, the MSP belt of the Nanodisc is labeled with TAMRA at position 73 and talin is labeled with UA at position 398 in the F3 domain or position 123 in the F1 domain. TAMRA labeled Nanodiscs encompassing 0, 10, 30, and 50% PS, PA and PG as well as 2.5%, 5% and 10% PIP2 were prepared and used to perform FRET binding assay with THD. Figure 2.6 shows a representative binding isotherm for the interaction of THD labeled at position 398 with UA (THD-398-UA) with TAMRA labeled Nanodiscs containing 50% DMPS/50% DMPC and 100% DMPC. The binding isotherms fit well to a single binding site model assuming one talin binds per Nanodsics leaflet. 50% DMPS membrane clearly induces tighter dissociation

constant than neutral lipid bilayer.

Figure 2.7 summarizes the dissociation constants for all lipids tested in this study. As expected, there exists a clear trend of increased affinity with increasing anionic lipid content. The weakest interaction is between pure DMPC bilayers with a dissociation constant of 3.3 μM and the tightest being interactions with membranes containing 10% PIP2 displaying a dissociation constant of 0.25 μM. The dissociation constant decreases 5 to 10 fold when in the presence of 50% DMPS, DMPA or DMPG compared to pure DMPC membrane. These results well reconciles with the previously reported dissociation constants of THD binding to lipid surface [72].

The weak interaction of THD to pure neutral DMPC membrane may due to the zwitterionic charge distribution on PC headgroup where the negative charged phosphate promotes THD binding, but strongly countered by the positive choline group. Comparing identical mole % anionic lipids, the dissociation constant differs by no more than a factor of 3 for PS, PA and PG while 5% PIP2 affinities are comparable to 50% PS, PG, and PA. This difference is presumably due to the multiple charges present on the PIP2 headgroups and a specific headgroup interaction. Although the importance of PIP2 in the activation of auto-inhibited talin has been suggested [99], it is still unclear if this preference is based solely on the differences in the charge of the membrane bilayer or if the structure of the headgroup is providing some specificity. Interestingly, in the binding of talin to Nanodiscs containing PIP2 or PI4P, only 2.5% is needed to reach a 3-fold increase in affinity. DMPC Nanodiscs contain 77 phospholipids per leaflet, thus approximately two PIP2 headgroups per bilayer results in a dramatic increase in membrane affinity. This clearly points to specificity towards PIP2 as the anionic phospholipid component.

For a more direct comparison, free energies of association versus formal bilayer charge of the Nanodisc samples was plotted (Figure 2.8). Since the titrations are performed at pH 7.2 to mimic the cytosol environment, the charge of each phospholipid headgroups is -1 for

PS, PA, and PG, -3 for PI4P, and -4 for PIP2. So that, formal charge of bilayer is calculated by multiplying the headgroup charge by the mole percentage of anionic lipids in Nanodiscs. An obvious linear grouping of the free energies of PG, PI4P, and PIP2 was observed on a line which is about 0.5 kcal/mol lower in free energy of association that the line formed by PS and PA lipid headgroups. The differences here could be explained by the identity of the charged moiety on the headgroup. Those that have the lower free energy of association possess a negatively charged phosphate group and a headgroup containing alcohol groups (Figure 2.9). This points to a subtle free energy preference to headgroups providing potential hydrogen bond donors in addition to the main electrostatic driving force. While on PS, the zwitterionic serine on prohibits such hydrogen bond formation, and on PA, the negatively charged phosphate may be masked by the bulky PC headgroup inhibiting the access of THD.

2.3.4 Interactions of THD subdomains with anionic membrane

The structural study of THD revealed an uncanonical linear arrangement with additional ubiquitin like F0 preceding F1 [34]. The exact functional role of F0F1 subdomain is not fully understand, although pioneer study suggests that several basic residues on the F1 inserted loop are required for THD binding to acidic phospholipids and facilitating subsequent talin mediated integrin activation [33]. Here, FRET based binding assay was used to directly measure the dissociation constants of UA labeled THD F0F1 and F2F3 subdomains. Table 2.1 summarizes the result of measured dissociation constants. On 10% PIP2 membrane surface, the dissociation constant for F0F1 is 0.86 μM, almost 4 fold larger than the dissociation constant for F2F3 of 0.18 μM, whereas the dissociation constant for full-length THD is 0.27 μM. This result is in a great agreement with a previous study[72] that uses SPR binding assay and report tighter affinity of F2F3 compared to both F0F1 and F0F3. Intriguingly, F0F1 binds to 50% DMPS Nanodiscs with a dissociation constant of 0.45 μM, comparable to the dissociation constant of full-length THD of 0.58 μM, but significantly

lower than the 1.24 μM dissociation constant of F2F3 (Table 2.1). The similar affinities of talin FERM subdomains and the intact THD with PS membrane surface suggest that there is little cooperativity between F0F1 and F2F3. In comparison, the clear preferential binding of PIP2 to talin F2F3 over F0F1 is consistent with the previous NMR study that the binding interface between PIP2 and talin resides in the F2F3 subdomain.

2.4 Conclusions

This chapter described the analysis of the lipid composition effect on talin membrane recruitment during integrin signaling. To accurately measure the affinity of THD to various phospholipid bilayers, a solution assay based on FRET and Nanodisc technology was developed allowing precise control of membrane compositions.

Result confirms that the overall formal charge on membrane governs the THD association. Higher anionic lipid percentage in Nanodiscs promotes tighter binding of THD in the range of sub-micromolar. Although, the detected difference of affinities between neutral membrane (DMPC) and highly negatively charged membrane (PIP2) is less than 10 fold, seem relatively small compared to a change of enzymatic reaction. The signal could be amplified by the downstream events that induced dramatic change of cell activity. Intriguingly, data suggests that THD possess a subtle preference for phospholipid headgroups. Small amount of phosphoinositides, such as 5% PIP2, supports the same THD affinity as 50% DMPS, which strongly suggests the specificity of PIP2 to THD. Furthermore, affinity measurement on THD subdomains also shows that F2F3 favors binding to PIP2 over PS. The comparison of association free energy versus formal charge across all the phospholipids tested indicates an additional hydrogen bond donor on PG, PI4P, and PIP2 beside the main electrostatic driving force.

2.5 Figures and Table

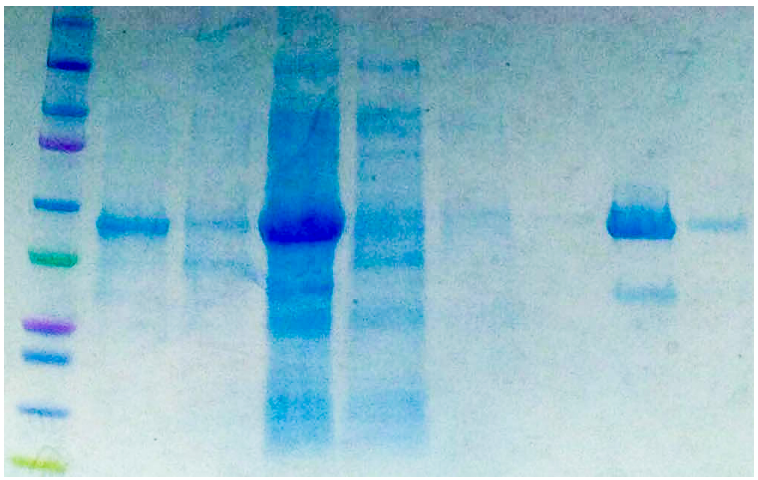

Figure 2.1: Purified THD analysis in SDS-PAGE. From left to right, Lane 1–All range Precision protein standards; Lane 2–total cell lysate; Lane 3–cell lysate supernatant; Lane 4–cell lysate debris; Lane 5–column loading flow through; Lane 6–column wash; Lane 7,8,9–column elution fractions.

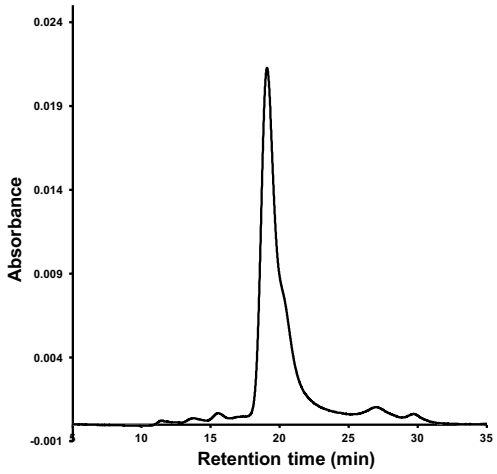

Figure 2.2: The sample size exclusion column chromatography of purified THD.

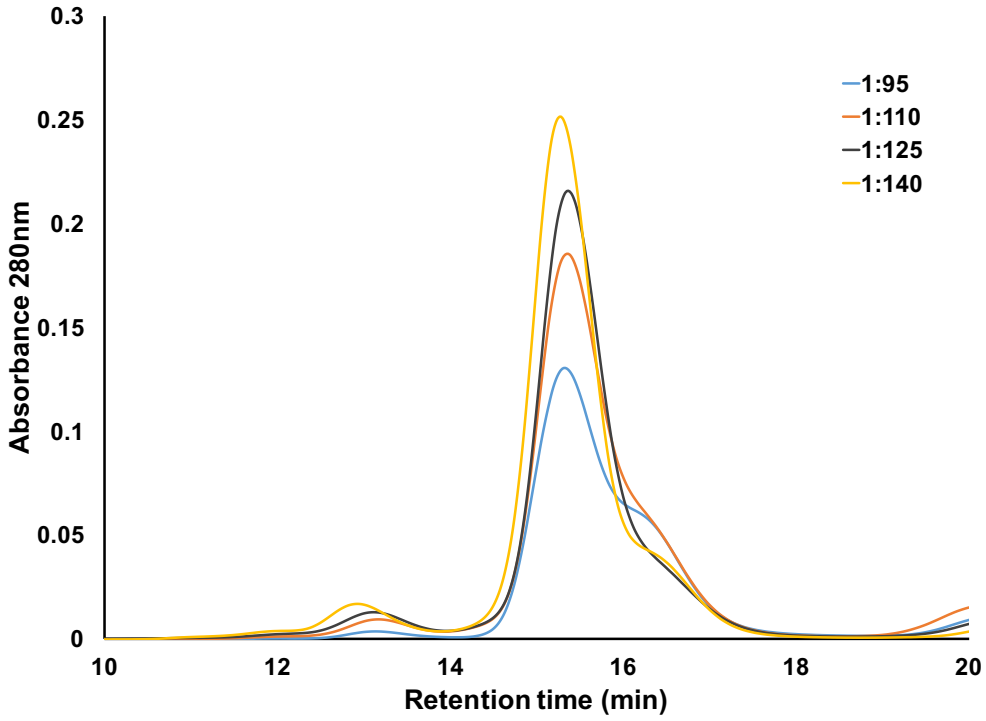

Figure 2.3: Lipid titration of TAMRA labeled MSP for Nanodiscs assembly. Blue trace–1:95 ratio; Orange trace–1:110 ratio; Dark grey–1:125 ratio; Yellow trace–1:140 ratio.

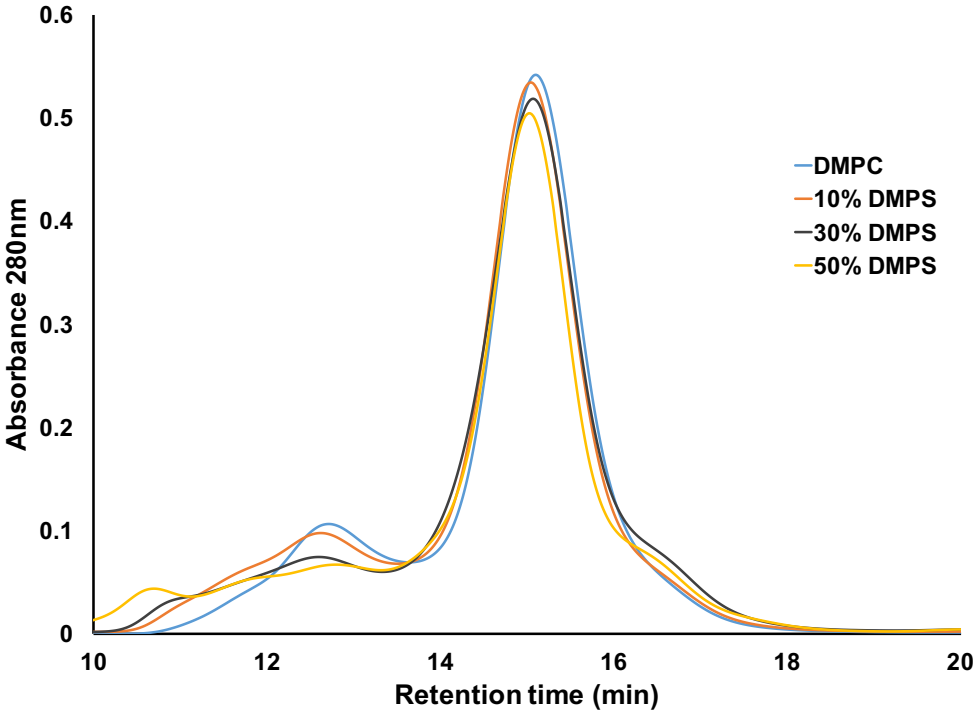

Figure 2.4: Purification of DMPS Nanodiscs.Blue trace–DMPC; Orange trace–10% DMPS; Dark grey–30% DMPS; Yellow trace–50% DMPS.

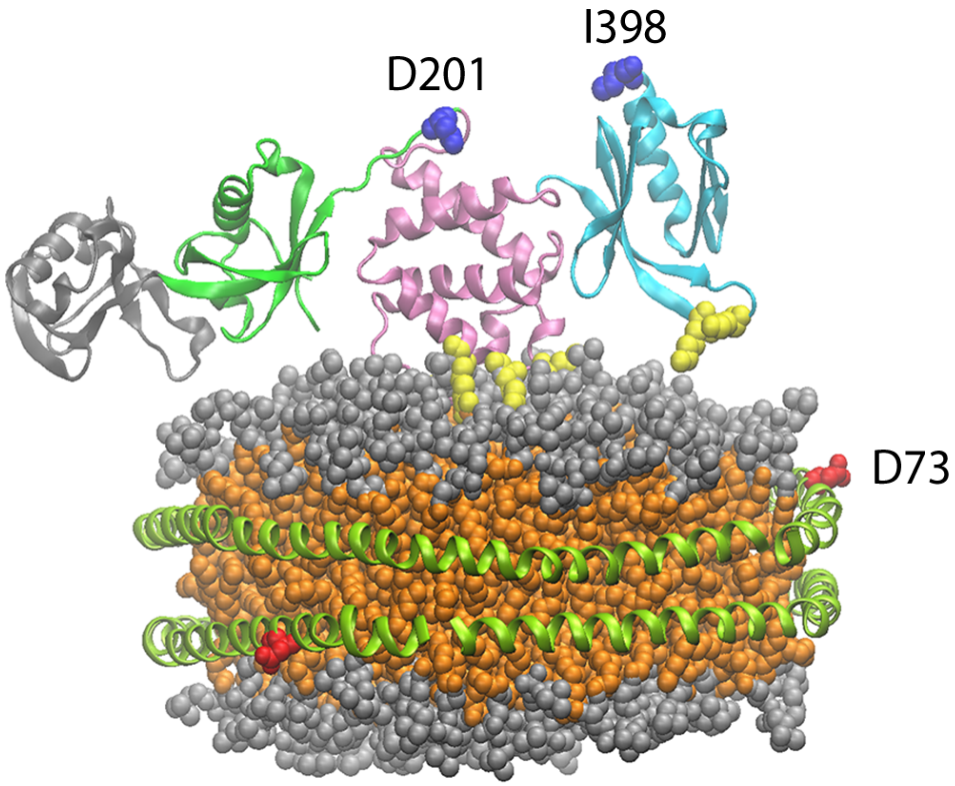

Figure 2.5: Talin Head Domain docked on the surface of a Nanodisc. THD colors: F0-gray, F1-green, F2-pink, F3-blue. The Nanodisc labeling sites are shown in red and the talin labeling sites in blue. The positively charged amino acids that make up the MOP and FAP are shown in yellow. For clarity, the binding of talin to the opposite bilayer was omitted.

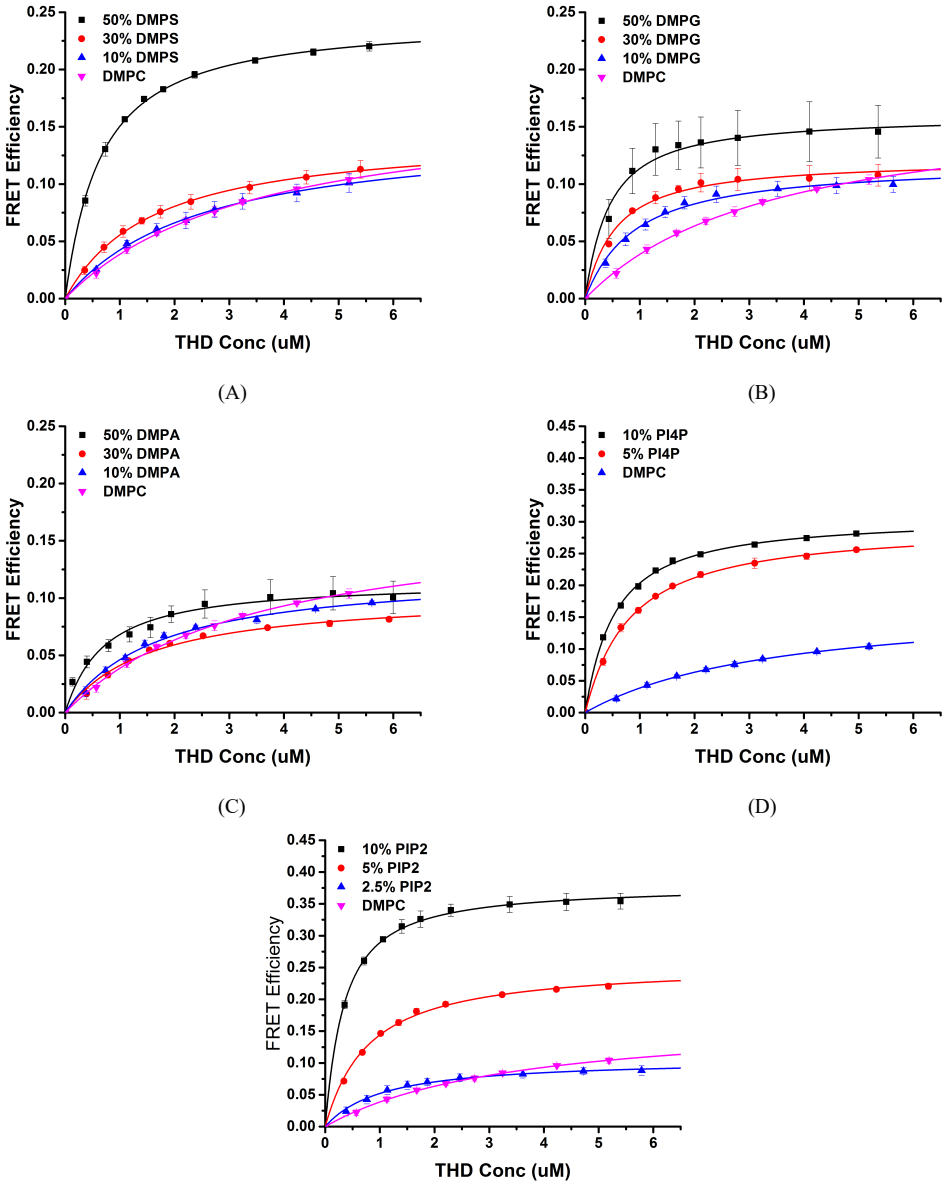

Figure 2.6: FRET based THD binding isotherms on DMPS (A), DMPG (B), DMPA (C), PI4P (D), and PIP2 (E) Nanodiscs.

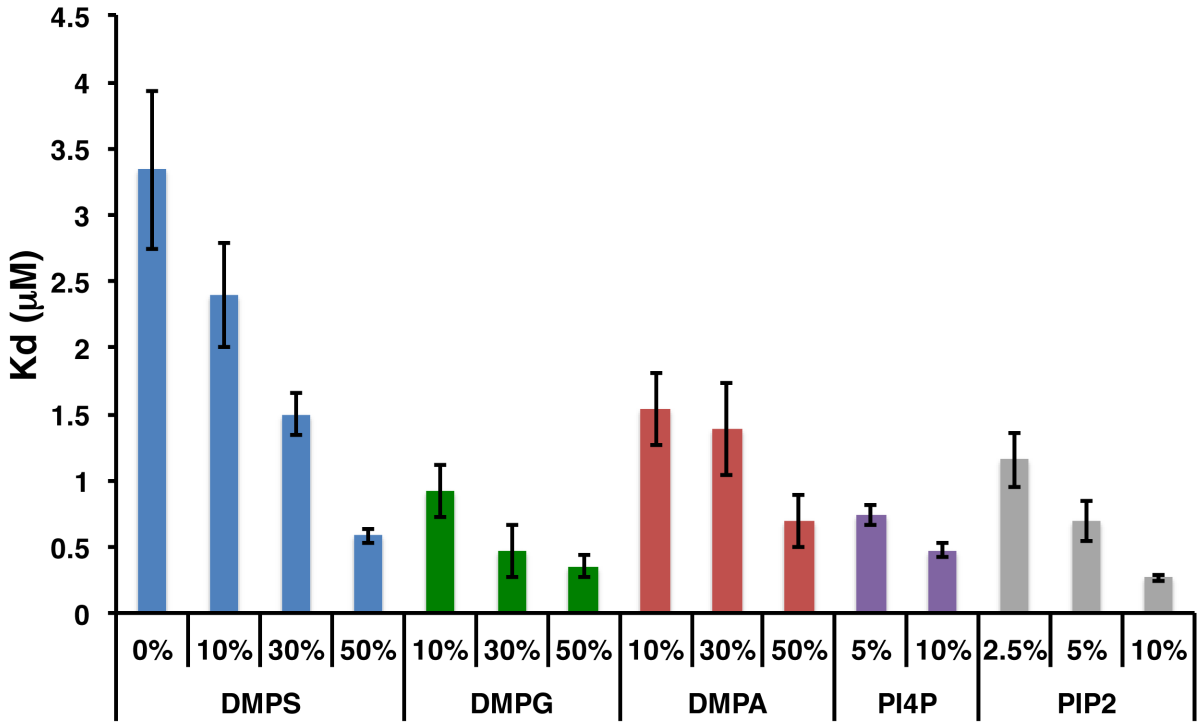

Figure 2.7: Dissociation constants of THD binding to bilayers composed of mixtures of DMPC and anionic lipids.Error bars represent the standard deviation calculated from a minimum of three trials.

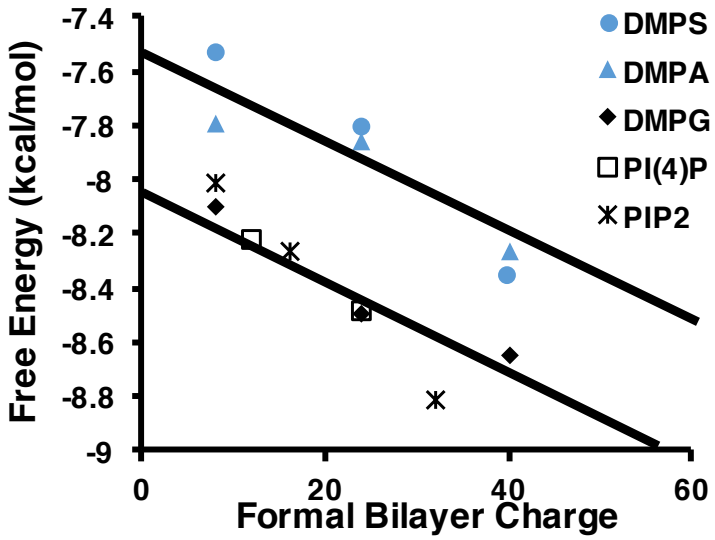

Figure 2.8: Free energy of association vs. bilayer formal charge. DMPS and DMPA grouped together blue triangles; DMPG, PI4P, and PIP2 grouped together green asterisks.

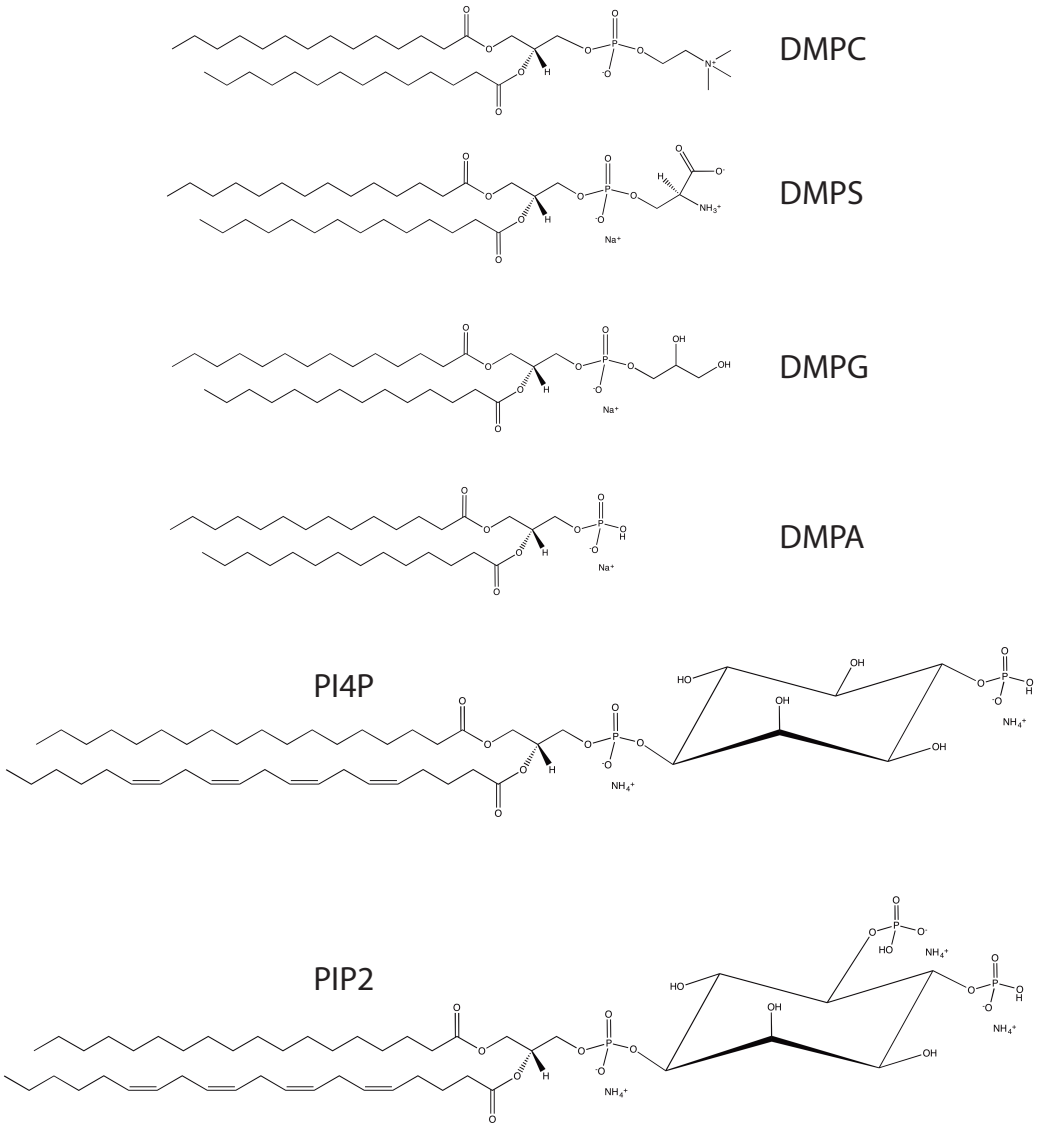

Figure 2.9: Structures of DMPC, DMPS, DMPG, DMPA, brain PI4P, and brain PIP2.

Table 2.1: Dissociation constant of THD subdomains on Nanodiscs

	F0F1 Kd (μM)	F2F3 Kd (μM)	F0F3 Kd (μM)
50% DMPS	0.45 ± 0.05	1.24 ± 0.17	0.58 ± 0.04
10% PIP2	0.86 ± 0.02	0.18 ± 0.01	0.27 ± 0.01

CHAPTER 3

CONFORMATIONAL DYNAMICS OF TALIN REGULATED BY ANIONIC LIPIDS

3.1 Introduction

The overall membrane charge has been previously shown to control the affinity of talin head domain (THD) for the bilayer surface. Many suggest that PIP2 plays a critical role in talin mediated integrin activation by activating the auto-inhibited talin and promoting conformational change [20, 34, 99]. However, the detail picture of talin interacting with membrane and integrin tails is lacking, especially how the F3 domain binds membrane and modifies the integrin β tail tilting angle.

Martel *et al.* first described the evidence for a lipid induced conformational change, which showed a differential sensitivity to proteolysis upon binding to phosphatidylinositides [20]. Recently, the advance of Molecular Dynamics (MD) simulations has allowed investigators to further study this problem. Kalli *et al.* showed that interaction of talin with the lipid bilayer converts the linear arrangement of the F0-F3 domains to a "V" shape conformation having an angle of 60 degrees between F0F1 and F2F3 [168]. This conformation is shown to optimize membrane contacts and increase the number of hydrogen bonds upon binding to β-tails.

In yet another MD simulation, Arcario *et al.* used a Highly Mobile Membrane Mimetic

Reproduced in part with permission from Ye Xin, McLean A. Mark, and Sligar G. Stephen. Conformational equilibrium of talin is regulated by anionic lipids. *Biochimica et Biophysica Acta-Biomembranes*, 1858(8), 1833–1840, 2016. Copyright 2016 Elsevier. The published version may be found online at http://doi.org/10.1016/j.bbamem.2016.05.005.

(HMMM) to capture snapshots of the interaction of the F2F3 domain and an anionic membrane surface [44]. The study suggests the important function of the MOP region of F2 domain in steering the THD toward the membrane in an orientation conducive to interaction with integrin tails. The simulations also identified an initially buried phenylalanine rich area that opens up and allows the embedding of phenylalanine residues 261 and 283 (F259 and F280 in talin 1). They may serve as a pair of membrane anchor that stabilize the THD/membrane complex. In the simulation, such conformational changes seem to be triggered by the snorkeling of the basic lysine residues in the MOP upon binding with anionic lipids. Most interestingly, the motions described above also promotes a large conformational change in the F3 domain, bringing K325 and K327 (K322 and K324 in talin 1) to the membrane surface in a preferable conformation for interaction with integrin tails. The F3 residues involved in the membrane interactions have been termed as the F3 Association Patch (FAP).

Although the simulation results are in a great agreement with many previous *in vivo* study that K322 and K324 are crucial for optimal integrin activation [9, 98]. There is no direct biochemistry or biophysics evidence of the F3 conformational change, to my best of knowledge. To further study and properly measure the protein-membrane binding topology, fluorescence resonance energy transfer (FRET) was chosen as the major technique due to the fact that FRET occurs between two proper fluorophores only when the distance between them is less than 10 nm [169, 170]. This is well suited to study the binding geometry change occurring on a comparable spatial scale. When FRET takes place in a sufficiently close proximity, energy of the fluorophore is coupled through the fluorescent dipoles rather than transferring by emitting a photon from the donor then absorbing by the acceptor. One particular useful phenomenon of the FRET is that the FRET efficiency changes as the sixth order of the distance between the FRET pair and their Förster distance where the FRET efficiency is 50% [171]. Researcher have widely applied this technique to study the protein conformational change [80, 172], protein-protein interaction [173, 174], biophysical

characteristic of membrane [175], and protein-membrane interaction [176].

This chapter describes the first evidence of anionic lipids regulating the conformational equilibrium of talin. To correctly probe the conformational change of talin during membrane binding, the Förster distance of FRET pair used in FRET THD binding assay. Data analysis suggests that talin F3 domain undergoes a large conformational change on highly negatively charged membrane surface as suggested in previous MD simulation. PIP2 induces the largest change. Mutagenesis studies of talin also implicates that several lysine and phenylalanine residues are important trigger residues for such binding topology alteration.

3.2 Experimental Methods

3.2.1 Materials

DMPC, DMPS, DMPG, DMPA, PI4P, and PIP2 were purchased from Avanti Polar Lipids (Alabaster, AL). *E.coli* BL21 DE3 and *E.coli* BL21 DE3 gold were purchased from Stratagene (San Diego, CA). Competent cells of NEB Turbo *E.coli* were obtained from New England Biolabs (Ipswich, MA). Tetramethylrhodamine-5 (and -6) C2 maleimide (TAMRA) was obtained from Anaspec (Fremont, CA). iProof polymerase kit was purchased from Bio-Rad (Hercules, CA). Uniblue A (UA), Amberlite XAD-2 beads, and sodium cholate were obtained from Sigma-Aldrich (St. Louis, MO). pET30A-THD plasmid DNA for expression of talin 1 head domain was a generous gift from Dr. Mark Ginsberg in University of California at San Diego (San Diego, CA).

3.2.2 Talin head domain (THD) mutagenesis

THD D201C was generated by using pET30A-THD as the template and designed primers for the aspartate to cysteine mutation (THD D201C Forward: 5'- GTT CTT TTA

CTC ATG CCA GAA TGT GGA TTC C -3'; THD D201C Reverse: 5'- GGA ATC CAC ATT CTG GCA TGA GTA AAA GAA C -3'). Expression plasmids of THD K274E, K322E, K324E, and F259A/F280A mutants were produced by using pET30A-THD I398C as the template and specific primers for each mutant (THD K274E Forward: 5'- CTG CCC AAG GAG TAC GTA AAG CAG GAA GGA GAG CGT AAG ATC -3'; THD K274E Reverse: 5'- GAT CTT ACG CTC TCC TTC CTG CTT TAC GTA CTC CTT GGG CAG -3'; THD K322E Forward: 5'- GGA AAA AAT GAA AGG GGA GAA CAA GCT TGT GCC CAG GCT TCT G -3'; THD K322E Reverse: 5'- CAG AAG CCT GGG CAC AAG CTT GTT CTC CCC TTT CAT TTT TTC C -3'; THD K324E Forward: 5'- GAA AGG GAA GAA CGA GCT CGT GCC CAG GCT TCT G -3'; THD K324E Reverse: 5'- CAG AAG CCT GGG CAC GAG CTC GTT CTT CCC TTT C -3'; THD F259A Forward: 5'- GCA CAA GGC TGG CGC ACT TGA CCT CAA GGA CTT CCT GCC -3'; THD F259A Reverse: 5'- GGC AGG AAG TCC TTG AGG TCA AGT GCG CCA GCC TTG TGC -3'; THD F280A Forward: 5'- GAA GGG AGA GCG TAA GAT AGC CCA GGC ACA CAA GAA TTG -3'; THD F280A Reverse: 5'- CAA TTC TTG TGT GCC TGG GCT ATC TTA CGC TCT CCC TTC -3'). The PCR reaction parameters and setup were adopted from the protocol described in chapter 2 except 3 minutes 30 seconds extension time. All PCR products were digested with DpnI and then purified by QIAquick PCR purification kit (QIAGEN, Valencia, CA). The recombinant plasmid constructs were amplified by transferring into NEB turbo competent cell and then send for DNA sequence validation by ACGT (Northbrook, IL) using a T7 promoter primer.

3.2.3 Expression, purification and labeling of THD mutants

The protocol for THD mutant purification and labeling was adapted from chapter 2. In brief, the expression vectors were transferred into the *E. coli* BL21 Gold (DE3). 50 mL starting culture was prepared for each mutant and then inoculated to 1 L in a ratio of 1:100.

Typically, 2 L of cell culture for each THD mutant were cultivated at 37 °C with shaking at 250 RPM followed by IPTG induction and additional 4-hour incubation. Cell pellet was harvested by centrifugation at 8,000 RPM for 10 minutes at 4 °C.

Purification started with preparation of cell lyse supernatant by suspension, sonication, and ultracentrifugation at 30,000 RPM 4 °C for 45 minutes. Then the cell supernatant was purified by loading onto a Ni^{2+} chelating Sepharose fast flow column. The THD proteins were eluted by 500 mM imidazole and dialysised against 8,000,000 volumes of labeling buffer (20 mM Tris, 150 mM KCl at pH 7.0).

To label the protein, four equivalents of TCEP (pH 7.4) were added added to THD D201C or other THD mutants in cytoplasmic mimetic buffer followed by 10-minute incubation at room temperature. Two-fold of UA in dry DMSO were added to the sample dropwisely and continue incubation for another 45 minutes. The excess dye was removed by gel filtration on an 80 mL Sephadex G25 column. The purity and labeling efficiency were examined as described in chapter 2.

3.2.4 Determination of TAMRA labeled MSP quantum yield and Förster distance

To precisely report the fluorophore pair distance measured by FRET binding assay, the quantum yield of TAMRA and the Föster distance of UA and TAMRA were determined. The quantum yield of the TAMRA labeled Nanodiscs was determined by comparing the fluorescence intensity to that of a quantum yield standard using the following equation:

$$Q = Q_R \cdot \frac{I}{I_R} \cdot \frac{OD_R}{OD} \cdot \frac{n^2}{n_R^2} \tag{3.1}$$

Here, Q_R is the quantum yield of rhodamine B in water (0.31). I, I_R, n, n_R are the intensities and indices of refraction of the sample and reference respectively. In the case of

TAMRA, the refraction indices are equal for sample and reference. Five samples of TAMRA labeled Nanodiscs and rhodamine B, prepared having optical densities ranging from 0.005 to 0.01 at 540 nm, were used to ensure a more accurate measurement for the quantum yield. Emission spectra of TAMRA samples and rhodamine B reference were collected scanning from 560 nm to 650 nm using 540 nm excitation. The integrated fluorescence intensity versus optical density was fit to a gradient function (Grad). The following equation was used to calculate the quantum yield:

$$Q = Q_R \cdot \left(\frac{Grad}{Grad_R} \right) \cdot \frac{n^2}{n_R^2} \tag{3.2}$$

The Föster distance (R_0) for the fluorophore donor-acceptor pair of TAMRA and UA was calculated using the equation below:

$$R_0 = 0.211 \left[\frac{\kappa^2 \Phi_D J(\lambda)}{n^2} \right] \tag{3.3}$$

Where κ_2 is a constant related to the orientation of the transition dipoles of the donor and acceptor. Under normal circumstance, it is assumed to be 2/3. Φ_D is the quantum yield of the donor, n is the index of refraction of the solution, and $J(\lambda)$ is the overlap integral of the donor's emission spectrum, and the acceptor's absorbance spectrum and is equal to:

$$J(\lambda) = \int_0^\infty \varepsilon_A(\lambda) \lambda^4 F_{D(\lambda)} d\lambda \tag{3.4}$$

where $\varepsilon_A(\lambda)$ is the absorption spectrum of the acceptor in the unites of $M^{-1}cm^{-1}$. $F_D(\lambda)$ is the emission spectrum of the donor normalized to unit area. Using 540 nm excitation wavelength, the emission spectra of TAMRA labeled MSP was measured and then normalized to an area of 1. The absorbance spectra of UA labeled THD was measured and normalized to an extinction of 11,000 $M^{-1}cm^{-1}$ at 595 nm. The a/e-V-Vis-IR Spectral Software (www.fluortools.com) was used to calculate the overlap integral from the normalized spectra. Utilizing the above equations yielded an R_0 of 41 Å for the TAMRA-UA fluorophore

pair.

3.2.5 FRET based binding assay

The FRET based binding assay was using the same method described in chapter 1. Briefly, 5 μM of UA labeled THD or THD mutants were titrated into around 100 nM TAMRA labeled Nanodisc in cytoplasmic mimetic buffer at 20 °C. Samples were thoroughly mixed by gentle pipetting and allowed to equilibrate until the fluorescence intensities were stabilized for recording. FRET efficiency was calculated using the equation 2.3. Data was fit to equation 2.4 to derive F_{max} and dissociation constant assuming one THD bound per leaflet of Nanodisc. Lastly, F_{max} was used to calculated the saturated dye pair distance in following equation:

$$E_{FRET} = \frac{1}{1 + (r/R_0)^6} \tag{3.5}$$

Where E_{FRET} is the calculated maximum FRET efficiency. R_0 is the determined Föster distance of TAMRA and UA, which is 41 Å.

3.3 Results and Discussion

In last chapter, a FRET based THD binding assay was developed to measure the affinity of THD-Nanodisc complexes, where the TAMRA is specifically labeled on MSP D73C and a dark quencher UA is engineered on THD I398C site to avoid potential interference of the MOP and FAP region. Thus, by nature of FRET, the average donor-acceptor distances can be easily measured from the FRET efficiencies. The Föster distance of the TAMRA-UA pair was determined to be 41 Å. Figure 3.1 shows the calculated relation plot of the FRET efficiencies and dye pair distances of TAMRA-UA where the FRET efficiency is expected

to be greater than 10% for 60 Å and smaller than 95% for 30 Å making this dye pair ideal for measuring donor acceptor distances of the THD-Nanodisc binding geometries. The measured dye separation distances represent the spacing between the labeled residue on talin and position 73 on the MSP belt (Figure 2.5). Here, THD is assumed binding to both sides of the Nanodisc in any azimuthal orientation and thus the measured distance represents the average of all orientations in the complex.

3.3.1 Measurements of THD-Nanodisc binding geometry by FRET

Figure 3.2 summarizes the donor acceptor distances for all the phospholipids tested where the UA is labeled in position 398 of THD F3 domain. On bilayers with higher anionic lipid content, the donor acceptor distances become shorter. Due to the labeling position of the dye, the distance changes on different phospholipid bilayers suggest that increased anionic lipid composition induce a geometry of the complex in which the THD F3 domain is closer to the bilayer. Intriguingly, PIP2 favors this geometry at just 5% mole fraction in Nanodisc.

Although there is an obvious general trend of decreasing dye separation with increasing anionic lipids, the degree of the change differs with different anionic lipid headgroups. Comparing DMPS, DMPA, and DMPA membrane which all have identical formal charges, F3 domain is 5–8 Å closer on 50% DMPS than on 50% DMPA or 50% DMPG bilayers. Comparably, on 5% and 10% PI4P and PIP2 bilayers, the distances between THD F3 domain and Nanodiscs are 10 Å closer than that on 50% DMPA and 50% DMPG membranes.

The significant difference here between 50% DMPS, PI4P, PIP2 bilayers and 50% DMPG and 50% DMPA could be attributed to two main reasons. First is the charge localization on the lipid headgroups. PA and PG membranes carry the charge on the glycerophosphate, while PS, PI4P, and PIP2 membranes carry the negative charge on the headgroup residue. The bulky zwitterionic head group of the background DMPC may render the PA

and PG charge inaccessible to the protein. In the contrast, the charge of PS, PI4P, and PIP2 are more expose to the outer solvent environment. Secondly, PI4P and PIP2 lipids have a charge of -3 and -4 creating a much higher charge density in the binding site. Taken as a whole, there is a requirement for a high charge density and that the charge must be localized distal to the glycerol backbone to promote the proposed conformational change. 50% PS, 5% PI4P, 10% PI4P, 5% PIP2 and 10% PIP2 all fall in this category.

These results also provide experimental support for MD simulations that predict a significant conformational change in the THD upon engaging a negatively charged bilayer [44]. In the model, 5–10 Å downward movement of the F3 domain was observed after initiral docking of the MOP and promoted the interaction of K325 and K327 (K322 abd K324 in talin 1) with the surface of the membrane. Such conformational change could be crucial for optimal interaction with integrin tails.

It seems that when a bilayer has a high change density, either local or in bulk, and that the headgroup possess the negative charge, the THD F3 domain binds in a topology nearly 10 Å than when the charge is localized on the glycerolphosphate. In the case of DMPS, only 50% PS bilayers present a local charge density comparable to that of PI4P and PIP2 thus inducing the large change of THD F3 domain. It is interesting to note that the magnitude of the conformational change on 50% PS membranes is smaller than that seen on 10% PIP2. This data is in a great agreement with the hypothesis suggested by the MD simulation that the F3 conformational change were performed on pure PS membranes therefore presenting a much higher charge density than the tasted 50% PS membrane and may better represent the local charge density of PIP2.

To understand if these key differences are purely due to bilayer charge or if PIP2 is preferentially promoting a change in binding geometry, we have plotted the dye separation distance versus formal bilayer charge (Figure 3.3). Clearly, just 5% phosphatidylinositides presented in bilayer are more effective at altering the equilibrium of THD conformation

than PS, PA, or PG at the same degree of formal charge. This observation impicates the regulatory role of PIP2 in integrin activation. Although the physiological concentration of PIP2 in cell membrane is 1–2%, it is known that talin can bind, activate and recruit PIPKIγ to the sites of focal adhesion and potentially giving rise to an increase in the local PIP2 concentration [38, 39]. 50% PS may be physiologically irrelevant, the PIP2 concentrations used are directly applicable. It has been shown that roughly 80 phospholipids occupy one leaflet in a DMPC Nanodisc, 5% represents just four PIP2 lipids per leaflet. Therefore, THD is quite sensitive to the local concentration of PIP2. A modest elevaion of PIP2 at the sites of Focal Adhesions (FAs) can trigger this change in binding geometry. Our results are consistent the importance of the interaction of talin with PIPKIγ and production of PIP2 at the site of adhesion.

In order to validate that the FRET based binding assay is indeed probing a large conformational change in the F3 domain, another labeling site was engineered in position 201 (THD-201-UA) located on the opposite site of MOP residues of THD F2 domain. Inspection of the fluorophore separation distances by the FRET based binding assay shows that, when the F2 domain is labeled, the distances between the dye pair are greater than 55 Å on either PS or PIP2 membrane surface (Figure 3.4). This confirm the previous interpretation that the THD F2 domain provides the anchor point after initial contact and would remain at a nearly fixed distance from the bilayer surface, while the F3 domain starts with a further position and later recruits toward anionic lipid bilayer by PIP2. Actually, the small decreased dye separation distance seen on THD-201-UA binding to PIP2 can be interpreted as the burying of the MOP membrane anchor, a step that may be critical in triggering the F3 conformational change.

On examination of previous FRET results, the measured distance alterations on different lipid headgroups might also due to a shift in the docking of the THD on Nanodiscs. The favored interaction of F0 or F1 domain with certain type of bilayer surface may result in the

F3 domain hanging off the edge of the Nanodisc causing closer dye separation distance. To confirm that the measured changes are localized to F2F3 domain, same FRET based binding experiments on isolated F2F3 domain labeled at position 398 were performed. Figure 3.5 shows that the distance measurements on the full-length THD and truncated THD F2F3 domain are nearly identical under all condition tested. The removal of the F0F1 domain does not notably change the overall docking location of the THD F2F3 domain , which is consistent with hypothesis that the changes in FRET distances are a result in a change in the F2F3 binding topology instead of a docking position shift.

3.3.2 Mutagenesis investigation of THD MOP and FAP

A long-time unresolved question in talin mediated integrin activation is that how does a single point mutation in the F2 domain strongly prohibit the ability of THD to activate integrin? Previous simulation results have identified key residues in the F2 MOP and the F3 FAP that are important in triggering the conformational change. Closer examination of the simulation shows that the lysine residues on the F2 domain are proposed to snorkel into the anionic lipid bilayer, exposing a phenylalanine rich pocket that provides further stabilization of the bound complex as membrane anchors. The formation of the membrane anchor induces a large conformation change in the F3 domain, bringing it to the membrane surface. Early studies also show that single charge reversal mutations in the MOP or in the FAP significantly weaken the talin mediated integrin activation *in vivo* [6, 43, 98].

In order to investigate the functional role of the MOP and FAP residues, the charge reversal mutants of K274E in the F2 domain and K322E and K324E in the F3 domain were generated to ascertain the effects on the measured dy separation distances. In the FRET based binding assay, the affinities of THD-membrane binding were not significantly affected by the single charge reversal mutations (less than a factor of two, WT = 0.6 μM, K324E = 1.2 μM, K322E = 0.4 μM, K274E = 0.9 μM, and F259A/F280A = 0.7 μM), consistent

with membrane recruitment being driven by the overall electrostatics of the bilayer surfaces. However, measurements of the dye separation distance of the THD mutants labeled in the F3 domain are 10–15 Å greater than the WT THD/membrane complex (Figure 3.6). It points to a considerable conformational change of the mutants compared to wild type. Recent MD simulation, mentioned above, have suggested that the interactions of the F2 lysines with the membrane induce the exposure of a pair of membrane anchor formed by residue F259 and F280. To further test this hypothesis, the proposed membrane anchor residues F259 and F280 were mutated to Alanine (F259A, F280A) and performed FRET based binding assay. Once again, the mutations in the F2 domain resulted in a longer donoracceptor distance in the bound complex.

All of the MOP and FAP mutants exert only a modest change in dissociation constant, increasing by no more than a factor of two. This result indicates that the remaining positive charges provide a significant portion of the overall free energy of association. Although the affinities are minimally affected, the lysine to glutamate mutations at positions 322, 324, and 274 significantly alter the conformation of the THD bilayer complex. This phenomenon can be explained in two ways. Firstly, the clash of the negatively charged glutamates at position 322 and 324 with the negatively charged bilayer does not allow the close association of the F3 domain. Secondly, K274E plays a pivot role in the snorkeling that is required to open up the membrane anchor pocket. Mutation at this position inhibits the trigger of the large conformational change. Similarly, alanine mutations of the phenylalanine residues implicated in the formation of the membrane anchor, once again, fail to trigger the change of binding geometry, and the F3 domain remains 10 Å further from the bilayer surface. It is important to note that the F259A/F280A mutant presumably has the same electrostatic interactions as the wild-type yet, the conformational change is inhibited. The correlation of the measured complex geometry and the ability of the mutant THD to activate integrin provide evidence that the conformational dynamics of the THD may play a significant role

in integrin activation.

3.4 Conclusions

In this chapter, measurements of the dye separation distance of the THD Nanodiscs complex were performed. Results suggest a rich interplay between electrostatics and conformational equilibrium during the talin FERM domain binding to phospholipid bilayers. THD binds to anionic bilayers with relative high affinity regardless of the identity of anionic lipid headgroup providing the charge. It is only when the bilayer provides a high charge density and the charge is localized on the headgroup does the F3 domain approach the bilayer surface in a confirmation conducive interacting with integrin cytoplasmic tails. Phosphatidylinositides provide the perfect scaffold for promoting the proposed conformational change, thus potentially implicating PIP2 and THD conformational dynamics in a regulatory role during talin mediated integrin activation. THD F3 undergoes a large conformational change in the process of talin recruitment, triggered by MOP residues and a pair of phenylalanine membrane anchors in F2 domain. Figure 3.7 depicts a schematic representation of the mechanism of this lipid headgroup induced change of binding topology.

3.5 Figures

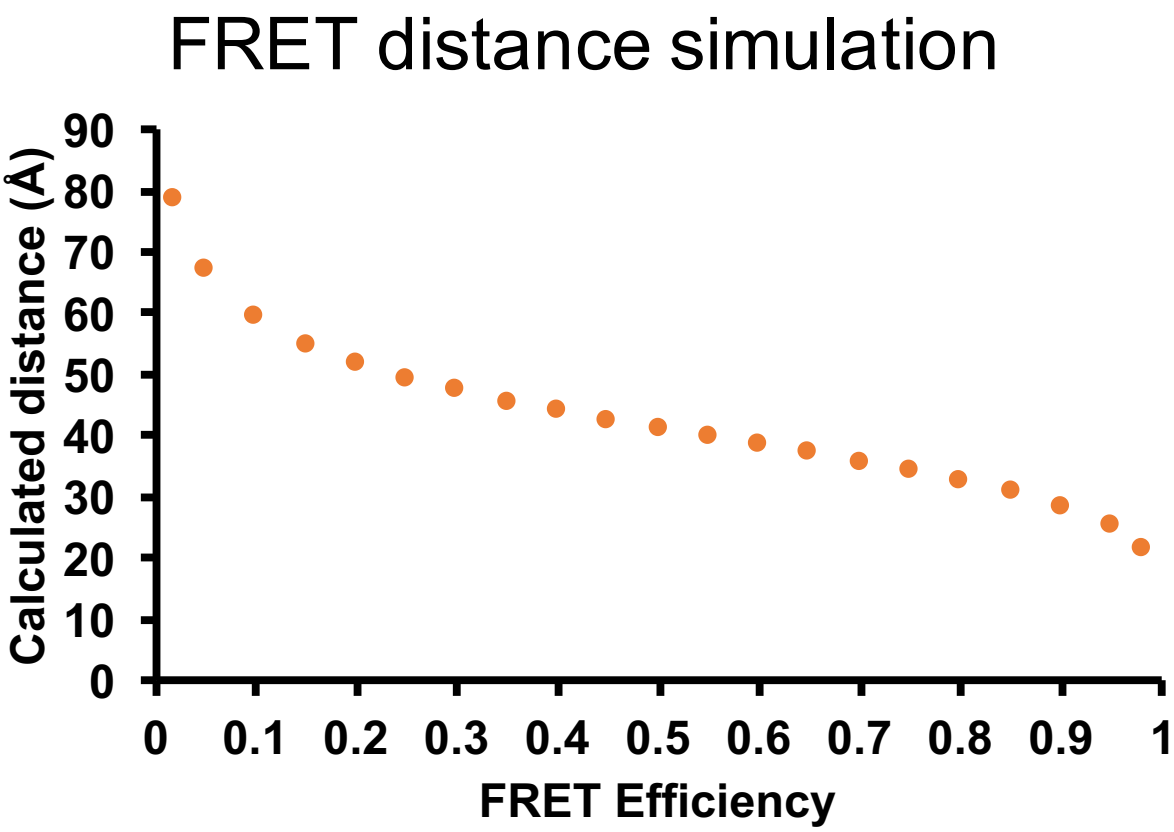

Figure 3.1: The plot shows the theoretical FRET distance calculation from a dye pair that has a Föster distance of 41 Å.

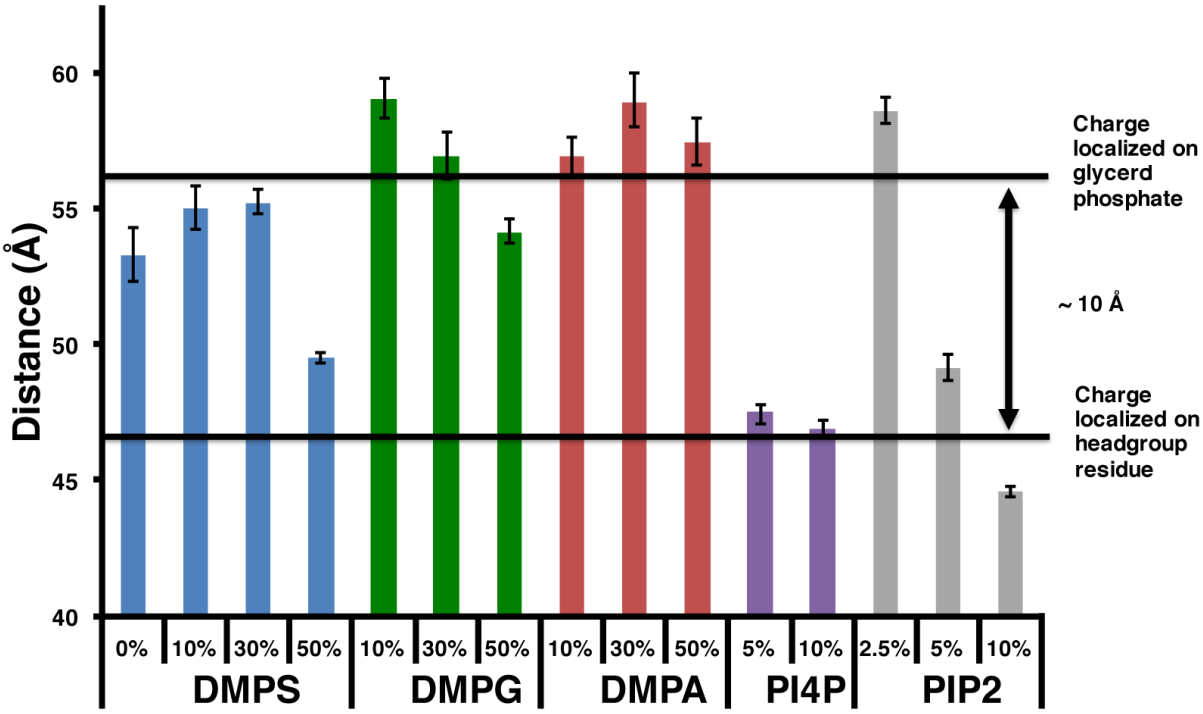

Figure 3.2: Dye separation distances of I398C labeled talin binding to bilayers containing anionic lipids. Distances are calculated from the F_{max} determined from the fitting of the binding isotherms. The error bars represent the standard deviation of a minimum of three trials.

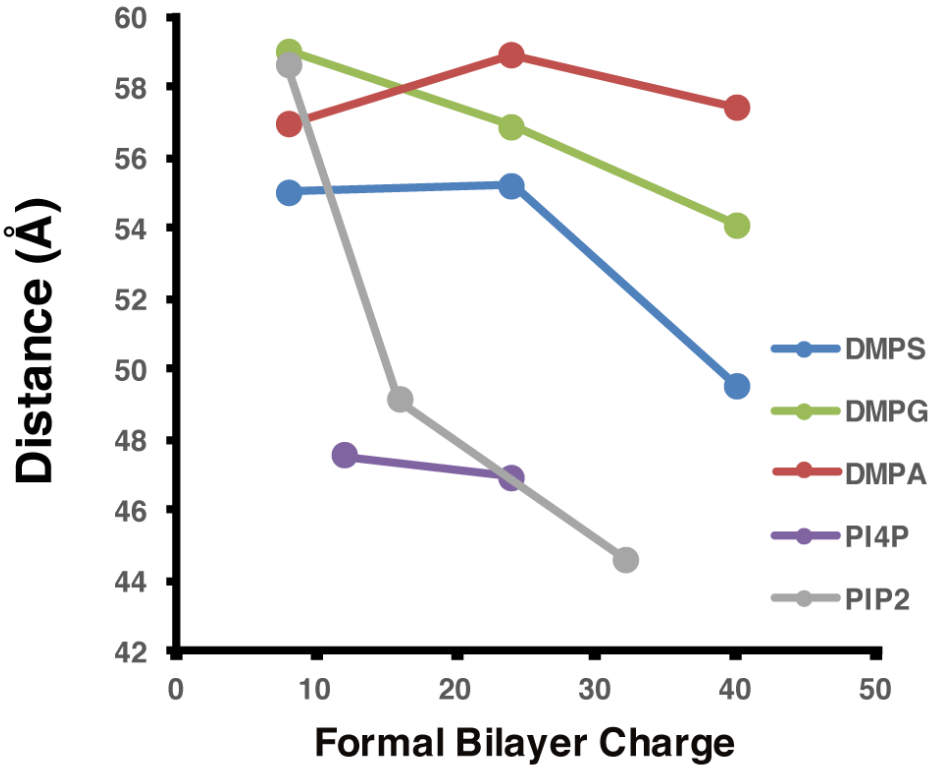

Figure 3.3: Dye separation distance of THD bound to DMPS, DMPG, DMPA, PI4P and PIP2 versus formal bilayer charge.

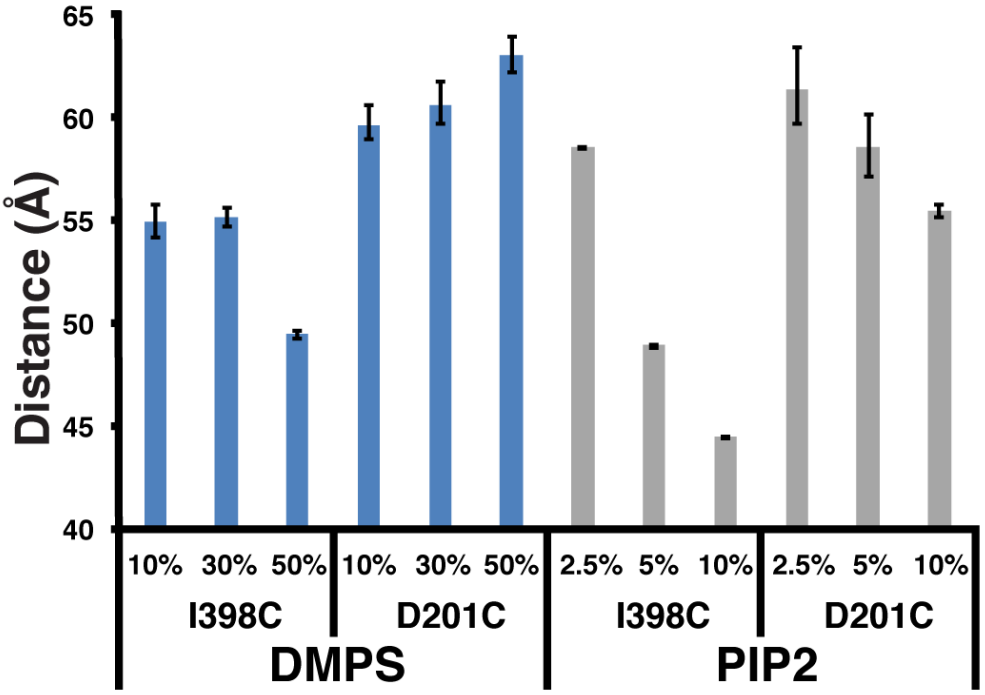

Figure 3.4: Comparison the dye separation distances of THD I398C and D201C labeling sites. The error bars represent the standard deviation of a minimum of three trials.

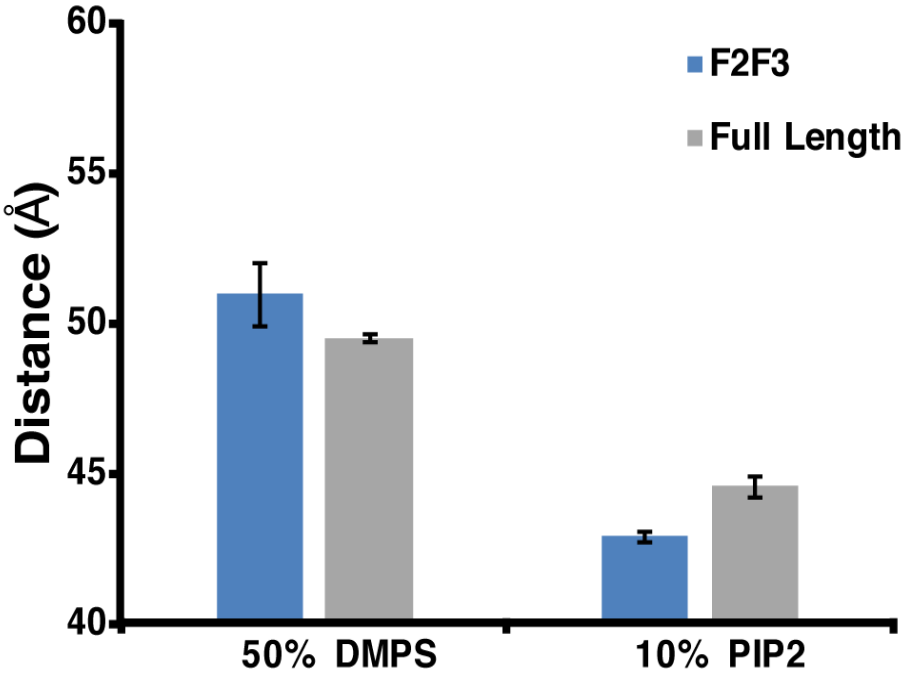

Figure 3.5: Comparison of the dye separation distances of THD F2F3 and full-length THD on Nanodiscs. The error bars represent the standard deviation of a minimum of three trials.

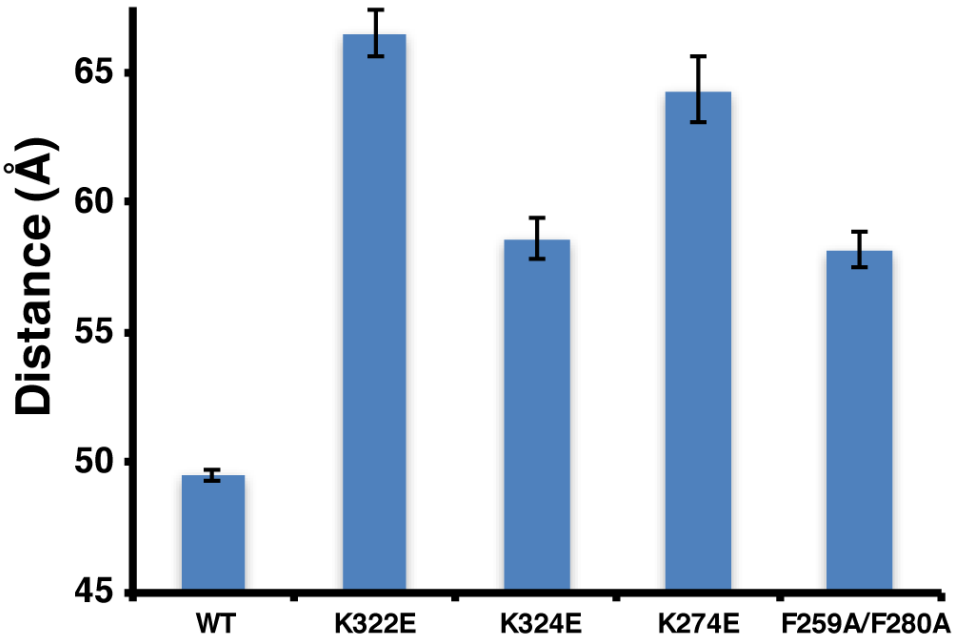

Figure 3.6: Effect of FAP and MOP mutants on the dye separation distances. Error bars represent the standard deviation of a minimum of three trials.

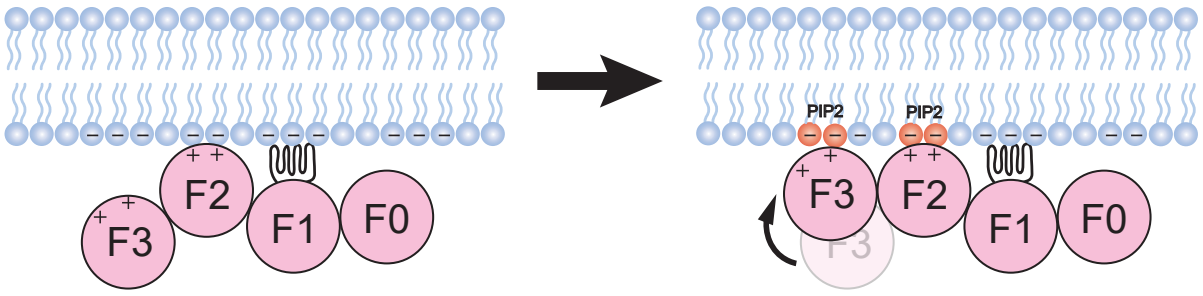

Figure 3.7: Regulation of THD conformation by PIP2. The presence of PIP2 in a bilayer promotes the conformational change that allows simultaneous interaction of F2 and F3 domains with the membrane surface.

CHAPTER 4

CHARACTERIZATION OF TALIN HEAD MEMBRANE ANCHOR

4.1 Introduction

For many membrane peripheral proteins, the insertion of hydrophobic anchors into the membrane's acyl chain core offers a crucial stabilization force for the membrane bound forms [177, 178]. Even though the electrostatic attractions provide the overall free energy of peripheral proteins binding to the membrane, water and metal ions in cytoplasmic solution can readily displace such electrostatic interactions. Thus, insertion of hydrophobic membrane anchor and general electrostatic engagements often work in orchestra for complete strong binding of peripheral proteins to the membrane.

Early experimental studies have predicted the existence of the hydrophobic anchor in talin [179, 180, 181]. However, the detail description and mechanism of the membrane anchor, which could be important to understanding the talin membrane recruitment and integrin signaling, has remain elusive to both biochemical and structural studies. The major hurdle is the difficulties in fully interrogating a membrane bound protein in its native environment. Another main reason that hampers further study of the membrane anchor is no apparent membrane anchor observed in the crystallographically determined structure of talin F2F3. Large conformational change may require to uncover the suggested hidden membrane anchors. Opposing to that, many other peripheral proteins, such as Ras family proteins and blood coagulation factors, possess obviously exposed hydrophobic anchors or lapidated domains that readily insert into the membrane [182, 183, 184].

A recent Molecular Dynamic (MD) simulation performed by Arcario *et al.* utilizes highly mobile membrane mimetic (HMMM) model to expedite the diffusion of lipid molecules [44]. In HMMM simulation, the full-length lipid bilayers are replaced by short tail lipids at the interface of an aqueous-organic biphasic system that allow shorter simulation time to observe lipid reorganization and protein insertion compared to conventional lipid setting. The simulation identified two connected conformational changes of talin FERM domain that contribute to membrane anchoring when THD approaches the surface of the membrane. First is the snorkeling of lysine residues of F2 domain (MOP) that drags the protein deeper into membrane. The protein local side chain rearrangement allows the secondary insertion of a phenylalanine rich membrane anchor which is originally buried within the protein and flips down into the membrane core. The snorkeling basic residues in the F2 domain may offer some stabilization to the membrane bound talin FERM. The inserted phenylalanine pair (F259 and F280 in talin 1) is expected to provide the majority of hydrophobic stabilization. Although another recent simulation fails to observe the same membrane anchor insertion [168].

In this chapter, MSP was engineered to remove all tryptophan residues in order to avoid fluorescence interference. The "dark" Nanodisc was assembled to provide precise lipid composition control and native membrane environment. Thus, mutagenesis study at proposed membrane anchor sites allow the visualization of side chain insertion upon binding of the Nanodisc by observing the emission spectrum shift of protein native tryptophan, which is sensitive to its polar environment. The result here shows the first experimental evidence of the existence of membrane anchor in talin FERM domain that inserts into membrane hydrophobic core.

4.2 Experimental Methods

4.2.1 Materials

DMPC, DMPS, and PIP2 were purchased from Avanti Polar Lipids (Alabaster, AL). *E.coli* BL21 DE3 and *E.coli* BL21 DE3 gold were purchased from Stratagene (San Diego, CA). Competent cells of NEB Turbo *E.coli* and Gibson assembly master mix were obtained from New England Biolabs (Ipswich, MA). iProof polymerase kit was purchased from BioRad (Hercules, CA). Uniblue A (UA), Amberlite XAD-2 beads, and sodium cholate obtained from Sigma-Aldrich (St. Louis, MO). Tetramethylrhodamine-5 (and -6) C2 maleimide (TAMRA) was obtained from Anaspec (Fremont, CA).

4.2.2 Preparation of dark Nanodiscs

The expression vector of non-tryptophan MSP was generated by DNA synthesis and Gibson assembly method. The DNA fragments were designed to contain about 10-15 base pair overlap with adjacent DNA sequence. Before the assembly reaction, plasmid backbone pET28A were digested by restricted enzyme NcoI and HindIII and purified by QIAquick PCR purification kit (QIAGEN, Valencia, CA) to create the sticky ends. To start the Gibson assembly, the digested pET28a plasmid and designed MSP DNA segments were mixed with a cocktail of three enzymes, including exonuclease, polymerase, DNA ligase, and other buffer components provided by the commercial available kit (New England Biolabs, Ipswich, MA). The exonuclease is responsible for creating 3' overhangs that allow the annealing of segments shared with complementarity overlap regions. Then the polymerase incorporates nucleotides to fill in the gaps between any annealed fragments. The DNA ligase removes any nicks in the assembled DNA.

The assembled DNA product was transferred into NEB turbo competent cells for am-

plification and purification. DNA sequence validation was performed by by ACGT (Northbrook, IL) using a T7 promoter primer. The expression and purification protocol of MSP was previously described [158, 159]. Concentration of the protein was determined using extinction coefficient 10.94 $mM^{-1}cm^{-1}$ at 276 nm wavelength. The Nanodiscs reconstitution was performed as described in chapter 2.

4.2.3 THD membrane anchor mutagenesis and preparation

THD F2F3 F259W, THD F2F3 F280W, THD F2F3 F259W I398C, THD F2F3 F280W I398C, and THD F2F3 F259W F280W with or without I398C mutation were generated by using pET30A-F2F3 or pET30-F2F3 I398C as the PCR template and designed primers for the phenylalanine to tryptophan mutation (F259W Forward: 5'- GCA CAA GGC TGG CGC ACT TGA CCT CAA GGA CTT CCT GCC -3'; F259W Reverse: 5'- GGC AGG AAG TCC TTG AGG TCA AGT GCG CCA GCC TTG TGC -3'; F280W Forward: 5'- GAA GGG AGA GCG TAA GAT ATG GCA GGC ACA CAA GAA TTG -3'; F280W Reverse: 5'- CAA TTC TTG TGT GCC TGC CAT ATC TTA CGC TCT CCC TTC -3'). Silent mutations were engineered in the primers to eliminate XmnI and BglII restricted digestion sites from F259W and F280W reaction for subsequent examination.

The detailed PCR reaction settings and parameters can be referred to chapter 2. All PCR products were digested with DpnI for 4 hours at room temperature. NEB turbo competent cells were used to amplify and extract recombinant plasmid. All miniprep samples were subject to digestion by XmnI or BglII and visualize by agarose electrophoresis. Samples, that were not cleaved by restricted enzyme, were sent for DNA sequence validation by ACGT (Northbrook, IL) using a T7 promoter primer.

4.2.4 FRET based binding assay

The UA labeled THD and TAMRA labeled Nanodiscs were prepared as described in previous chapter. Detail protocol of the fluorescence titration can be found in chapter 2.

4.2.5 Label free tryptophan fluorescence binding assay

The label free tryptophan fluorescence assay was developed to visualize the hydrophobic change of tryptophan environment. The fluorescence binding experiments were performed in a ISS K2 multi-frequency cross correlation phase and modulation fluorometer connected with a circulating water bath for temperature control at 20 °C. An excitation wavelength of 295 nm and 8 nm bandwidth for both excitation and emission were used for all experiments.

The binding assays started by adding 5 μM dark Nanodiscs in a 1 mL solution containing 20 mM HEPES pH 7.2, 4 mM KH_2PO_4, 125 mM KCl, 14 mM NaCl, 1mM $MgCl_2$, 0.02 mM EGTA to mimic cytoplasmic environment. The Nanodiscs containing buffer was equally split into two fluorescence cuvettes followed by adding 5 μM THD F2F3 wild type or mutants into one cuvette and same volume of cytoplasmic buffer into the other one as the reference. Then the binding samples and blanks were incubated at 20 °C for 10 minutes with gentle stirring. The final emission spectra were obtained by scanning from 310 nm to 410 nm in 1 nm/second rate. The data were imported into Vinci software to perform spectrum manipulations for blank subtraction and normalization.

4.3 Results and Discussion

4.3.1 Tryptophan mutations do not perturb THD membrane binding

To visualize the membrane anchor insertion, F280 and F259 were mutated into tryptophan for two rationales. Firstly, the structures of the two amino acids are very similar

that both possess an aromatic residue allowing hydrophobic interactions with lipid bilayer, although the tryptophan side chain is slightly less hydrophobic than phenylalanine. The second reason is that tryptophan fluorescence is sensitive to its polar environment. Using the tryptophan fluorescence maximum information, a tryptophan can be assigned as buried and in a hydrophobic environment if the peak of emission is near 330 nm; A tryptophan in more polar environment can induce a longer maximum wavelength, which is commonly used to imply side chain solvent exposure in protein.

In chapter 3, alanine mutations at F259 and F280 in the talin F2 significantly impede the F3 domain conformational change to the membrane in a preferable geometry for integrin interaction. In order to assess the effects of mutating phenylalanine to tryptophan on talin FERM domain functions, FRET based binding assay was performed with UA labeled F2F3 phenylalanine mutants on 5% PIP2 and 50% DMPS Nanodiscs. Figure 4.1 shows the results of the FRET titration experiments on 5% PIP2 Nanodisc. Only modest effects on dissociation constant were detected. The biggest change observed with F2F3 F259W is less than a factor of two compared to wild type THD and the dissociation constant remains at a dissociation constant of 0.89 μM in a tight binding range. Similar results were also obtained with 50% DMPS Nanodiscs (Data not show). Substitutions of phenylalanine with tryptophan do not noticeably alter the affinity between THD F2F3 and anionic membrane surfaces. This result fits to the previously suggested model that the general electrostatic attraction governs the talin FERM binding to membrane and the lysine residues in F2 MOP and FAP are the major interface.

Moreover, calculation of the FRET donor-acceptor distance reveal a unchanged dye separation of THD F2F3 phenylalanine mutants binding to lipid bilayers containing PIP2 (Figure 4.1 bottom panel). The F2F3 F280W mutant gives rise to the biggest increase of FRET pair distance, which is less than 0.2 nm longer than that of wild type F2F3. The phenylalanine mutations at F280 and F259 do not perturb the MOP residues inducing

the subsequent large F3 conformational change. Thus, the mutants are suitable to further investigate the membrane anchor insertion.

4.3.2 F259W inserts into lipid bilayer upon talin membrane binding

The original membrane scaffold protein (MSP) used in previous chapter for FRET based binding assay contains two native tryptophan that may interfere the detection of membrane anchor insertion. Figure 4.2 shows that MSP structure and each MSP possess two tryptophan, four tyrosine, and four phenylalanine. To exclusively measure the environmental change of talin tryptophan, all MSP tryptophan were mutated into phenylalanine by Gibson assembly method with designed MSP DNA segments containing desire mutated codons.

Figure 4.3 presents the comparison of the size exclusion chromatography traces from Nanodiscs prepared by regular MSP or tryptophan mutated MSP. The identical retention time of the absorbance peak at 280 nm indicates that homogeneous Nanodiscs were produced by both versions of MSP. Thus, alanine mutations at tryptophan sites in MSP do not perturb the assembly process of the Nanodiscs.

In order to determine the solvent exposure of the tryptophan in THD wild type and mutants, 5 μM protein were dissolved in cytoplasmic mimic environment and excited with 295 nm wavelength. The 295 nm excitation wavelength was selected to minimize the fluorescence from tyrosine due to the fact that its significantly absorbsance from 250 to 295 nm and emission from 280 to 350 nm.

Figure 4.4 is the crystallographic structure of talin F2F3 generated from the previously reported linear talin FERM domain structure (PDB: 3IVF). Two tryptophan residues can be found and are buried in talin F3 domain. This is in a great agreement with the normalized emission scanning results (Figure 4.5), where the maximum emission is detected at 330 nm. Mutating phenylalanine into tryptophan induces a slightly red shift of the emission spectra, and double mutation further promote a larger peak wavelength at about 350 nm. The result

here implicates that F259 and F280 are semi-exposed to the solvent environment, that allow them to readily flip down and insert into lipid bilayer.

To investigate the membrane anchor insertion upon binding to membrane, 5 μM THD F2F3 mutants, which is roughly ten times more than the determined dissociation constant to ensure completed binding, were incubated with 5 μM neutral or negatively charged Nanodiscs. Interestingly, the emission spectrum of F259W binding to 50% DMPS noticeably shifts to 330 nm maximum compared to protein alone. On the other hand, interactions of F280W and anionic lipid membrane yields a slightly red shifted emission spectrum (Figure 4.6). It should be noted that both THD mutants bind to the 50% DMPS with similar dissociation constants (Figure 4.1) and thus the shift is specific to side chain membrane insertion rather than the difference in binding strength.

A closer exanimate on the simulation result of Arcario *et al.* may provide a plausible explanation to the difference between the two sites. In their simulation, although both F259 (F261 in talin 2) and F280 (F281 in talin 2), induced by the lysine snorkeling and local side chain rearrangement, insert into the membrane but the depths of insertion are distinctive. The F259 residue penetrate deeper into the hydrophobic acyl chain layer comparing to the charged lipid headgroup where the F280 stays. It is also possible that only F259 exerts as the membrane anchor and inserts into membrane, and the local conformational change provides larger solvent exposure for F280. Another observation for membrane anchor insertion is the require of negatively charged membrane surface. Neither of the mutants show significant shift on the neutral DMPC Nanodisc. This could be explained by the lack of MOP lysine snorkeling, which requires high formal negatively charge and is prerequisite for subsequent local side chain reorganization. And those motions are critical to trigger buried phenylalanine flipping down and provide stabilization force for membrane bound talin FERM domain.

4.4 Conclusions

To summarize this chapter, a label free fluorescence assay was developed to probe the hydrophobic environment of protein tryptophan. To eliminate the interference from Nanodisc, the membrane scaffold protein used for assembly was engineered to contain no tryptophan residues. Previous proposed membrane anchor sites in talin F2 domain were mutated into tryptophan to further investigate the insertion of those side chains. The result of FRET based binding assay suggests that those mutations do not perturb the talin membrane interactions and F3 conformational change. The emission spectra scan for talin F2F3 Nanodisc complexes indicates that the initial buried F259 flips down into the membrane. It is still not clear whether F280 would provide stabilizing force by inserting into membrane or remain in protein hydrophobic pocket. It is nevertheless that talin could interplay with lipid bilayer by additional hydrophobic force but solely rely on electrostatic attraction.

4.5 Figures

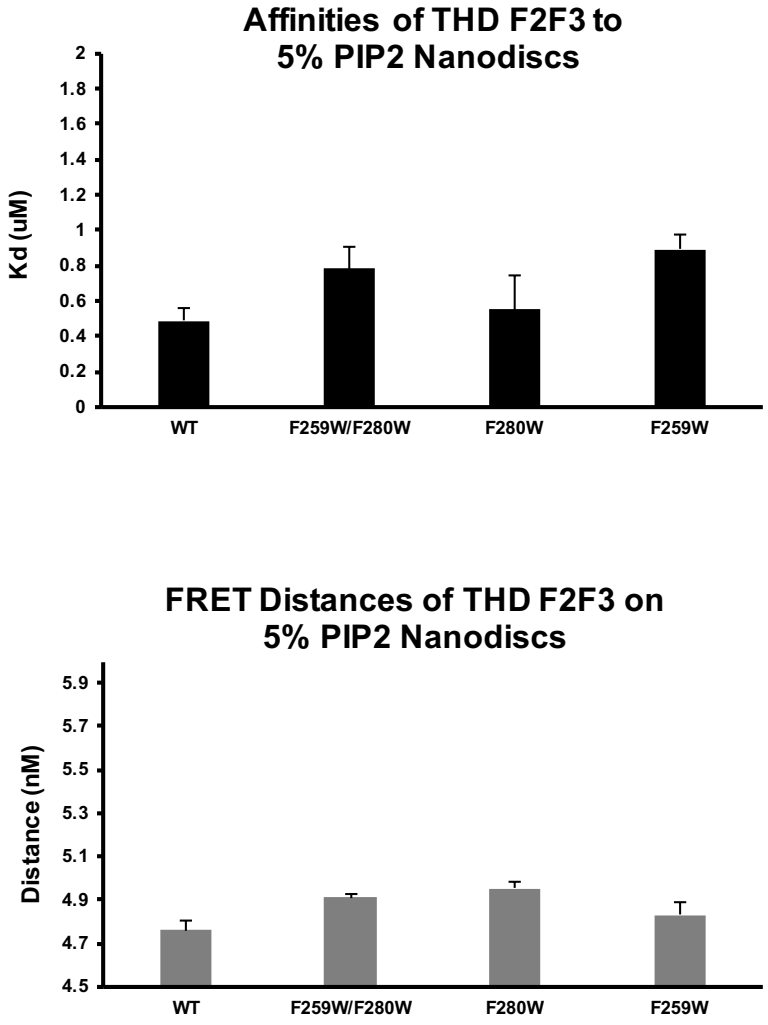

Figure 4.1: Comparisons of THD and THD mutants binding to 5% PIP2 Nanodiscs in dissociation constants and FRET pair distance.

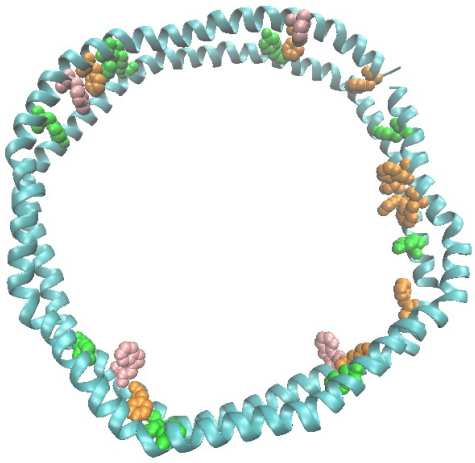

Figure 4.2: The structure of MSP. Each MSP contains two tryptophan (pink), four tryosine (green), and four phenylalanine (orange).

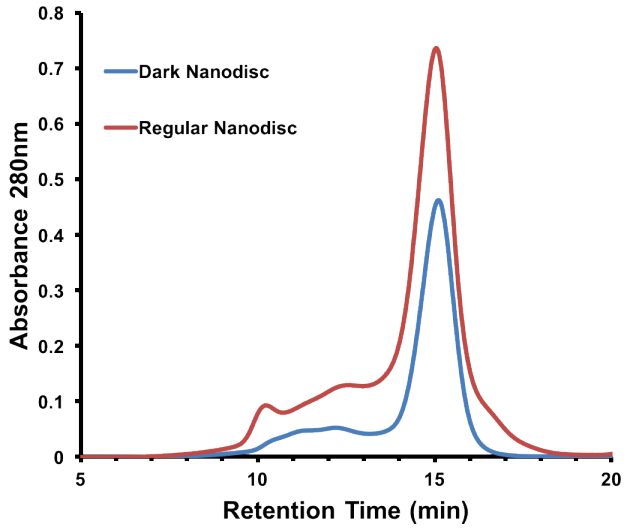

Figure 4.3: The structure of MSP. Each MSP contains two tryptophan (pink), four tryosine (green), and four phenylalanine (orange).

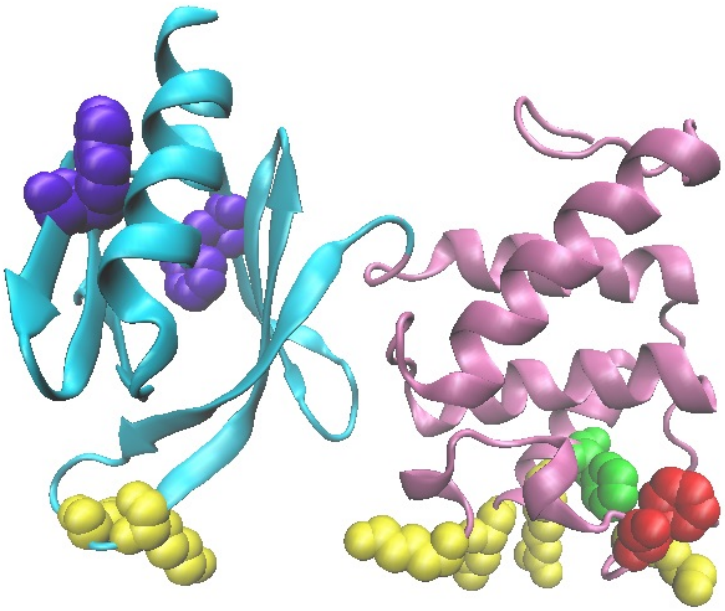

Figure 4.4: The structure of talin F2F3 domain. THD F2 domain is labeled in pink. The F3 is depicted in cyan. The yellow side chains are MOP and FAP residues. Native tryptophan residues are buried in F3 domain and labeled in navy. F259W and F280W are labled in green and red, respectively.

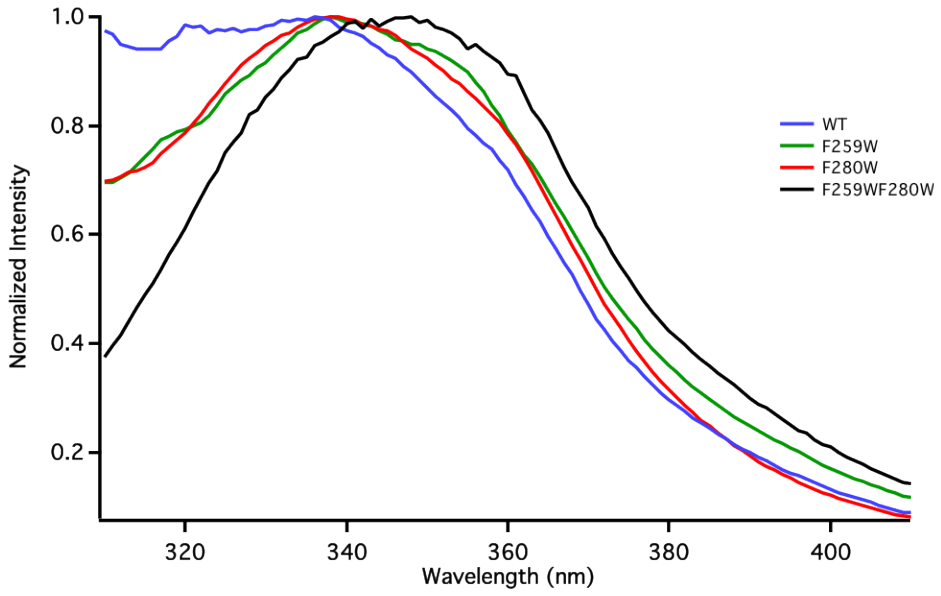

Figure 4.5: The normalized emission spectra of THD F2F3 wild type and tryptophan mutants. Tryptophan mutation of F259 and F280 induce a red shift.

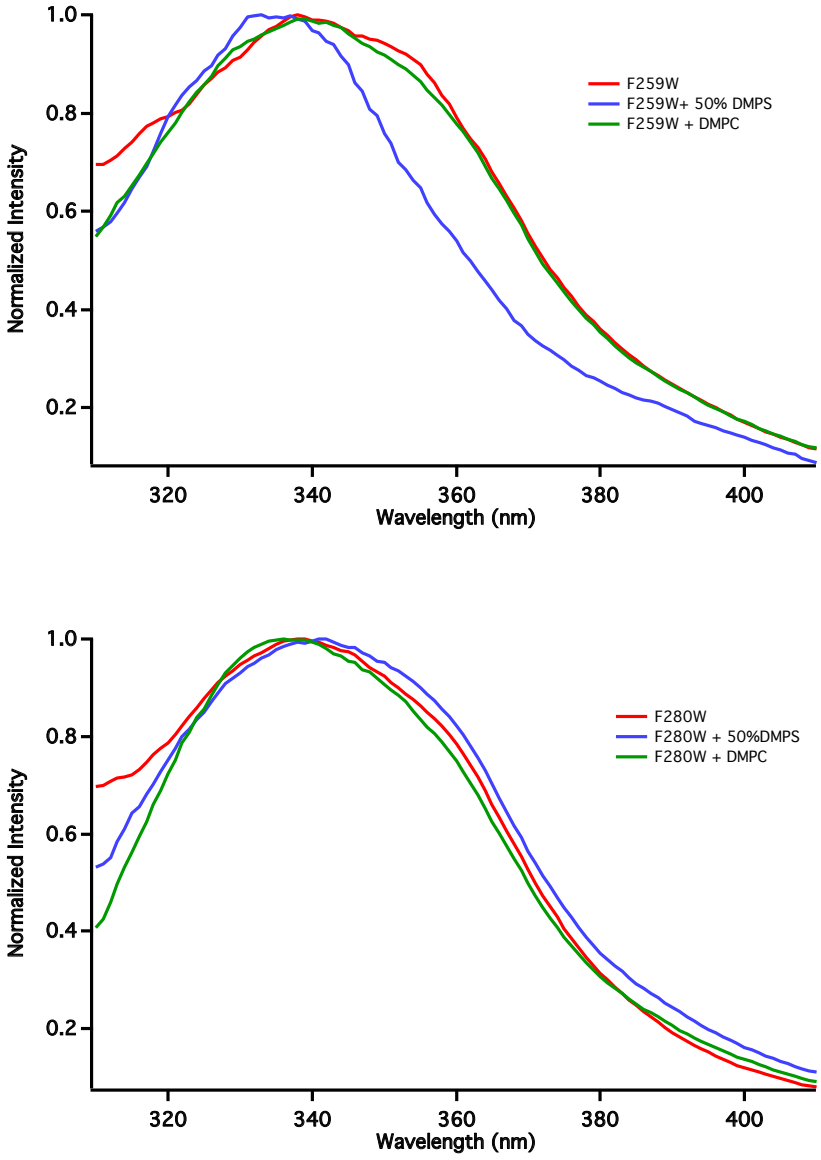

Figure 4.6: The normalized emission spectra of THD F2F3 Nanodisc complexes.

CHAPTER 5

TALIN AUTO-INHIBITION AND ACTIVATION BY PIP2

5.1 Introduction

Talin adopts an auto-inhibited conformation, where the talin rod packs against the talin FERM domain and inhibits its approach to the phospholipid bilayers [97, 98, 100, 102]. Figure 5.1 shows that the talin rod domain consists of 13 helical bundles, R1-R13, and an N-terminal dimerization sequence [102]. Some of the subdomains of talin rod have identified as the binding site of many other cytoplasmic proteins, such as vinculin and actin, making a central hub of protein-protein interaction between transmembrane receptors and cytoskeleton [10, 50, 51, 54]. Previous structural and NMR studies indicates that segments R1R2, R9, and R12R13 are the subdomains in the talin rod that bind to the FERM domain (Figure 5.2), masking the PTB binding site within the F2F3 subdomains [97, 98, 99, 102]. In addition, Goult *et al.* report that full-length talin exists as a "donut" shape dimer structure where rod helical bundles encircle the FERM domain as the auto-inhibited conformation [102]. Several pathways have been identified to disrupt the talin head-rod interactions. Major routes include the interaction of complexes of Rap1-RIAM [47, 49], talin linker specific cleavage by calpain [35, 45, 106], and binding of PIPKIγ [40, 38, 154], which subsequently gnereates PIP2 form PI4P [185]. The protein-protein interactions of talin activation have been extensively explored, yet the detail lipid-protein interactions of the process remain elusive.

In the plasma membrane, PIP2 only comprises a small fraction (1-2%) of the total phospholipid and is evenly distributed throughout the membrane [186]. PIP2 has been

recognized as an indispensable messenger molecule and plays an important role in focal adhesion assembly [187, 188]. Multiple allosteric regulation mechanisms have been shown to relied on the presence of PIP2. For instance, vinculin is expressed in a closed, inactive conformation in the cytosol. PIP2 binding to the regulatory site of the vinculin tail domain opens up the self-inhibitory form [12]. PIP2 is also crucial for FAK regulation through interactions with the positive charge patch in the F2 subdomain of the FAK FERM domain, resulting in release of the auto-inhibited conformation [189].

In previous chapters as well as early study, it has been shown that the affinity of THD for lipid bilayers is mainly controlled by overall formal membrane charge [72], the presence of PIP2 facilitates talin membrane localization [20]. Recent studies show that talin binds to various phosphatidylinositides and hypothesis that PIP2 plays a role in disrupting the head to rod domain interactions that are important in maintaining talin auto-inhibited conformation [72, 99]. Furthermore, PIP2 was found playing a role in the talin mediated integrin activation and clustering [154]. The recruitment of PIPKIγ is responsible for converting PI4P into PIP2 and well correlate with the enrichment of local concentration of PIP2 at focal adhesion site [185]. Specific deletion of PIPKIγ in focal adhesion could remarkably reduce the talin localization to membrane and adhesion sites. Other biophysics measurements, such as SPR and NMR, demonstrate that several residues in talin F2F3 domain binds to PIP2, and soluble C4- or C8-PIP2 disrupts the THD/R9 interactions. A recent research hypothesis a push-pull mechanism model for talin activation as the high charge density of PIP2 headgroup pulling THD to the bilayer surface, in the meanwhile pushing away talin R9 domain [99].

In this chapter, affinities of the THD towards various phospholipid bilayers were examined utilizing Nanodisc technology to provide native membrane environment. To investigate the role of PIP2 during the activation process of the auto-inhibited talin, FRET based binding assay was used to measure the inhibition of THD-Nanodisc association in the presence of purified rod domain segments. Results show that THD is insensitive to the inhibitory

effect by talin rod subdomains, which strongly inhibit THD binding to other anionic lipid bilayers. In addition, the interface of activating auto-inhibited talin between PIP2 and THD is located within talin F2F3 domain.

5.2 Experimental Methods

5.2.1 Materials

DMPC, DMPS, DMPG, DMPA, PI4P, and PIP2 were purchased from Avanti Polar Lipids (Alabaster, AL). *E.coli* BL21 DE3 and *E.coli* BL21 DE3 gold were purchased from Stratagene. Competent cells of NEB Turbo *E.coli* were obtained from New England Biolabs (Ipswich, MA). Tetramethylrhodamine-5 (and -6) C2 maleimide (TAMRA) was obtained from Anaspec (Fremont, CA). iProof polymerase kit was purchased from BioRad (Hercules, CA). Uniblue A (UA), Amberlite XAD-2 beads, and sodium cholate obtained from Sigma-Aldrich (St. Louis, MO).

5.2.2 Preparation of talin rod subdomains

THD R1R2 (482-786), R9 (1654-1848), and R12R13 (2225-2234) was generated by using pET28A full-length talin as the template and designed primers for the truncated talin rod domains (R9 Forward: 5'- AGA CAT ATG GCT CCA GGG CAG CTG GAG -3'; R9 Reverse: 5'- GCC TCG AGA CCT TCT GGT TCA CCC ATT G -3'; R12R13 Forward: 5'- GCG CAT ATG CAC CCA GAA GTG G -3'; R12R13 Reverse: 5'- GCA CTC GAG CTG CTC CTC AAA GTT C -3'; R1R2 Forward: 5'- AT AT AT CAT ATG CGA GGA CAC ATG CCT CCT CTG -3'; R1R2 Reverse: 5'- AT AT AT CTC GAG TTT CAC ATG CTG CAG CAG CTC -3'.). The PCR reaction parameter and setup are similar as described in Chapter 1using iProof polymerase and 60 seconds for extension. All PCR

products were visualized by agarose gel electrophoresis and then purified by QIAquick gel extraction kit (QIAGEN, Valencia, CA) followed by digestion of Xho I and Nde I for 4 hours at room temperature. The digested produce was purified by QIAquick PCR purification kit (QIAGEN, Valencia, CA) and mixed with pET30A backbone in the ratio of 3:1 of insert to vector. The ligation reaction was performed at room temperature over night with T4 ligase (New England Biolabs, Ipswich, MA). The ligation product was enriched by transforming into NEB turbo competent cells and plasmid extraction. The recombinant plasmid constructs were send for DNA sequence validation by ACGT (Northbrook, IL) using a T7 promoter primer.

The protocol for THD rod purification is adapted from chapter 2. In brief, the seqeuce verified expression vectors were transformed into the *E. coli* BL21 Gold (DE3). 50 mL starting culture was prepared for each rod subdomains and then inoculated to 1 L in a ratio of 1:100. Typically, 4 L of cell culture for each talin rod subdomains were cultivated at 37 °C with shaking at 250 RPM followed by IPTG induction and additional 4-hour incubation. Cell pellet was harvested by centrifugation at 8,000 RPM for 10 minutes at 4 °C.

Purification started with preparation of cell supernatant by suspension, sonication, and ultracentrifugation at 30,000 RPM 4 °C for 45 minutes. Then the cell supernatant was purified by loading onto a Ni (II)-chelating Sepharose fast flow column. The talin rod proteins were eluted by 500 mM imidazole and dialysised against 8,000,000 volumes of cytoplasmic mimetic buffer (20 mM HEPES pH 7.2, 4 mM KH_2PO_4, 125 mM KCl, 14 mM NaCl, 1mM $MgCl_2$, 0.02 mM EGTA).

5.2.3 FRET based binding assay

The TAMRA labeled Nanodiscs and UA labeled THD were prepared as described in chapter 2. To start the FRET based titration, designated concentrations of talin rod subdomains were mixed with 100 nM Nanodisc in order to evaluate the inhibitory effect on

THD-membrane interactions. Other detailed parameters and setup of FRET based binding assay can be found in the method section of chapter 2.

5.3 Results and Discussion

5.3.1 Talin rod subdomains inhibit THD binding to anionic lipid bilayers

In order to understand the interplay of protein-protein and membrane-protein interactions in the regulation of talin auto-inhibition, Nanodiscs is used to provide a defined lipid composition membrane. Goksoy *et al.* first identified a middle segment of talin rod, spanning from 1654 to 2344 residues, masks the integrin tail binding site in the talin FERM domain [97]. It has been further narrowed down by a later study that indeed talin R9 (1655-1822) binds to F3 of the THD and compete with the β3-integrin cytoplasmic tail for interaction of THD. Vesicles consisting of a mixture PC and PIP2 disturb such interaction [98]. Talin R12R13 (2225-2344) is also recognized as a potential THD inhibitory rod subdomain albeit with a weaker affinity to talin F3 domain compared to R9. In this work, the inhibitory effects of talin rod domain on THD binding to anionic lipid bilayer were directly measured using the FRET based binding assay.

Figure 5.3 shows the binding isotherms of labeled THD titrating into TMARA labeled Nanodiscs containing 50% DMPC in the presence of talin R9 and R12R13. Table 5.1 summarizes the dissociation constants obtained from further data analysis in Matlab software. In the presence of 0.5 μM talin rod subdomains, THD binds to 50% DMPS Nanodiscs with a dissociation constant of 1.6 μM, which increases three fold compared to the titration in the absence of any inhibitory domains. The dissociation constants further increase with higher concentrations of talin R9 and R12R13. At 32 μM of talin inhibitory domains, the interactions of THD with Nanodiscs are nearly abrogated. A cell membrane typically contains only

about 20% PS and it is the most abundant anionic lipid headgroup, yet no talin activation effect on 50% PS Nanodiscs was observed. The local concentration of the rod domains is expected to be much higher than what is tested here. The volume of the full-length talin dimer calculated from a previously reported structure is approximately 1300 nm^3, which represents roughly 2 mM inter-domain concentration considering the dimer contains two rod domains.In cellular environment, the local concentration of inter-domain interaction could be much higher than 32 μM tested here, thus both subdomains of talin rod are strong inhibitory segments that regulate the membrane recruitment of THD.

The FRET efficiency can be used to calculate the distance of fluorescence donor-acceptor. It is interestingly to note that the maximum FRET efficiency obtained from isotherm fitting is not affected by the presence of both THD inhibitory subdomains (data not show). Here, Lineweaver-Burk plots of the titrations at increasing concentration of talin inhibitory domains were used for better visualization (figure 5.4). The shared Y axis intercept in the plot for different titrations implicates that both talin R9 and R12R13 are canonical competitive inhibitors of the interaction between THD and DMPS membrane surface. The topology of THD Nanodisc complex is similar in the presence and absence of the inhibitory rod subdomains. These results are in a great agreement with previous NMR studies that the R9 and R12R13 are directly binding to the MOP region in F2F3 domain [98, 102, 99] and not altering the overall geometry of THD Nanodisc complex. Thus, the association of THD and membrane is tightly regulated by R9 and R12R13 masking the membrane and/or integrin binding sites on THD.

Gingras *et al.* identified a second integrin binding site (IBS2: 1974-2293) in talin rod domain, which is a pair of helical bundles encompassed by R9 and R12R13 [76]. It has been linked to maintain integrin clustering and stabilize focal adhesion site [94, 86, 109]. Another important feature of talin rod is connecting actin cytoskeleton to membrane receptors for mechanic force transduction and signaling. One of two recognized actin binding within talin

rod is located in R13 subdomain [76]. Several vinculin binding site also have been identified in talin R1-R3, R6-R8, R10-R11 subdomains [50]. Thus, the duel-inhibition of R9 and R12R13 to THD may, conversely, covers the binding sites and interfaces of other proteins in talin rod, regulating many talin functions, such as integrin clustering, actin binding, vinculin engagement.

A recent structural study proposed a novel "donut" shape dimer of talin auto-inhibited conformation, where the R1R2 rod subdomain covers the FERM domain and provides additional inhibitory effect [102]. In the FRET based binding assay, only modest effect of R1R2 on talin FERM domain binding to membrane was observed (Table 5.1), displaying only a factor of 4 increase in dissociation constant, which is remarkably weaker than R9 an R12R13. This is consistent with other NMR studies that talin R1 fails to promote noticable chemical shifts, suggesting that binding of talin R1 to THD F2F3 appears to be non-specific and weak [100]. The data presented here fits to a model that the association of THD to membrane is inhibited by the covering of the FERM domain by rod segments R9 and R12R13, Talin R1R2, on the other hand, has a closely packed arrangement with R3R4 and does not play a role in talin auto-inhibition. It has been implicated that the first five helical bundles exist in a compact form occluding vinculin binding sites of the rod domain in the absence of force [104].

5.3.2 PIP2 activates inhibited THD

A major unresolved question in talin mediated integrin activation is the mechanism of releasing the compact auto-inhibited form of full-length talin, especially the role of protein-membrane interactions. It has been shown that the recruitment of PIPKIγ promotes the synthesis of PIP2 from PI4P at the sites of focal adhesion [20]. Studies of NMR and SPR demonstrated an unique bivalent mode of PIP2 interacting with THD, revealing that F2 membrane orientation patch and F3 residues K322-K324 (FAP) are the key interfaces. In

chapter 3, result shows that charge reversal mutation in the MOP or K322-K324 positions prevent the closer membrane binding geometry of F3 domain, which may be preferable for integrin interactions.

To directly quantify the effects of PIP2 on auto-inhibited talin, affinities of THD to 10% PIP2 Nanodiscs was measured in the presence of talin rod inhibitory subdomains. Figure 5.5 panel A and B show the binding isotherms of the titration of THD into 10% PIP2 Nanodiscs and R9 or R12R13 segments. Lineweaver-Burk plots of the titrations unveil that both R9 and R12R13 have very little effect on THD-PIP2 interactions (Figure 5.5 C and D). 50% DMPS membrane surface is used as a convenient comparison to 10% PIP2 owing to a similar overall formal change since the charge on PIP2 headgroup at 7.2 is between -4 and -5, depending on the counter ions and the local environment [186]. PIP2 supports THD tight binding in the presence of the inhibitory subdomains. Only 4-fold increase in the dissociation constants, at or below 1 μM, were detected at highest concentration of talin rod subdomains tested, which is in a sharp contrast to the inhibition seen on DMPS Nanodiscs (Figure 5.5 E and F).

10 % PI4P, 50 % DMPG, and 50% DMPA Nanodiscs were prepared for FRET based binding assay for the purpose of further investigating the activation effects of lipid headgroup specificity. Previously in chapter 2, it has shown that talin FERM domain binds to DMPG, DMPA, and PI4P at around 0.5 μM dissociation constant similar to DMPS and PIP2. As expected, neither DMPG and DMPA are able to support tight binding of THD in the presence of talin rod subdomains R9 and R12R13 (Figure 5.6). This can be explained by the charges on DMPG and DMPA are located at the glycerol phosphate, which could be less accessible to talin FERM due to bulkiness of background PC headgroup. Intriguingly, PI4P also fail to support the high affinity binding of THD in the presence of the talin inhibitory segments despite the fact that molecular structure of PI4P differ only by a single phosphate group from PIP2 (Figure 2.9). These findings is consistent with the hypothesis that high charge density

on lipid head group but not the overall formal charge of the membrane surface is critical for unmasking the talin rod inhibitory domains and subsequently talin functions. Therefore, this finding demostrates that the presence of PIP2 at the protein membrane interface is a key player in dislodging talin rod inhibitory domains and activating talin. At the focal adhesion site, the presence of PIPKIγ, which is responsible for converting PI4P to PIP2, might be indispensable for talin activation.

5.3.3 PIP2 specifically interacts with THD F2F3 domain

In order to further understand the role of the THD subdomains in the process of talin activation, the binding of isolated F0F1 and F2F3 to DMPS and PIP2 in the presence of talin rod inhibitory subdomains were measured with the FRET based binding assay (Table 5.2). In chapter 2, it has been described that F0F1 does not discriminate between anionic lipids, while F2F3 has a strong preference for PIP2 over DMPS, almost 6-fold increase of affinity. Adding talin rod inhibitory segments induces almost 10-fold higher dissociation on F2F3 binding to 50% DMPS, similar to full-length talin FERM domain, but fail to impede F2F3 binding to 10% PIP2 with a tight dissociation constant of 0.36 μM. In striking contrast, the presence of both R9 and R12R13 prohibit F0F1 binding to 10% PIP2 by a factor of 10 higher dissociation constants and complete abrogates interacting to 50% DMPS.

A unique feature of talin head FERM domain is the large unstructured polypeptide loop (around 30 amino acids) within F1 domain. It has a propensity to form a α-helix when encounter with anionic lipids. The helix formation is considered to be important to talin-membrane interaction and talin activation due to the fact that no other talin head to rod interaction has been identified in F0F1 domain. In addition, deletion of this F1 loop has been shown to substantially inhibit talin mediated integrin activation *in vivo*, but does not affect the affinity of talin head to integrin tails [33].

The FRET binding assay of truncated talin FERM domains deconvolute the mechanism

of talin activation by PIP2. Clearly, F2F3 has a strong binding preference of PIP2 over PS while F0F1 shows similar dissociation constants on both membrane surfaces. Result suggests that there is no cooperativity between F0F1 and F2F3 regarding interaction with overall charge. Both talin R9 and R12R13 are able to impede F0F1 and F2F3 binding to PS membrane, yet it is not clear how F0F1 interacts with talin rod inhibitory subdomains. One possible explanation could be the electrostatic interaction between the F0F1 positively charged loop and the extensively negatively charged surface on talin R9 [99]. Surprisingly, F2F3 is insensitive to the inhibitory effect by both talin R9 and R12R13 yet the binding of F0F1 to PIP2 membrane is significantly inhibited by the presence of talin rod segments. Although many researchers suggest that the unstructured loop of F1 could be a potential site to activate talin by forming helix upon contacting anionic membrane [135, 190]. However, in this work, the results are not consistent with this hypothesis. The rod domains inhibit F2F3 by a tight specific interaction that is efficiently disrupted by the high density charge headgroup of PIP2, while the talin rod segments may mask membrane-binding sites of F0F1 through general electrostatic interaction by competing with anionic phospholipid bilayers with negatively charged rod domain surface.

5.4 Conclusions

This chapter described a unique role of the membrane in regulating talin mediated integrin transmembrane signaling. Figure 5.7 depicts a schematic representation of the lipid dependent mechanism of talin activation through a complex interplay of protein-protein and protein-membrane interactions. PIP2 promotes the dislodging of talin rod inhibitory subdomains on talin FERM domain through a process that is extremely sensitive to the lipid headgroup identity. Enhanced PIP2 local concentration from converting PI4P at the membrane induce the unraveling of the auto-inhibited talin, allowing optimal talin membrane

engagement and effective communication with integrin cytoplasmic tails. This leads to a suggestion for a role of other effector proteins in talin activation, particularly PIPKIγ. One likely scenario is that the interplay between PIPKIγ and talin at the site of focal adhesion results in the amplification of talin activation through the production of PIP2 from PI4P. Clearly, among common phospholipid head groups, PIP2 seems to be a key player in an orchestra involving many other adaptor protein partners, such as Rap1-RIAM, calpain, and the aforementioned PIPKIγ, that promotes efficient talin mediated integrin activation.

5.5 Figures and Tables

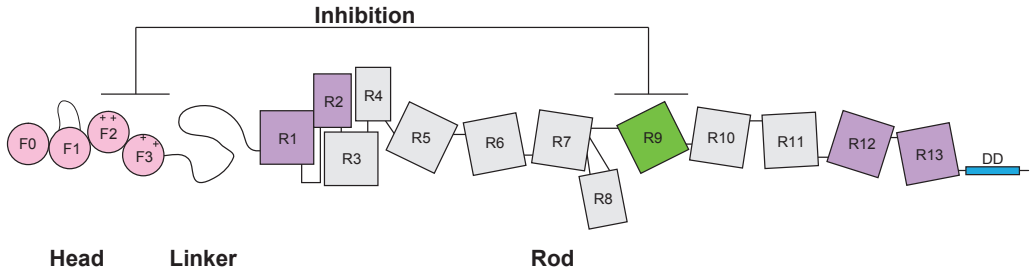

Figure 5.1: The schematic representation of full-length talin protein structure. The talin FERM domain is colored in pink. The talin rod subdomains are depicts as squares in various color. The previous suggested THD inhibitory domains are labeled in purple and green.

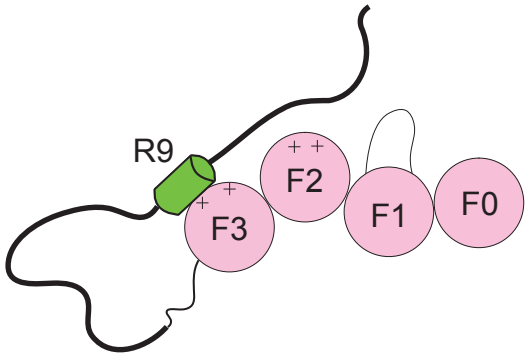

Figure 5.2: The schematic representation of full-length talin auto-inhibited conformation in cytosol. R9 covers the THD F3 domain inhibiting subsequent binding of membrane and integrin β tails.

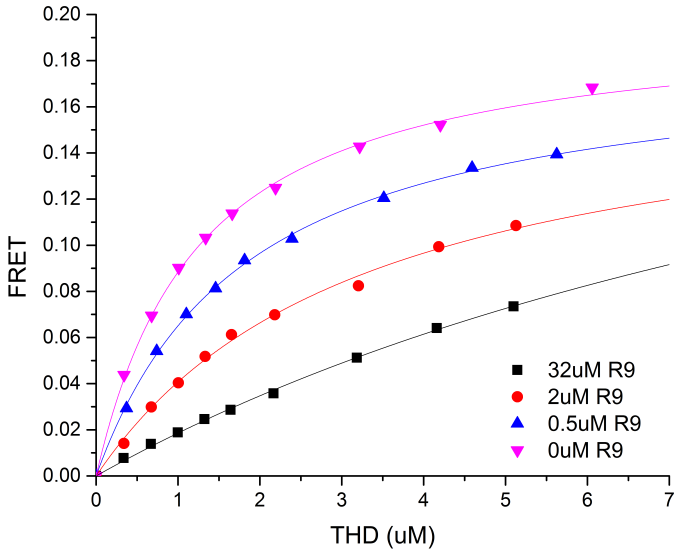

(A)

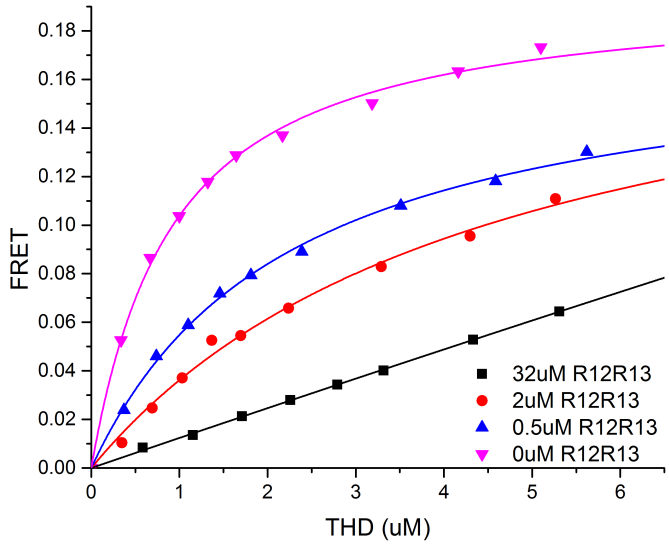

(B)

Figure 5.3: Binding isotherms of THD on DMPS with talin R9 and R12R13. (A and B) Data for 32 μM, 2 μM, 0.5 μM, and 0 μM of talin R9 or R12R13 subdomains, are shown in pink, blue, red, and black, respectively.

Table 5.1: Inhibitory effects of talin rod subdomains on Nanodiscs

Rod domain	Dissociation constant (μM)	Fold increase
None	0.58 ± 0.04	NA
0.5 μM R9	1.6 ± 0.1	2.8
2 μM R9	2.6 ± 0.5	4.6
32 μM R9	18 ± 19	30
0.5 μM R12R13	2.2 ± 0.2	3.8
2 μM R12R13	4.4 ± 0.5	7.5
32 μM R12R13	180 ± 40	300
0.5 μM R1R2	0.43 ± 0.01	0.7
2 μM R1R2	0.65 ± 0.06	1.1
32 μM R1R2	2.4 ± 0.2	4.2

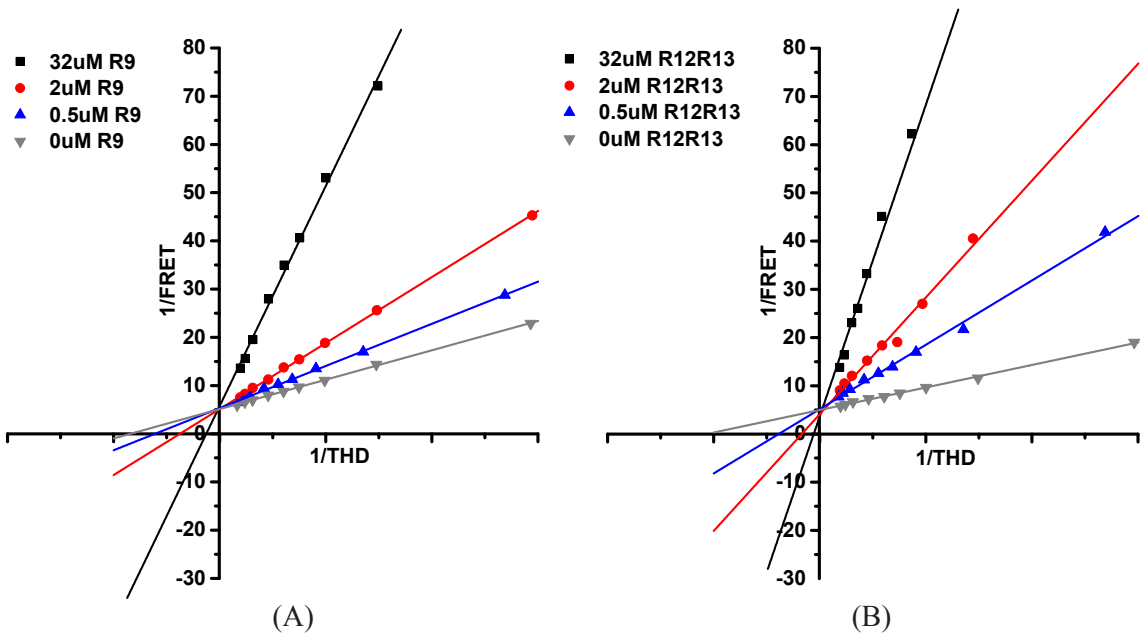

Figure 5.4: Linweaver-Burk Plot of fluorescence titrations in the presence of talin Rod subdomains. (A and B) 32 μM, 2 μM, 0.5 μM, and 0 μM of talin R9 or R12R13 subdomains are shown in black, red, blue, and grey, respectively.

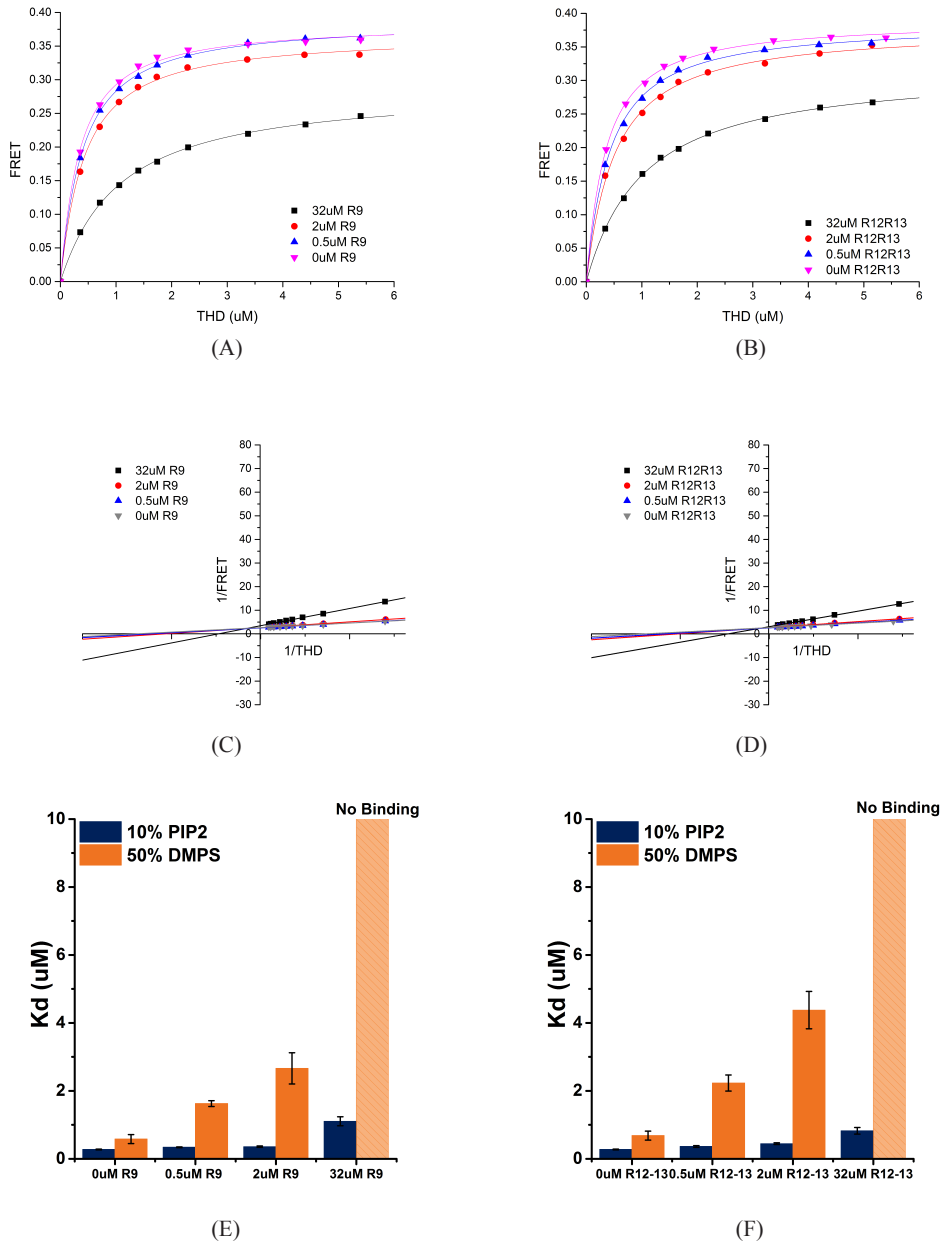

Figure 5.5: PIP2 activates inhibited THD in the presence of R9 and R12R13. (A and B) Binding isotherms of THD binding to 10% PIP2 Nanodiscs. 32 μM, 2 μM, 0.5 μM, and 0 μM of talin R9 or R12R13 subdomains are shown in black, red, blue, and pink, respectively. (C and D) Linweaver-Burk Plot of fluorescence titrations in the presence of talin Rod subdomains on PIP2. (E and F) Comparisons of affinities of THD on DMPS and PIP2 in the presence of talin rod.

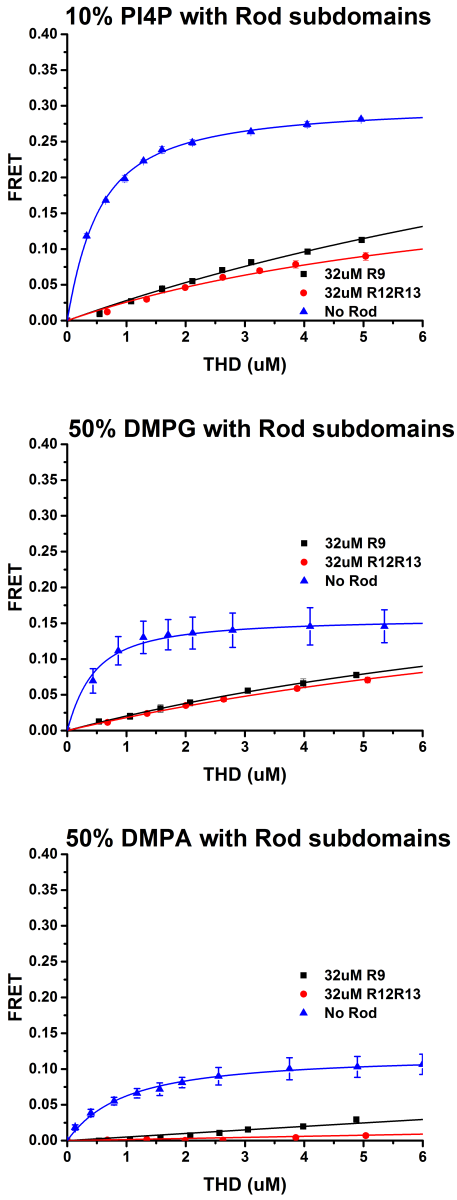

Figure 5.6: Binding isotherms of THD on DMPA, DMPG, and PI4P in the presence of talin rod domains.

Table 5.2: Inhibitory effects

	F0F1		F2F3	
Rod domain	50% DMPS	10% PIP2	50% DMPS	10% PIP2
None	0.45 ± 0.09	0.86 ± 0.25	1.2 ± 0.3	0.18 ± 0.01
32 μM R9	No Binding	14 ± 1	11 ± 2	0.36 ± 0.03
32 μM R12R13	No Binding	9 ± 4	10 ± 3	0.36 ± 0.03

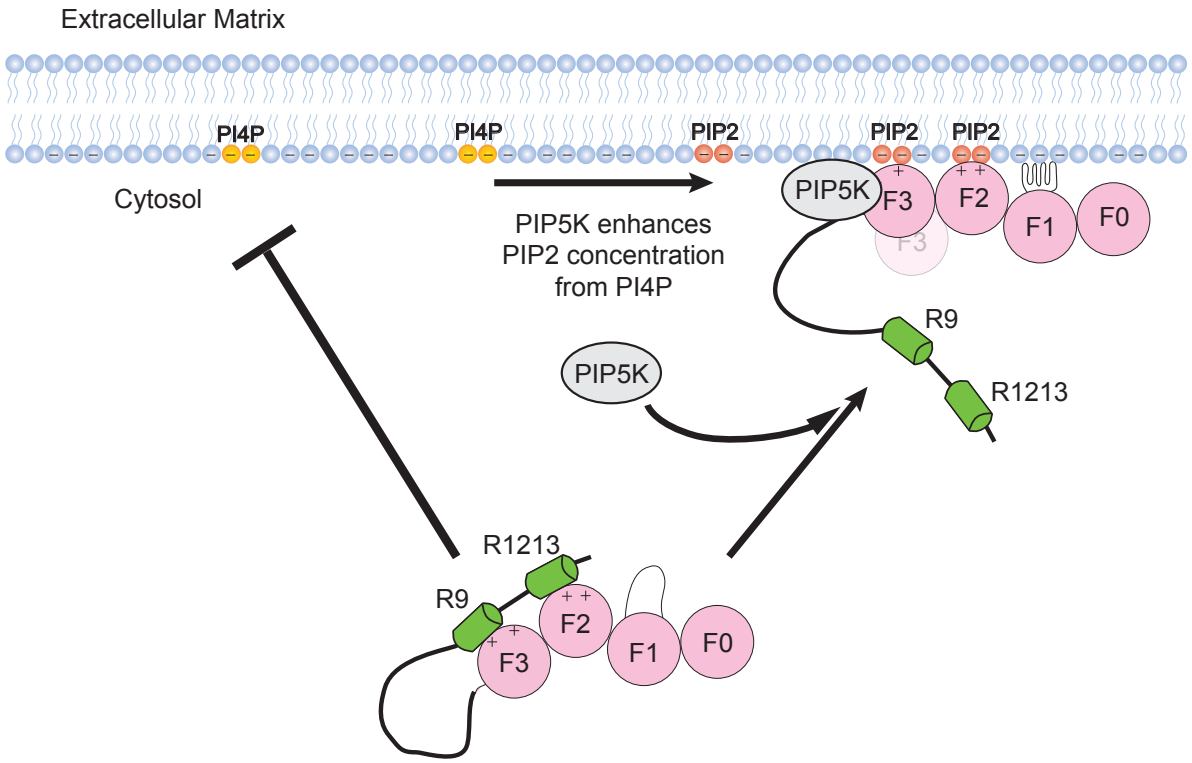

Figure 5.7: Regulation of talin activation by PIP2. PIP5K promotes local synthesis of PIP2 form PI4P. The presence of PIP2 in a bilayer promotes the dissociation of talin R9 and R12R13.

CHAPTER 6

INTERACTION OF TALIN AND INTEGRIN TAIL

6.1 Introduction

The final regulation step of integrin inside out signaling is the disruption of integrin cytoplasmic subunits mediated by talin integrin interaction. Significant efforts have spent on understand the protein-protein interactions in this process. Structural studies reveal that the talin F3 domain recognizes two interface sites in β tail.

First is on the membrane proximal NPxY/F sequence motif [7, 78]. Mutagenesis study of the interaction between talin F3 W359 and Y747 of the integrin β tail mid portion is specific and strongly resembles a Phospho-tyrosine binding (PTB) domain interactions with peptide ligands. Alanine substitutions in either position fail to support talin/integrin complex forming and subsequent integrin activation [78].

Second is the conserved membrane proximal region of integrin cytoplasmic tail encompassing the inner membrane clasp and salt bridge (αR995-βD723) that are critical for maintaining integrin inactive state. It has been shown that talin FERM domain interactions with the membrane proximal region of integrin β tail cause disruption of α/β heterodimer promoting the conformational change of integrin extracellular domains [64]. Another fluorescence research elegantly shows that binding of talin alters the topology of integrin β transmembrane domain. This tilting angel change is pivotal for transducing the activation signal across membrane [84].

Early studies emphasized the protein interactions, yet the interplays of talin, membrane

composition, and integrin tail are poorly studied. The affinities of talin FERM domain for integrin β tails measured by solution NMR and SPR are ranging from 100 nM to hundreds of μM [7, 36, 65, 66, 67, 68]. The difference could be correlated with the integrins various subcellular distributions and major responses.

It is interesting to note that talin FERM domain and integrin $\beta 3$ cytoplasmic tail do not interact noticeably. But in mark contrast, the dissociation constant rises to 860 nM measured by isothermal titration calorimetry in the presence of anionic lipids [71, 72]. Previous study also indicate that the binding of talin to negatively charge membrane is pre-requisite for altering integrin transmembrane topology and following activation [5, 19]. Results of recent MD simulations and previous chapter also suggest that the lipid bilayer may play a crucial role in forming a stable complex with talin FERM domain and steering the talin head into a preferable geometry to interact with integrin cytoplasmic tails[44].

In this chapter, a novel protocol was developed to assembly unclustered integrin $\beta 3$ tails into anionic lipid bilayer utilizing Nanodiscs technology. To ensure single insertion of integrin, the protein was engineered and expressed as a fusion with maltose binding protein. This method allows researcher to precisely tailor membrane environment and dissect the free energy contribution from membrane and integrin tail during the talin membrane recruiting process. The FRET based binding assay result shows that talin interactions with integrin tail provide the majority of the free energy for forming the trimeric complex. The FAP residues of THD mediate the membrane engagement of talin F3 domain. Talin rod inhibitory subdomain R9 and R12R13 may employ different interface on the FERM domain, in which, the R9 sterically blocks the binding site of integrin on THD F3.

6.2 Experimental Methods

6.2.1 Materials

DMPC, DMPS, and PIP2 were purchased from Avanti Polar Lipids (Alabaster, AL). *E.coli* BL21 DE3 (gold) was purchased from Stratagene. pMAL-c2e expression vector and competent cells of NEB Turbo *E.coli* were obtained from New England Biolabs (Ipswich, MA). iProof polymerase kit was purchased from BioRad (Hercules, CA). Uniblue A (UA), Amberlite XAD-2 beads, and sodium cholate obtained from Sigma-Aldrich (St. Louis, MO). Tetramethylrhodamine-5 (and -6) C2 maleimide (TAMRA) was obtained from Anaspec (Fremont, CA). Integrin DNA G-block sequence was purchased from Integrated DNA Technologies (Coralville, IA).

6.2.2 MBP-β3 TM/tail pMAL vector construction

To reconstitute the expression vector of MBP-β3 TM/tail, the sequence of integrin β3 TM/tail (residues 685-762) was engineered with a AvrII site on 5'-terminal and a XbaI site on 3'-terminal for subsequent digestion and ligation. In addition, a poly-histidine sequence and a Tobacco Etch Virus (TEV) was designed preceding to integrin sequence for later purification and Nanodisc assembly (Integrin 5'- GCG GAA ACC CTA GGT CAT CAT CAT CAT CAT CAT CAT GAT TAT GAT ATT CCG ACC ACC GAA AAT CTG TAT TTT CAG GGA TCC CCG GAA TGT CCG AAA GGT CCG GAT ATT CTG GTT GTT CTG CTG AGC GTT ATG GGT GCA ATT CTG CTG ATT GGT CTG GCA GCA CTG CTG ATT TGG AAA CTG CTG ATT ACC ATT CAT GAT CGT AAA GAA TTT GCA AAA TTT GAA GAA GAA CGT GCA CGT GCA AAA TGG GAT ACC GCA AAT AAT CCG CTG TAT AAA GAA GCA ACC AGC ACC TTT ACC AAT ATT ACC TAT CGT GGT ACC TAA TAA TCT AGA TAT ACG -3').

The blunt-ended DNA fragments were synthesis by Integrated DNA Technologies Inc. and cut with XbaI and AvrII to create sticky ends. The linearized vector which possesses marching restricted digestion sites was incubated with the integrin DNA fragments in a mole ratio of 1 to 3. T4 ligase was used to ligate the insert and backbone. The reconstructed plasmid was enriched by transforming into competent NEB turbo *E. Coli* cell follow by plasmid extraction using Miniprep spin column kit (NEB, Ipswich, MA). DNA sequence confirmation was performed by ACGT (Northbrook, IL) using M13 promoter primers.

6.2.3 Expression and purification of MBP-β3 TM/tail pMAL

E. Coli. BL21 DE3 (gold) was chosen for expression in the reason of fast growing rate and compatibility with lactose induction. 0.5 μL expression vector was transform into competent BL21 DE3 (gold) *E. Coli.* cell. One colony of cells containing the fusion plasmid was inoculated into 50 mL rich broth with glucose and ampicillin (per liter borth: 10 g tryptone, 5 g yeast extract, 5 g NaCl, 2 g glucose autoclave; add sterile ampicillin to 100 g/ml). The starting culture was grow to OD_{600} 0.6 at 37 °C, 250 RPM. 1 L culture broth was inoculated with 10 mL of the starting culture and incubated in the same condition. A typical expression scale is 4 liters. Upon the cell density reach OD_{600} 0.5, IPTG was added to a final concentration of 0.3 mM for expression induction. The cell culture was continued to incubate for 2 hours after IPTG induction. Cell pellets were harvested by centrifugation at 8000 RPM for 10 minutes and discard the supernatant. For long term storage, cells were frozen and stored at -80 °C.

The purification started with resuspend cell pellets in 5 volume excess column buffer (20 mM Tris-HCl pH 7.4, 200 mM NaCl, 1mM EDTA, 0.5% Triton X-100, 1mM DTT). Protease inhibitor cocktail tablets (1 tablets per 10 g of cell pellet) and DNase (1 mg per 5 g of cell pellet) were used to prevent target degradation and facilitate lysis. After 45 minutes stirring at 4°C for completed suspension, sample was placed on ice and incubated

with 0.25 mg/mL lysozyme over night with gentle stirring. The cell lysate was centrifuged at 30,000 RPM for 30 minutes to obtain the cell supernatant and discard the cell debris. Then the crude extraction was loaded into the amylose affinity column equilibrated with column buffer. The maximum flow rate of loading should not exceed 5 mL/min. Then the column was washed with 10 column volumes of column buffer at a flow rate no more than 10 mL/min. The fusion protein was eluted with column buffer containing additional 10 mM maltose. 20 fractions of 1/5 column volume each were collected. The protein usually starts to elute within the first 5 fractions and can be easily detected by the Bradford protein assay (Thermo Fisher, Waltham, MA). The protein fractions were pooled together and dialyzed against column buffer with no detergent. The final product was exanimated by SDS-PAGE and electro-spray Mass spectrometry.

6.2.4 Assembly integrin β3 TM/tail into Nanodisc

To ensure single integrin insertion, large excess Nanodiscs were used for assembly. The typical stoichiometry of lipid, TAMRA MSP, and protein is 525:5:1. The purified MBP-integrin β3 TM/tail protein was concentrated in 10,000 Da centrifugal concentrator (EMD Millipore, Billerica, MA) to 50 μM. The protein stock was incubated with 6 M urea for 1 hour at room temperature. The lipid stock in chloroform was dried under steady flow of nitrogen gas followed by overnight incubation in vacuum desiccator. The dried lipid powder was resuspend with 100 mM sodium cholate to a final concentration of 50 mM. The designated amount of TAMRA labeled MSP were mixed with lipid and denatured integrin β3 TM/tail. The mixture was incubated at room temperature for 45 minutes. The self-assembly process started with removing detergent and urea by buffer exchange with 8,000,000 volumes standard Nanodisc buffer (20 mM Tris-HCl pH7.4, 150 mM NaCl) at room temperature.

The dialyzed Nanodisc sample was further purified by amylose resin , which is an affinity matrix used for isolating MBP, in a batch incubation method. In brief, around

500 μL amylose resin equilibrated with standard Nanodisc buffer were mixed with crude Nanodiscs sample and gently rotated at 4 °C for 90 minutes. Then sample was centrifuged at 6,400 RPM for 90 seconds. The supernatant was removed and kept at 4 °C for later test. The precipitated resin was washed by 5 bed volumes of standard Nanodisc buffer to eliminate residual empty Nanodiscs. The integrin containing Nanodiscs were eluted with 10 mM maltose. Normally, protein elutes within first 2 bed volumes. The Nanodisc fractions were pooled and digested by TEV protease (100:1 protein to protease ratio) overnight at 4 °C. A 2 mL amylose column was used to eliminate residual cleaved MBP. The flow through and wash fractions of the column were concentrated to a volume smaller than 400 μL. The concentrated product was further purified by size exclusion and injected into the Superdex 200 increase column connected to Water HPLC system and equilibrated with cytoplasmic mimetic buffer (20 mM HEPES pH 7.2, 4 mM KH_2PO_4, 125 mM KCl, 14 mM NaCl, 1mM $MgCl_2$, 0.02 mM EGTA). The fractions of Nanodiscs containing integrin should elute slightly earlier than the plain membrane Nanodiscs. Samples of every purification steps were collected and analyzed by SDS-PAGE.

6.2.5 FRET based binding assay

The FRET based binding assay was adapted from the experimental methods described in chapter 1 and 5.

6.3 Results and Discussion

6.3.1 Reconstitute unclustered integrin β3 TM/tail in Nanodiscs

Early studies of talin interactions with integrin often adopt lipid vesicle to incorporate integrin tails. However, it is difficult to resolve the inserting direction and clustering state

which might hamper the understanding of protein-protein interactions. Also in liposomes, anionic lipids have strong tendency of aggregation which does not fully represent the native membrane environment. To overcome these obstacles, here Nanodiscs were utilized to ensure single protein insertion and provide precisely controlled membrane surface. Integrin $\beta 3$ TM/tail was first cloned and expressed in a fusion form with Maltose binding protein (MBP) in order to improve solubility. Figure 6.1 illustrate the cloning strategy and cartoon representation of the fusion protein. A TEV digestion site was engineered in between of MBP and integrin allowing subsequent digestion in later Nanodisc assembly.

Preliminary expression and purification of MBP-integrin $\beta 3$ TM/tail with amylose affinity column yielded the protein polymers that cannot be dissociated by SDS-PAGE. Incubation with 10 mM DTT at 99 °C fully reverse the polymers back to monomers (data not show). Thus, 1% Triton X100 were added to all the buffers during cell pellet resuspension and purification to mitigate aggregation formation. One possible explanation of this phenomenon is that the highly soluble MBP connecting with a more hydrophobic integrin $\beta 3$ TM/tail resembles the structure of a lipid molecule where MBP is the polar headgroup and integrin tail is the hydrophobic chain. The fusion proteins are likely to aggregate in the manner of lipid forming liposomes. The purified fusion protein was digested by TEV protease and exanimated by electro-spray mass spectrometry. Result shows a main 8.9 kDa peak which is correspond to the molecular weight of integrin $\beta 3$ TM/tail.

To breakdown the soluble aggregation of MBP-integrin fusion protein, 6 M urea was used to completely denature the protein. This denaturing step enhance the insertion rate by a factor of 3 in comparison of using only detergents. The Nanodiscs assembly starts with mixing 5 molar excess MSP to the integrin $\beta 3$ TM/tail in order to provide suitable stoichiometry ratio for single insertion. The top panel of figure 6.2 shows the size exclusion chromatography of the purification process. The flow through fraction of the first amylose affinity column contains mostly empty Nanodiscs without integrin insertion. Second amylose

column targets cleaved MBP and the flow through fraction includes mostly integrin embedded Nanodiscs and residual free MBP (20-minute retention fraction). SDS-PAGE analysis (Figure 6.2 bottom) revealed that 15-minute SEC fraction contains only MSP and integrin β3 tail, thus integrin β3 TM/tail successfully assembles into Nanodiscs. The final integrin to MSP ration is roughly 1:1 based on the calculation from absorbance spectra, in another work, one Nanodisc leaflet possesses one integrin β3 tail.

6.3.2 Binding of talin to integrin β3 tail in concert with membrane

To investigate the mechanism of talin membrane recruitment in the presence of integrin β3 TM/tail, FRET based binding assay was performed with TAMRA labeled Nanodiscs with single inserted integrin tail. Figure 6.3 summaries the fitting results of UA labeled wild type THD or THD mutants titrating into integrin tail containing Nanodiscs. Wild type THD binds to β3 tail DMPC Nanodisc with a dissociation constant of 0.74 μM. Compared to the plain DMPC membrane surface, the mere presence of integrin tail promotes the affinity of THD by a factor of 5. Introducing anionic lipid, on 50% DMPS membrane, further induce a two-fold increased affinity of THD binding to integrin tail Nanodiscs. Intriguingly, on 5% PIP2 membrane surface, adding integrin β3 tail only results in a minimal tighter binding, from 0.72 μM on plain membrane to 0.58 μM with integrin tail. Thus, although anionic membrane facilitates the talin recruitment, the integrin β tails provide the majority of the binding free energy of forming the talin-integrin-membrane trimer.

In chapter 3, it has been shown that the binding geometry of talin F3 subdomain is sensitive to the lipid headgroup identity. Higher charge density of the lipid headgroup, like phosphatidylinositols, gives rise to a closer binding distance. Interestingly, the presence of integrin β3 tail on membrane leads to a noticeable further distance between the fluorescence dye pairs, from 5.3 Å to 6.1 Å on DMPC bilayer and 4.9 Å to 5.5 Å on 50% DMPS membrane. This observation may be explained by two-fold. Firstly, integrin tails contain two

NPxY motifs targeted by the PTB domain of talin in addition to the inner membrane clasp. Although talin preferably binds to the membrane proximal NPxY motifs, it is possible that talin also interacts with the distal one and results in a longer FRET pair distance. Secondly, the insertion of integrin tail in Nanodiscs could occupy certain area on the membrane surface obstructing talin F3 domain access lipid bilayer in an optimal conformation. It should be noted that 5% PIP2 Nanodisc promotes similar FRET pair distances, around 5 nm, with or without the presence of integrin β tail. Comparing to the dye separation on integrin inserted PC and PS Nanodiscs, it is significantly shorter on PIP2 containing integrin Nanodiscs. This result, combining the previous data, directly points to the specificity of PIP2 to talin as well as its ability of facilitating talin to position into a preferable geometry for disrupting the clasp between α and β integrin subunits.

It has been shown that K322 and K324 residues in F3 FAP region are critical for talin membrane engagement and subsequent integrin activation. Reverse charge mutation on these sites abrogate talin mediated integrin activation *in vivo* and impede talin F3 subdomain conformational change (Figure 3.2). Here, UA labeled talin K322E and K324E were prepared and used for titration with integrin inserted Nanodiscs. Figure 6.3 compares the titration fitting results of wild type and FAP mutants. The glutamate substitution does not affect the overall affinity of talin to integrin inserted Nanodiscs. This result is compatible with the previous suggested model that MOP residues in F2 domain mediate the major electrostatic contact with anionic lipid bilayer and PTB domain in F3 domain act as the primary binding interface of integrin β tail. The FAP reverse charge mutations result in a significantly increased fluorescence dye separation as seen on plain membrane Nanodiscs. This supports the hypothesis that a large conformational change of talin F3 domain, which may allow FAP residues access the α-β salt bridge, is required for optimal integrin activation.

6.3.3 Talin activation in the presence of integrin β tail

To further investigate the talin auto-inhibition, in particular the difference of identified talin rod inhibitory domain, series of FRET based binding assays were performed with integrin tail inserted Nanodiscs in the presence of talin rod inhibitory domains. 50% DMPS and 5% PIP2 membrane surface were selected for direct comparison as they provide similar affinities toward THD, and have been previously shown that PIP2 is the specific activator for R9 or R12R13 inhibited THD while no activation was observed on PS lipid bilayer.

Figure 6.4 (top panels) show the binding isotherms of the FRET titrations. 32 μM talin R9 subdomain completely inhibits the interactions of THD with 50% DMPS membrane and integrin tail. The maximum fluorescence change is within 1%. One other hand, the dissociation constants are minimally affected by adding same concentration of the talin R12R13 segments and the maximum FRET efficiency is reduced to 5% from 13% without the presence of rod subdomains. On 5% PIP2 Nanodisc, THD engages the membrane and integrin β3 tail with a similar affinity as seen on 50% DMPS membrane, besides a slightly increased maximum FRET efficiency at 18%. The presence of both talin inhibitory subdomains leads to comparable dissociation affinities and around 10% decrease in maximum FRET efficiencies compared to titrations excluding inhibitory domains. It is interesting to note that the differences of FRET efficiencies with R9 and R12R13 on PIP2 membrane are not as distinctive as that on PS membrane.

Figure 6.4 (bottom) summarizes distance calculations from the measured maximum FRET efficiencies. 5% PIP2 Nanodiscs promote a closer binding geometry than it found on 50% DMPS. Particularly in the presence of talin R9 inhibitory subdomains, adding THD yields undetectable change on 50% DMPS membrane while 5% PIP2 Nanodiscs still give rise to sub-micromolar dissociation constant and a dye separation distance of 6 nm. The inhibitory effect of R12R13 on THD binding topology is weaker on both integrin inserted PS and PIP2 membranes with unchanged dissociation constant and moderately increased FRET

pair distance. The data shown here indicates that the interfaces of THD, integrin tail and PS membrane, namely the FAP residues and PTB domain, may be sterically blocked by talin R9 but not R12R13. This is distinctive from what previously observed in chapter 3 where both talin inhibitory subdomains are classic competitive inhibitors of DMPS Nanodiscs to THD. The R12R13 might inhibit the talin membrane recruitment by covering the F2 MOP region to impede THD membrane binding, yet the NPxY motif on integrin tail is still accessible for THD. Thus integrin tail could still arrest THD but with a further binding topology due to the lack of MOP interactions to trigger F3 conformational change. The result also reassures the activator role of PIP2 during talin membrane engagement due to the fact that the presence of 5% PIP2 on lipid bilayer partially promotes high affinities and closer binding geometry of the rod subdomains inhibited THD compared to PS membrane. It should be note that the formal charge of 5% PIP2 roughly equals to 20-30% DMPS, thus the high charge density on PIP2 lipid headgroup may be critical for encouraging the disruptions of THD and talin rod inhibitory domains. However the PIP2 alone does not fully rescue talin activation, other protein partners, such as RIAM-RAP1, PIPKγ, and calpain, may need to work in orchestra with PIP2 for complete talin activation and optimal integrin activation.

6.4 Conclusions

This chapter detailed the development and optimization of assembling single integrin β3 tail inserted Nanodiscs. This represents the first application of combining Nanodisc technology to provide native membrane environment for unclustered integrin cytoplasmic domain in order to investigate talin interaction and activation. The FRET titration results shown in this chapter suggest that the interaction between integrin β tail and talin offer the majority of binding free energy for talin membrane recruitment. However, the binding geometry of the complex remains sensitive to the lipid head group identity in the presence

of integrin cytoplasmic domain. High local charge density lipids, such as PIP2, may be required in triggering the conformational change of F3 domain for disrupting integrin α/β salt bridge and integrin activation. Furthermore, the date indicates the distinctive interfaces of different talin rod inhibitory domains, where R9 may directly mask the binding site of integrin tail on talin F3 while R12R13 may block the MOP residues in F2 domain to inhibit talin engagement. It should be noted that PIP2 remains a key activator of auto inhibited talin in the presence of integrin tail. However, it may work in concert with other identified talin activation pathway to achieve fully activation.

6.5 Figures

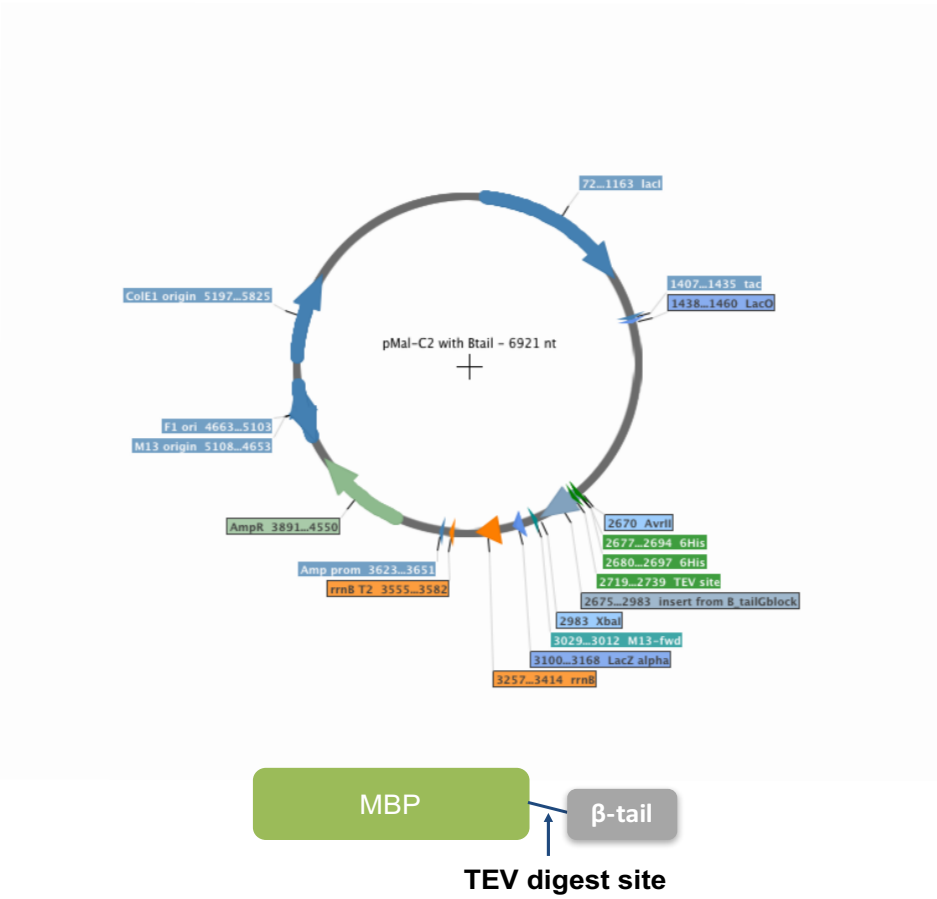

Figure 6.1: Schematic representation of the MBP-β3 tail construct. The top panel shows the graphical description of MBP-β3 tail expression vector in pMAL-c2e backbone. The bottom panel shows a cartoon of the protein structure. A TEV digestion site is engineered between MBP and β-tail.

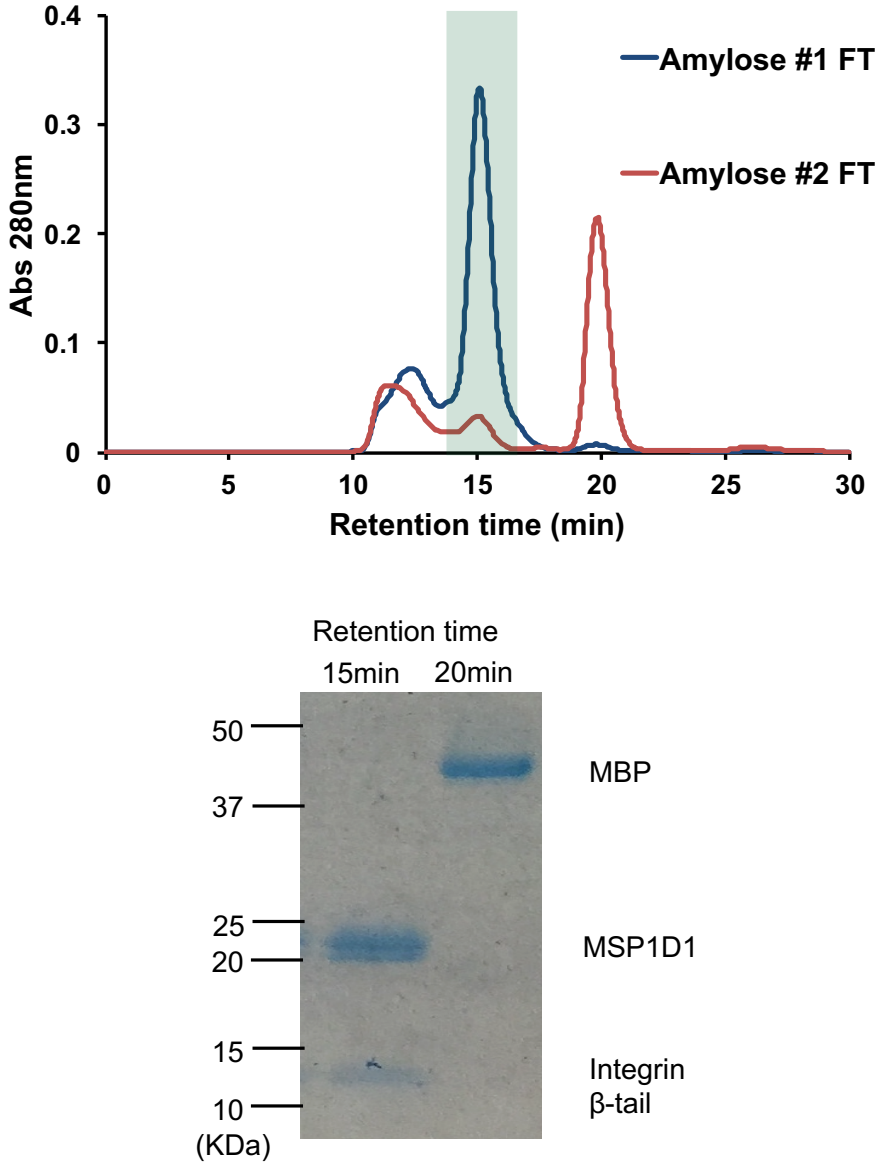

Figure 6.2: Nanodiscs containing integrin $\beta 3$ TM/tail. Size exclusion chromatography (top) shows the purification process. Flow through fraction of the first amylose column is in blue trace, the second amylose column flow through is in red trace, the light green shade encircles the fraction of 10 nm elutent. The SDS-PAGE analysis (bottom) reveals the insertion of integrin $\beta 3$ TM/tail and the a complete TEV digestion.

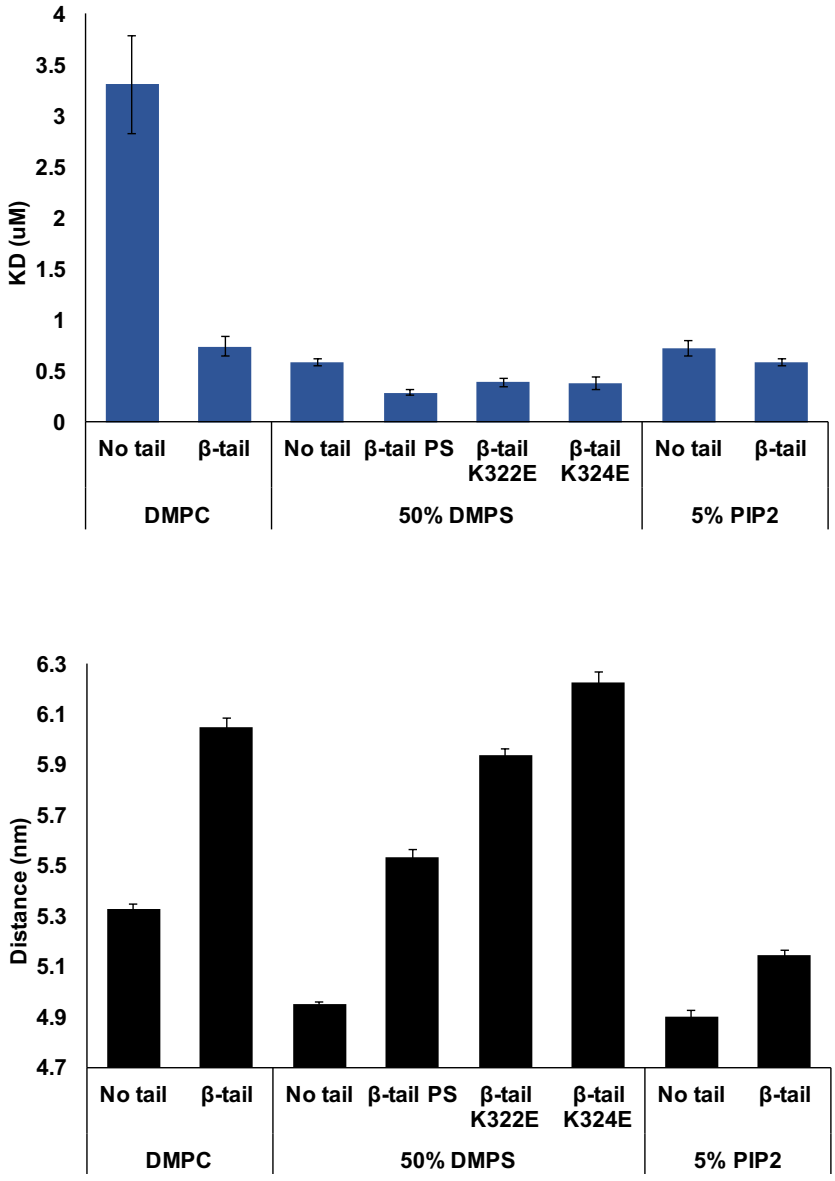

Figure 6.3: Results of FRET based binding assay with integrin inserted Nanodiscs. The top panel summarizes the dissociation constants of THD WT and THD mutants binding to Nanodiscs with or without integrin $\beta 3$ tail. The bottom panel compares the fluorophore separation distances.

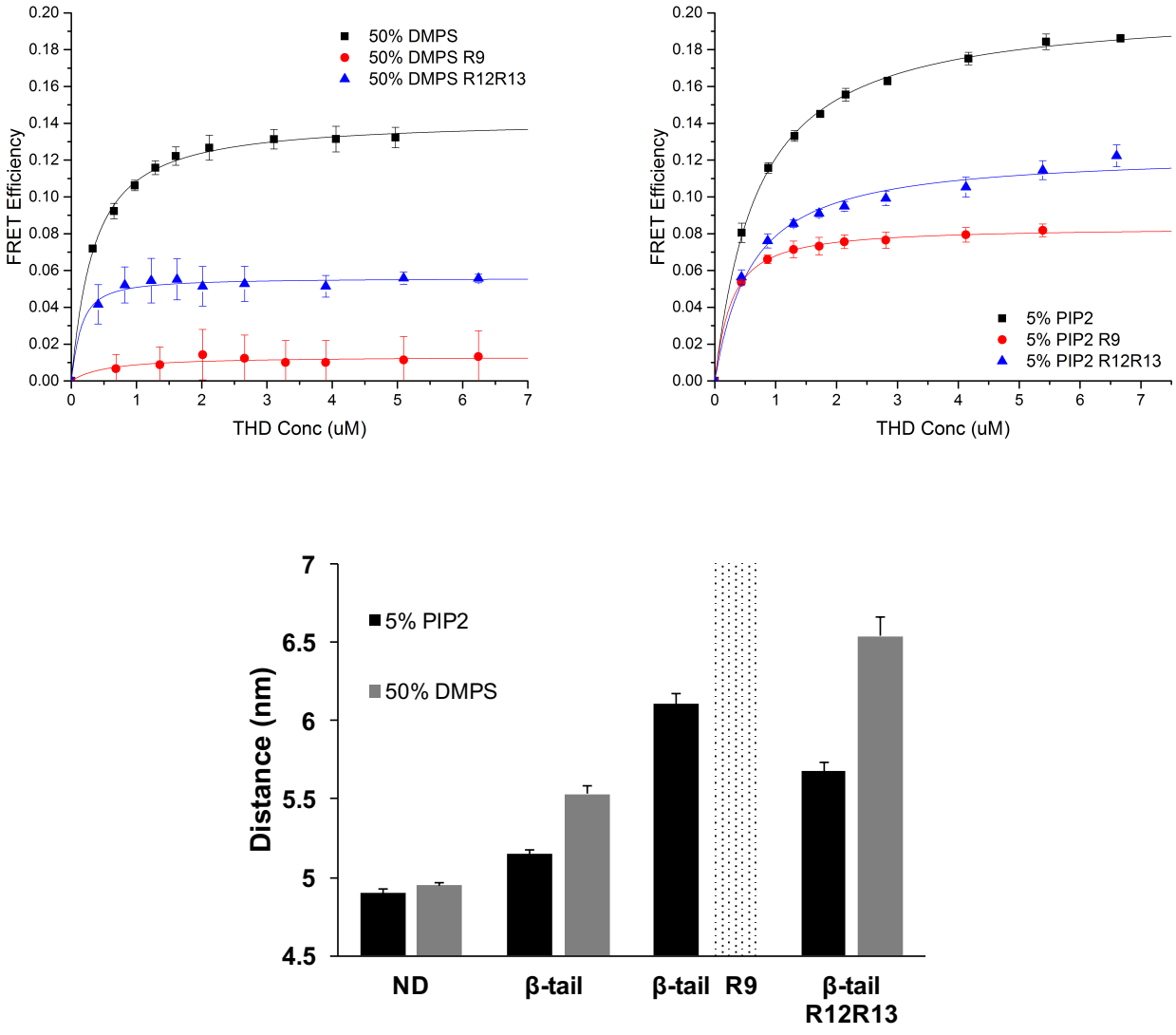

Figure 6.4: Titrations of THD into integrin inserted Nanodiscs in the presence of talin rod inhibitory subdomains. The top two panels show the binding isotherms of 50% DMPS and 5% PIP2. The bottom panel summarizes fluorophore distance analysis of the titrations.

CHAPTER 7

DISCUSSIONS AND FUTURE DIRECTIONS

Integrin plays an undisputed role in cell-cell and cell-ECM interactions that closely relate to many cell events. The activation and function of integrin are tightly regulated by the protein-protein and protein-membrane interactions of talin. It is therefore critical to study and understand the complex biochemical reactions that occur on the lipid bilayer surface. Early researches have employed heterogeneous and ill-defined membrane system, such as surface tethered lipid monolayers and liposomes, to investigate membrane proteins and their functions. In comparison, Nanodiscs offer a homogeneous, well-defined, native-like lipid bilayer for solubilizing membrane protein and characterizing membrane related events *in vitro*.

Chapter 2 described a novel Nanodisc based titration assay to probe the talin FERM domain binding to a membrane with precisely controlled composition utilizing specific labeling and FRET. This technique allows researcher fine tuning the membrane lipid identity, charge density and lipid mobility in order to differentiate any lipid preference. The talin membrane recruitment is mainly governed by the electrostatic interaction between the positively charged patch on THD and anionic lipid surface. The measured dissociation constants with different flavors of phospholipids are in the range of sub-micromolar in exception of pure DMPC membrane. Further association free energy analysis demonstrates a linear grouping of PG, PI4P, and PIP2, which is subtly lower than PS and PA. The common features of negatively charged phosphate group and additional alcohol group are hypothesized to potentially form hydrogen bonds with THD contributing to the binding preference.

Measurements of FRET efficiency enable the calculation of fluorescence dye separations that hold great potential to shed light on the detail binding topology of talin and membrane. Chapter 3 compares the FRET pair distances of talin FERM binding to various phospholipid bilayers. THD F3 undergoes a large conformational change, that brings FAP residues K322 and K324 to a closer proximity to integrin IMC, upon binding to membrane. This conformational equilibrium is highly sensitive to the charge density of lipid headgroup and PIP2 promotes the largest protein topology alteration. Mutagenesis investigations also demonstrate that K274, and F259/F280 residues in talin 1 are the key triggering position for the F3 downward motion, which is compatible with the result of previous computational simulation [44]. This work creates a paradigm for future studies of the protein-membrane interaction in vitro.

Besides electrostatic binding, membrane or peripheral membrane protein often employ hydrophobic interaction, such as transmembrane domain or membrane anchor, to stabilize the membrane-protein complex. Chapter 4 developed a Nanodisc based label free assay to probe the hydrophobicity of intrinsic tryptophan in protein. The observation of the tryptophan emission spectra identified a potential membrane anchor F259 in talin F2 domain. The F259W mutant exhibits significant red shifted emission spectrum upon binding anionic lipid bilayer indicating a local conformational flip down and insertion into the hydrophobic core of membrane.

Talin is self-regulated by adopting a compact homodimer conformation and interactions between FERM domain and rod inhibitory subdomains. To allow THD accessing the cell inner membrane and integrin tail, the talin rod domain must be dislodged. Chapter 5 depicts the distinctive role of the membrane composition in talin activation. Talin R9 and R12R13 inhibitory subdomains exhibit a classic competitive inhibition of THD binding DMPS, DMPG, DMPA, and PI4P lipid bilayer. The mere presence of PIP2 renders THD insensitive to both rod segments and promotes tight talin-membrane interaction. The lipid

headgroup identity is extremely important to membrane induced THD activation. The failure of PI4P activating inhibited THD indicates the recruitment of PIPKIγ converting PI4P to PIP2 may be a prerequisite mechanism for talin engagement and integrin activation.

Early investigations using lipid vesicle inserted or surface tethered integrins fail to characterize the assembly direction or clustering status that may hinder precise measurements of talin binding. Nanodisc technology provides an ideal platform to reconstitute transmembrane or membrane anchored proteins demonstrated by several previous studies [162, 191, 192]. Chapter 6 utilizes Nanodisc to assembly single unclustered integrin β3 transmembrane and cytoplasmic domains with controlled lipid bilayers. The major free energy of forming membrane/talin/integrin complex is provided by integrin THD interaction. PIP2 facilitates positioning THD into an optimal geometry for disrupting integrin α/β clasp and alter β integrin tansmembrane topology, which are critical for activating integrin in rest state. The presence of integrin tail allows differentiating the interfaces of two identified talin rod inhibitory subdomains. R9 sterically block the integrin binding sites of THD, which are located at F3 subdomain. On the other hand, R12R13 might impede THD recruitment by masking the MOP residues in F2 domain that are key for membrane binding. Although PIP2 remains important to dislodge the inhibitory domains, other activation pathways, such as RAP1-RIAM, calpain, and PIPKγ, may need to work in concert with membrane to achieve fully THD activation.

There are several interesting future directions for studying talin mediated integrin pathway in Nanodisc system. One is assembly the Nanodiscs with full-length αIIbβ3 integrin. It would allow researchers to access both extracellular and cellular side of this transmembrane receptor, so that the integrin activation can be determined by measuring integrin binding to ligands or monitoring integrin extracellular conformational change *in vitro*. The complexity of this Nanodisc based assay can be increased by introducing other protein partners, like RIAM and PIPKγ, to deconvolute the contribution and define the hierarchy of each

component during the talin mediated integrin activation.

In this thesis, the utility of Nanodiscs is extended to study the detailed molecular mechanism of talin mediated integrin activation through development of *in vitro* assay using fluorescence. This assay is amendable to measure protein-membrane binding, protein insertion, and protein-protein interaction in conjugation with lipid bilayers. It creates a paradigm of for future studies of membrane related signaling pathways that are vital to understand many sever diseases.

REFERENCES

[1] Richard O. Hynes. Integrins: A family of cell surface receptors. *Cell*, 48(4):549–554, feb 1987.

[2] Richard O. Hynes. Integrins: Bidirectional, allosteric signaling machines. *Cell*, 110(6):673–687, sep 2002.

[3] Aguang Dai, Feng Ye, Dianne W. Taylor, Guiqing Hu, Mark H. Ginsberg, and Kenneth A. Taylor. The structure of a full-length membrane-embedded Integrin bound to a physiological Ligand. *Journal of Biological Chemistry*, 290(45):27168–27175, nov 2015.

[4] Mark H. Ginsberg, Anthony Partridge, and Sanford J. Shattil. Integrin regulation. *Current Opinion in Cell Biology*, 17(5 SPEC. ISS.):509–516, oct 2005.

[5] Feng Ye, Guiqing Hu, Dianne Taylor, Boris Ratnikov, Andrey A. Bobkov, Mark A. McLean, Stephen G. Sligar, Kenneth A. Taylor, and Mark H. Ginsberg. Recreation of the terminal events in physiological integrin activation. *Journal of Cell Biology*, 188(1):157–173, jan 2010.

[6] Seiji Tadokoro, Sanford J Shattil, Koji Eto, Vera Tai, Robert C Liddington, Jose M de Pereda, Mark H Ginsberg, and David A Calderwood. Talin binding to integrin beta tails: a final common step in integrin activation. *Science*, 302(5642):103–6, oct 2003.

[7] David A. Calderwood, Yosuke Fujioka, Jose M. de Pereda, B. Garcia-Alvarez, Tetsuya Nakamoto, Ben Margolis, C Jane McGlade, Robert C. Liddington, and Mark H. Ginsberg. Integrin cytoplasmic domain interactions with phosphotyrosine-binding domains: A structural prototype for diversity in integrin signaling. *Proceedings of the National Academy of Sciences*, 100(5):2272–2277, mar 2003.

[8] David A. Calderwood, Boxu Yan, Jose M. de Pereda, Begoña García Alvarez, Yosuke Fujioka, Robert C. Liddington, and Mark H. Ginsberg. The phosphotyrosine binding-like domain of talin activates integrins. *The Journal of biological chemistry*, 277(24):21749–58, jun 2002.

[9] Kate L. Wegener, Anthony W. Partridge, Jaewon Han, Andrew R. Pickford, Robert C. Liddington, Mark H. Ginsberg, and Iain D. Campbell. Structural Basis of Integrin Activation by Talin. *Cell*, 128(1):171–182, jan 2007.

[10] Paul Atherton, Ben Stutchbury, De-Yao Wang, Devina Jethwa, Ricky Tsang, Eugenia Meiler-Rodriguez, Pengbo Wang, Neil Bate, Roy Zent, Igor L. Barsukov, Benjamin T. Goult, David R. Critchley, and Christoph Ballestrem. Vinculin controls talin engagement with the actomyosin machinery. *Nature Communications*, 6:10038, dec 2015.

[11] Lindsay B. Case, Michelle A. Baird, Gleb Shtengel, Sharon L. Campbell, Harald F. Hess, Michael W. Davidson, and Clare M. Waterman. Molecular mechanism of vinculin activation and nanoscale spatial organization in focal adhesions. *Nature cell biology*, 17(7):880–892, jun 2015.

[12] Andrew P. Gilmore and Keith Burridge. Regulation of vinculin binding to talin and actin by phosphatidyl-inositol-4-5-bisphosphate. *Nature*, 381(6582):531–535, jun 1996.

[13] Tiffany Truong, Hengameh Shams, and Mohammad R. K. Mofrad. Mechanisms of integrin and filamin binding and their interplay with talin during early focal adhesion formation. *Integrative Biology*, 7(10):1285–1296, 2015.

[14] Tiila Kiema, Yatish Lad, Pengju Jiang, Camilla L. Oxley, Massimiliano Baldassarre, Kate L. Wegener, Iain D. Campbell, Jari Ylänne, and David A. Calderwood. The molecular basis of filamin binding to integrins and competition with talin. *Molecular Cell*, 21(3):337–347, feb 2006.

[15] David S. Harburger, Mohamed Bouaouina, and David A. Calderwood. Kindlin-1 and -2 directly bind the C-terminal region of integrin cytoplasmic tails and exert integrin-specific activation effects. *Journal of Biological Chemistry*, 284(17):11485–11497, apr 2009.

[16] Yan Qing Ma, Jun Qin, Chuanyue Wu, and Edward F. Plow. Kindlin-2 (Mig-2): A co-activator of β3 integrins. *Journal of Cell Biology*, 181(3):439–446, oct 2008.

[17] Coert Margadant, Maaike Kreft, Giovanna Zambruno, and Arnoud Sonnenberg. Kindlin-1 regulates integrin dynamics and adhesion turnover. *PLoS one*, 8(6):e65341, jun 2013.

[18] Hiroaki Hirata, Masahiro Sokabe, and Chwee Teck Lim. Molecular mechanisms underlying the force-dependent regulation of actin-to-ECM linkage at the focal adhesions. In *Progress in Molecular Biology and Translational Science*, volume 126, pages 135–154. Elsevier Inc., 1 edition, jan 2014.

[19] Carsten Grashoff, Brenton D. Hoffman, Michael D. Brenner, Ruobo Zhou, Maddy Parsons, Michael T. Yang, Mark A. McLean, Stephen G. Sligar, Christopher S. Chen, Taekjip Ha, and Martin A. Schwartz. Measuring mechanical tension across vinculin reveals regulation of focal adhesion dynamics. *Nature*, 466(7303):263–266, jul 2010.

[20] Véronique Martel, Claire Racaud-Sultan, Sandra Dupe, Christiane Marie, Frédérique Paulhe, Antoine Galmiche, Marc R. Block, and Corinne Albiges-Rizo. Conformation,

localization, and integrin binding of talin depend on its interaction with phosphoinositides. *Journal of Biological Chemistry*, 276(24):21217–21227, jun 2001.

[21] Sarah L Veatch and Sarah L Keller. Separation of liquid phases in giant vesicles of ternary mixtures of phospholipids and cholesterol. *Biophysical journal*, 85(5):3074–83, 2003.

[22] Keith Burridge and Laurie Connell. A new protein of adhesion plaques and ruffling membranes. *The Journal of cell biology*, 97(2):359–67, aug 1983.

[23] Melissa A. Senetar and Richard O. McCann. Gene duplication and functional divergence during evolution of the cytoskeletal linker protein talin. *Gene*, 362(1-2):141–152, dec 2005.

[24] Susan J. Monkley, Xiao Hong Zhou, Sarah J. Kinston, Susan M. Giblett, Lance Hemmings, Helen Priddle, Jane E. Brown, Catrin A. Pritchard, David R. Critchley, and Reinhard Fässler. Disruption of the talin gene arrests mouse development at the gastrulation stage. *Developmental Dynamics*, 219(4):560–574, dec 2000.

[25] Francesco J. Conti, Sue J. Monkley, Malcolm R. Wood, David R. Critchley, and U. Muller. Talin 1 and 2 are required for myoblast fusion, sarcomere assembly and the maintenance of myotendinous junctions. *Development*, 136(21):3597–3606, nov 2009.

[26] Ana Maria Manso, Ruixia Li, Susan J. Monkley, Nathalia M. Cruz, Shannon Ong, Dieu H. Lao, Yevgeniya E. Koshman, Yusu Gu, Kirk L. Peterson, Ju Chen, E. Dale Abel, Allen M. Samarel, David R. Critchley, and Robert S. Ross. Talin1 has unique expression versus talin 2 in the heart and modifies the hypertrophic response to pressure overload. *Journal of Biological Chemistry*, 288(6):4252–4264, feb 2013.

[27] Jie Liu, Xiaowen He, Yanmei Qi, Xiaoxiang Tian, Susan J Monkley, David R Critchley, Siobhan a Corbett, Stephen F Lowry, Alan M Graham, and Shaohua Li. Talin1 regulates integrin turnover to promote embryonic epithelial morphogenesis. *Molecular and Cellular Biology*, 31(16):3366–3377, aug 2011.

[28] Nicholas H. Brown, Stephen L. Gregory, Wayne L. Rickoll, Liselotte I. Fessler, Mary Prout, Robert A.H. White, and James W. Fristrom. Talin Is essential for integrin function in Drosophila. *Developmental Cell*, 3(4):569–579, oct 2002.

[29] Erin J. Cram. Talin loss-of-function uncovers roles in cell contractility and migration in C. elegans. *Journal of Cell Science*, 116(19):3871–3878, oct 2003.

[30] David R. Critchley. Biochemical and structural properties of the integrin-associated cytoskeletal protein talin. *Annual Review of Biophysics*, 38(1):235–254, jun 2009.

[31] Susan J. Monkley, Vassiliki Kostourou, Lorraine Spence, Brian Petrich, Stacey Coleman, Mark H. Ginsberg, Catrin A. Pritchard, and David R. Critchley. Endothelial cell

talin1 is essential for embryonic angiogenesis. *Developmental Biology*, 349(2):494–502, jan 2011.

[32] Bernhard Nieswandt, Markus Moser, Irina Pleines, David Varga-Szabo, Sue Monkley, David Critchley, and R. Fassler. Loss of talin1 in platelets abrogates integrin activation, platelet aggregation, and thrombus formation in vitro and in vivo. *Journal of Experimental Medicine*, 204(13):3113–3118, dec 2007.

[33] Benjamin T. Goult, Mohamed Bouaouina, Paul R. Elliott, Neil Bate, Bipin Patel, Alexandre R. Gingras, J. Günter Grossmann, Gordon C. K. Roberts, David A. Calderwood, David R. Critchley, and Igor L. Barsukov. Structure of a double ubiquitin-like domain in the talin head: a role in integrin activation. *The EMBO Journal*, 29(6):1069–1080, mar 2010.

[34] Paul R. Elliott, Benjamin T. Goult, Petra M. Kopp, Neil Bate, J. Günter Grossmann, Gordon C.K. Roberts, David R. Critchley, and Igor L. Barsukov. The structure of the talin head reveals a novel extended conformation of the FERM domain. *Structure*, 18(10):1289–1299, oct 2010.

[35] Santos J. Franco, Mary A. Rodgers, Benjamin J. Perrin, Jaewon Han, David A. Bennin, David R. Critchley, and Anna Huttenlocher. Calpain-mediated proteolysis of talin regulates adhesion dynamics. *Nature Cell Biology*, 6(10):977–983, oct 2004.

[36] David A. Calderwood, Roy Zent, Richard Grant, D. Jasper G. Rees, Richard O. Hynes, and Mark H. Ginsberg. The talin head domain binds to integrin β subunit cytoplasmic tails and regulates integrin activation. *Journal of Biological Chemistry*, 274(40):28071–28074, oct 1999.

[37] Mark L. Borowsky and Richard O. Hynes. Layilin, a novel talin-binding transmembrane protein homologous with C- type lectins, is localized in membrane ruffles. *Journal of Cell Biology*, 143(2):429–442, oct 1998.

[38] Kun Ling, Renee L Doughman, Ari J Firestone, Matthew W Bunce, and Richard a Anderson. Type Iγ phosphatidylinositol phosphate kinase targets and regulates focal adhesions. *Nature*, 420(6911):89–93, nov 2002.

[39] Gilbert Di Paolo, Lorenzo Pellegrini, Kresimir Letinic, Gianluca Cestra, Roberto Zoncu, Sergei Voronov, Sunghoe Chang, Jun Guo, Markus R Wenk, and Pietro De Camilli. Recruitment and regulation of phosphatidylinositol phosphate kinase type 1γ by the FERM domain of talin. *Nature*, 420(6911):85–89, nov 2002.

[40] Kyle R Legate, Seiichiro Takahashi, Navid Bonakdar, Ben Fabry, David Boettiger, Roy Zent, and Reinhard Fässler. Integrin adhesion and force coupling are independently regulated by localized PtdIns(4,5)2 synthesis. *The EMBO Journal*, 30(22):4539–4553, 2011.

[41] Hong-Chen Chen, Paul A. Appeddu, J. Thomas Parsons, Jeffrey D. Hildebrand, Michael D. Schaller, and Jun-Lin Guan. Interaction of focal adhesion kinase with cytoskeletal protein talin. *Journal of Biological Chemistry*, 270(28):16995–16999, jul 1995.

[42] Christine Lawson, S.-T. Lim, Sean Uryu, Xiao Lei Chen, David A. Calderwood, and David D. Schlaepfer. FAK promotes recruitment of talin to nascent adhesions to control cell motility. *The Journal of Cell Biology*, 196(2):223–232, jan 2012.

[43] Nicholas J. Anthis, Kate L. Wegener, Feng Ye, Chungho Kim, Benjamin T. Goult, Edward D. Lowe, Ioannis Vakonakis, Neil Bate, David R. Critchley, Mark H. Ginsberg, and Iain D. Campbell. The structure of an integrin/talin complex reveals the basis of inside-out signal transduction. *The EMBO Journal*, 28(22):3623–3632, nov 2009.

[44] Mark J. Arcario and Emad Tajkhorshid. Membrane-induced structural rearrangement and identification of a novel membrane anchor in talin F2F3. *Biophysical Journal*, 107(9):2059–2069, nov 2014.

[45] Neil Bate, Alexandre R. Gingras, Alexia Bachir, Rick Horwitz, Feng Ye, Bipin Patel, Benjamin T. Goult, and David R. Critchley. Talin contains a C-terminal calpain2 cleavage site important in focal adhesion dynamics. *PLoS one*, 7(4):e34461, apr 2012.

[46] Laurent Tremuth, Stephanie Kreis, Chantal Melchior, Johan Hoebeke, Philippe Rondé, Sébastien Plançon, Kenneth Takeda, and Nelly Kieffer. A fluorescence cell biology approach to map the second integrin-binding Site of talin to a 130-amino acid sequence within the rod domain. *Journal of Biological Chemistry*, 279(21):22258–22266, may 2004.

[47] Ho-Sup Lee, Chinten James Lim, Wilma Puzon-McLaughlin, Sanford J. Shattil, and Mark H. Ginsberg. RIAM activates integrins by linking talin to ras GTPase membrane-targeting sequences. *The Journal of biological chemistry*, 284(8):5119–27, feb 2009.

[48] Ho-Sup Lee, Praju Anekal, Chinten James Lim, Chi-Chao Liu, and Mark H Ginsberg. Two modes of integrin activation form a binary molecular switch in adhesion maturation. *Molecular biology of the cell*, 24(9):1354–62, may 2013.

[49] Benjamin T. Goult, Thomas Zacharchenko, Neil Bate, Ricky Tsang, Fiona Hey, Alexandre R. Gingras, Paul R. Elliott, Gordon C. K. Roberts, Christoph Ballestrem, David R. Critchley, and Igor L. Barsukov. RIAM and vinculin binding to talin are mutually exclusive and regulate adhesion assembly and turnover. *Journal of Biological Chemistry*, 288(12):8238–8249, mar 2013.

[50] Jonas Emsley Alexandre R. Gingras, Wolfgang H. Ziegler, Ronald Frank, Igor L. Barsukov, Gordon C K Roberts, David R. Critchley. Mapping and consensus sequence Identification for multiple vinculin binding sites within the talin rod. *Journal of Biological Chemistry*, 280(44):37217–37224, aug 2005.

[51] Alexandre R. Gingras, Neil Bate, Benjamin T. Goult, Larnele Hazelwood, Ilona Canestrelli, J Günter Grossmann, HongJun Liu, Nicholas S. M. Putz, Gordon C. K. Roberts, Niels Volkmann, Dorit Hanein, Igor L. Barsukov, and David R. Critchley. The structure of the C-terminal actin-binding domain of talin. *The EMBO Journal*, 27(2):458–469, jan 2008.

[52] L. Molony, D. McCaslin, J. Abernethy, B. Paschal, and K. Burridge. Properties of talin from chicken gizzard smooth muscle. *The Journal of biological chemistry*, 262(16):7790–5, jun 1987.

[53] J Winkler, H Lünsdorf, and B M Jockusch. Energy-filtered electron microscopy reveals that talin is a highly flexible protein composed of a series of globular domains. *European journal of biochemistry / FEBS*, 243(1-2):430–6, jan 1997.

[54] Wolfgang H. Goldmann, Andreas Bremer, Markus Häner, Ueli Aebi, and Gerhard Isenberg. Native talin Is a dumbbell-shaped homodimer when it interacts with actin. *Journal of Structural Biology*, 112(1):3–10, jan 1994.

[55] Chungho Kim, T.-L. Tong-Lay Lau, Tobias S Ulmer, and Mark H Ginsberg. Interactions of platelet integrin alphaIIb and beta3 transmembrane domains in mammalian cell membranes and their role in integrin activation. *Blood*, 113(19):4747–53, may 2009.

[56] Jun Yang, Y.-Q. Ma, Richard C Page, Saurav Misra, Edward F Plow, and Jun Qin. Structure of an integrin alphaIIb beta3 transmembrane-cytoplasmic heterocomplex provides insight into integrin activation. *Proceedings of the National Academy of Sciences*, 106(42):17729–17734, oct 2009.

[57] Tong-Lay Lau, Varun Dua, and Tobias S. Ulmer. Structure of the integrin alphaIIb transmembrane segment. *The Journal of biological chemistry*, 283(23):16162–8, jun 2008.

[58] Tong-Lay Lau, Chungho Kim, Mark H Ginsberg, and Tobias S Ulmer. The structure of the integrin αIIbβ3 transmembrane complex explains integrin transmembrane signalling. *The EMBO Journal*, 28(9):1351–1361, may 2009.

[59] Tong-Lay Lau, Anthony W. Partridge, Mark H. Ginsberg, and Tobias S. Ulmer. Structure of the integrin β3 transmembrane segment in phospholipid bicelles and detergent micelles. *Biochemistry*, 47(13):4008–4016, apr 2008.

[60] Federico Diaz-Gonzalez. Breaking the Integrin Hinge. *Journal of Biological Chemistry*, 271(12):6571–6574, mar 1996.

[61] Wei Li, Douglas G Metcalf, Roman Gorelik, Renhao Li, Neal Mitra, Vikas Nanda, Peter B Law, James D Lear, William F Degrado, and Joel S Bennett. A push-pull mechanism for regulating integrin function. *Proceedings of the National Academy of Sciences of the United States of America*, 102(5):1424–9, feb 2005.

[62] Bing-Hao Luo, Christopher V Carman, Junichi Takagi, and Timothy a Springer. Disrupting integrin transmembrane domain heterodimerization increases ligand binding affinity, not valency or clustering. *Proceedings of the National Academy of Sciences of the United States of America*, 102(10):3679–84, mar 2005.

[63] Anthony W. Partridge, Shouchun Liu, Sanguk Kim, James U. Bowie, and Mark H. Ginsberg. Transmembrane domain helix packing stabilizes integrin αIIbβ3 in the low affinity state. *Journal of Biological Chemistry*, 280(8):7294–7300, feb 2005.

[64] Olga Vinogradova, Algirdas Velyvis, Asta Velyviene, Bin Hu, Thomas A. Haas, Edward F. Plow, and Jun Qin. A atructural mechanism of integrin αIIbβ3 Inside-Out activation as regulated by its cytoplasmic face. *Cell*, 110(5):587–597, sep 2002.

[65] Sonali Patil, Arom Jedsadayanmata, June D. Wencel-Drake, Wei Wang, Irina Knezevic, and S. C.-T. Lam. Identification of a talin-binding site in the integrin β3 subunit distinct from the NPLY Regulatory Motif of post-ligand binding functions: The talin N-terminal head domain interacts with the membrane-proximal region of the β3 cytoplasmic tail. *Journal of Biological Chemistry*, 274(40):28575–28583, oct 1999.

[66] Martin Pfaff, Shouchun Liu, David J. Erle, and Mark H. Ginsberg. Integrin beta cytoplasmic domains differentially bind to cytoskeletal proteins. *Journal of Biological Chemistry*, 273(11):6104–6109, mar 1998.

[67] Rangarajan Sampath. Cytoskeletal interactions with the leukocyte integrin beta 2 Cytoplasmic Tail. activation-dependent regulation of associations with talin and alpha-actin. *Journal of Biological Chemistry*, 273(50):33588–33594, dec 1998.

[68] Sukhwinder Singh, Veera D'mello, Paul van Bergen en Henegouwen, and Raymond B Birge. A NPxY-independent β5 integrin activation signal regulates phagocytosis of apoptotic cells. *Biochemical and Biophysical Research Communications*, 364(3):540–548, dec 2007.

[69] Nicholas J. Anthis, Kate L. Wegener, David R. Critchley, and Iain D. Campbell. Structural diversity in integrin/talin interactions. *Structure*, 18(12):1654–1666, 2010.

[70] Mohamed Bouaouina, Yatish Lad, and David A. Calderwood. The N-terminal domains of talin cooperate with the phosphotyrosine binding-like domain to activate 1 and 3 integrins. *Journal of Biological Chemistry*, 283(10):6118–6125, jan 2008.

[71] Antreas C. Kalli, Kate L. Wegener, Benjamin T. Goult, Nicholas J. Anthis, Iain D. Campbell, and Mark S. P. Sansom. The structure of the talin/integrin complex at a lipid bilayer: An NMR and MD simulation study. *Structure*, 18(10):1280–1288, oct 2010.

[72] David T Moore, Patrik Nygren, Hyunil Jo, Kathleen Boesze-Battaglia, Joel S Bennett, and William F DeGrado. Affinity of talin-1 for the 3-integrin cytosolic domain is modulated by its phospholipid bilayer environment. *Proceedings of the National Academy of Sciences*, 109(3):793–798, jan 2012.

[73] Takaaki Hato, Jun Yamanouchi, Tatsushiro Tamura, Yoshihiro Yakushijin, Ikuya Sakai, and Masaki Yasukawa. Cooperative role of the membrane-proximal and -distal residues of the integrin beta3 cytoplasmic domain in regulation of talin-mediated alpha IIb beta3 activation. *The Journal of biological chemistry*, 283(9):5662–8, feb 2008.

[74] Nicholas J. Anthis, Jacob R. Haling, Camilla L. Oxley, Massimiliano Memo, Kate L. Wegener, Chinten J. Lim, Mark H. Ginsberg, and Iain D. Campbell. β Integrin Tyrosine Phosphorylation Is a conserved mechanism for regulating talin-induced integrin activation. *Journal of Biological Chemistry*, 284(52):36700–36710, dec 2009.

[75] I Knezevic, T. M. Leisner, and S. C.-T. Lam. Direct binding of the platelet Integrin αIIb β3 (GPIIb-IIIa) to talin: Evidence that interaction is mediated through the cytoplasmic domains of both αIIb and β3. *Journal of Biological Chemistry*, 271(27):16416–16421, jul 1996.

[76] Alexandre R. Gingras, Wolfgang H. Ziegler, Andrey A. Bobkov, M. Gordon Joyce, Domenico Fasci, Mirko Himmel, Sven Rothemund, Anett Ritter, J. Günter Grossmann, Bipin Patel, Neil Bate, Benjamin T. Goult, Jonas Emsley, Igor L. Barsukov, Gordon C K Roberts, Robert C. Liddington, Mark H. Ginsberg, and David R. Critchley. Structural determinants of integrin binding to the talin rod. *The Journal of biological chemistry*, 284(13):8866–76, mar 2009.

[77] Markus Raab, Heide Daxecker, Richard J. Edwards, Achim Treumann, Derek Murphy, and Niamh Moran. Protein interactions with the platelet integrin αIIb regulatory motif. *Proteomics*, 10(15):2790–2800, jul 2010.

[78] Begoña Garca-Alvarez, José M. de Pereda, David A. Calderwood, Tobias S. Ulmer, David Critchley, Iain D. Campbell, Mark H. Ginsberg, and Robert C. Liddington. Structural determinants of integrin recognition by talin. *Molecular Cell*, 11(1):49–58, jan 2003.

[79] Tobias S. Ulmer, David a. Calderwood, Mark H. Ginsberg, and Iain D. Campbell. Domain-Specific Interactions of Talin with the Membrane-Proximal Region of the Integrin β3 Subunit. *Biochemistry*, 42(27):8307–8312, jul 2003.

[80] Minsoo Kim, Christopher V Carman, and Timothy A Springer. Bidirectional transmembrane signaling by cytoplasmic domain separation in integrins. *Science*, 301(5640):1720–5, sep 2003.

[81] Olga Vinogradova, Julia Vaynberg, Xiangming Kong, Thomas a Haas, Edward F Plow, and Jun Qin. Membrane-mediated structural transitions at the cytoplasmic face during

integrin activation. *Proceedings of the National Academy of Sciences*, 101(12):4094–4099, mar 2004.

[82] Anirban Bhunia, Xiao-Yan Tang, Harini Mohanram, Suet-Mien Tan, and Surajit Bhattacharjya. NMR solution conformations and interactions of integrin alphaLbeta2 cytoplasmic tails. *The Journal of biological chemistry*, 284(6):3873–84, feb 2009.

[83] Jieqing Zhu, Bing-Hao Luo, Patrick Barth, Jack Schonbrun, David Baker, and Timothy A. Springer. The structure of a receptor with two associating transmembrane domains on the cell surface: Integrin αIIbβ3. *Molecular Cell*, 34(2):234–249, apr 2009.

[84] Chungho Kim, Feng Ye, Xiaohui Hu, and Mark H Ginsberg. Talin activates integrins by altering the topology of the β transmembrane domain. *The Journal of Cell Biology*, 197(5):605–611, may 2012.

[85] Lisa Kurtz, Liyo Kao, Debra Newman, Ira Kurtz, and Quansheng Zhu. Integrin αIIbβ3 inside-out activation: an in situ conformational analysis reveals a new mechanism. *The Journal of biological chemistry*, 287(27):23255–65, jun 2012.

[86] Michèle Moes, Sophie Rodius, Stacey J. Coleman, Susan J. Monkley, Erik Goormaghtigh, Laurent Tremuth, Corinne Kox, Patrick P. G. van der Holst, David R. Critchley, and Nelly Kieffer. The integrin binding site 2 (IBS2) in the talin rod domain is essential for linking integrin beta subunits to the cytoskeleton. *The Journal of biological chemistry*, 282(23):17280–8, jun 2007.

[87] Charito Buensuceso, Maddalena de Virgilio, and Sanford J. Shattil. Detection of integrin alpha IIbbeta 3 clustering in living cells. *The Journal of biological chemistry*, 278(17):15217–24, apr 2003.

[88] Caroline Cluzel, Frédéric Saltel, Jost Lussi, Frédérique Paulhe, Beat A. Imhof, and Bernhard Wehrle-Haller. The mechanisms and dynamics of αvβ3 integrin clustering in living cells. *The Journal of Cell Biology*, 171(2):383–392, oct 2005.

[89] Jaewon Han, Chinten James Lim, Naohide Watanabe, Alessandra Soriani, Boris Ratnikov, David A. Calderwood, Wilma Puzon-McLaughlin, Esther M. Lafuente, Vassiliki A. Boussiotis, Sanford J. Shattil, and Mark H. Ginsberg. Reconstructing and deconstructing agonist-induced activation of integrin αIIbβ3. *Current Biology*, 16(18):1796–1806, sep 2006.

[90] Thomas A. Bunch. Integrin alphaIIbbeta3 activation in Chinese hamster ovary cells and platelets increases clustering rather than affinity. *The Journal of biological chemistry*, 285(3):1841–9, jan 2010.

[91] Teresa L. Helsten, Thomas A. Bunch, Hisashi Kato, Jun Yamanouchi, Sharon H. Choi, Alison L. Jannuzi, Chloe C. Féral, Mark H. Ginsberg, Danny L. Brower, and Sanford J. Shattil. Differences in regulation of Drosophila and vertebrate integrin affinity by talin. *Molecular biology of the cell*, 19(8):3589–98, aug 2008.

[92] Mirko Himmel, Anett Ritter, Sven Rothemund, Björg V. Pauling, Klemens Rottner, Alexandre R. Gingras, and Wolfgang H. Ziegler. Control of High Affinity Interactions in the Talin C Terminus: How talin domains coordinate protein dynamics in cell adhesions. *Journal of Biological Chemistry*, 284(20):13832–13842, may 2009.

[93] Stephanie J. Ellis, Mary Pines, Michael J. Fairchild, and Guy Tanentzapf. In vivo functional analysis reveals specific roles for the integrin-binding sites of talin. *Journal of Cell Science*, 124(11):1844–1856, jun 2011.

[94] Pengbo Wang, Christoph Ballestrem, and Charles H. Streuli. The C terminus of talin links integrins to cell cycle progression. *The Journal of Cell Biology*, 195(3):499–513, oct 2011.

[95] Andrew Smith, Yolanda R. Carrasco, Paula Stanley, Nelly Kieffer, Facundo D. Batista, and Nancy Hogg. A talin-dependent LFA-1 focal zone is formed by rapidly migrating T lymphocytes. *The Journal of Cell Biology*, 170(1):141–151, jul 2005.

[96] Guy Tanentzapf. Multiple factors contribute to integrin-talin interactions in vivo. *Journal of Cell Science*, 119(8):1632–1644, apr 2006.

[97] Esen Goksoy, Yan-qing Ma, Xiaoxia Wang, Xiangming Kong, Dhanuja Perera, Edward F Plow, and Jun Qin. Structural basis for the autoinhibition of talin in regulating integrin activation. *Molecular cell*, 31(1):124–133, 2009.

[98] Benjamin T. Goult, Neil Bate, Nicholas J. Anthis, Kate L. Wegener, Alexander R. Gingras, Bipin Patel, Igor L. Barsukov, Iain D. Campbell, Gordon C. K. Roberts, and David R. Critchley. The structure of an interdomain complex that regulates Talin activity. *Journal of Biological Chemistry*, 284(22):15097–15106, may 2009.

[99] Xianqiang Song, Jun Yang, Jamila Hirbawi, Sheng Ye, H Dhanuja Perera, Esen Goksoy, Pallavi Dwivedi, Edward F Plow, Rongguang Zhang, and Jun Qin. A novel membrane-dependent on/off switch mechanism of talin FERM domain at sites of cell adhesion. *Cell Research*, 22(11):1533–1545, jun 2012.

[100] Asoka Banno, Benjamin T. Goult, HoSup Lee, Neil Bate, David R. Critchley, and Mark H. Ginsberg. Subcellular localization of talin is regulated by inter-domain interactions. *Journal of Biological Chemistry*, 287(17):13799–13812, apr 2012.

[101] Maria E. Bertagnolli and Mary C. Beckerle. Evidence for the selective association of a subpopulation of GPIIb-IIIa with the actin cytoskeletons of thrombin-activated platelets. *The Journal of cell biology*, 121(6):1329–42, jun 1993.

[102] Benjamin T. Goult, Xiao-Ping Xu, Alexandre R. Gingras, Mark Swift, Bipin Patel, Neil Bate, Petra M. Kopp, Igor L. Barsukov, David R. Critchley, Niels Volkmann, and Dorit Hanein. Structural studies on full-length talin1 reveal a compact auto-inhibited dimer: Implications for talin activation. *Journal of Structural Biology*, 184(1):21–32, oct 2013.

[103] Wolfgang H. Ziegler, Alex R. Gingras, David R. Critchley, and Jonas Emsley. Integrin connections to the cytoskeleton through talin and vinculin. *Biochemical Society transactions*, 36(Pt 2):235–9, apr 2008.

[104] Armando Rio, Raul Perez-jimenez, Ruchuan Liu, Pere Roca-cusachs, Julio M Fernandez, and Michael P Sheetz. Stretching Single Talin Rod. *Science*, 323(January):638–641, 2009.

[105] Jenson Lim, Aurélien G. Dupuy, David R. Critchley, and Emmanuelle Caron. Rap1 controls activation of the $\alpha M\beta 2$ integrin in a talin-dependent manner. *Journal of Cellular Biochemistry*, 111(July):999–1009, nov 2010.

[106] Boxu Yan, David a. Calderwood, Brian Yaspan, and Mark H. Ginsberg. Calpain cleavage promotes talin binding to the $\beta 3$ integrin cytoplasmic domain. *Journal of Biological Chemistry*, 276(30):28164–28170, jul 2001.

[107] D. J. G. Rees, Sarah E Ades, S J Singer, and Richard O Hynes. Sequence and domain structure of talin. *Nature*, 347(6294):685–689, oct 1990.

[108] Lisa Dreolini and Fumio Takei. Activation of LFA-1 by ionomycin is independent of calpain-mediated talin cleavage. *Biochemical and Biophysical Research Communications*, 356(1):207–212, apr 2007.

[109] Sophie Rodius, Olivier Chaloin, Michèle Moes, Elisabeth Schaffner-Reckinger, Isabelle Landrieu, Guy Lippens, Minghui Lin, Ji Zhang, and Nelly Kieffer. The talin rod IBS2 alpha-helix interacts with the beta3 integrin cytoplasmic tail membrane-proximal helix by establishing charge complementary salt bridges. *The Journal of biological chemistry*, 283(35):24212–23, aug 2008.

[110] Nikolay L. Malinin, Edward F. Plow, and Tatiana V. Byzova. Kindlins in FERM adhesion. *Blood*, 115(20):4011–4017, may 2010.

[111] Kamila Bledzka, Jianmin Liu, Zhen Xu, H. D. Perera, Satya P. Yadav, Katarzyna Bialkowska, Jun Qin, Y.-Q. Ma, and Edward F. Plow. Spatial coordination of kindlin-2 with talin head domain in interaction with beta Integrin cytoplasmic tails. *Journal of Biological Chemistry*, 287(29):24585–24594, jul 2012.

[112] Bethsaida Nieves, Christopher W Jones, Rachel Ward, Yasutaka Ohta, Carlos G Reverte, and Susan E LaFlamme. The NPIY motif in the integrin 1 tail dictates the requirement for talin-1 in outside-in signaling. *Journal of Cell Science*, 123(8):1216–1226, apr 2010.

[113] Weizhi Liu, Kyle M. Draheim, Rong Zhang, David A. Calderwood, and Titus J. Boggon. Mechanism for KRIT1 release of ICAP1-mediated suppression of integrin activation. *Molecular Cell*, 49(4):719–729, 2013.

[114] W H Goldmann, V Niggli, S Kaufmann, and G Isenberg. Probing actin and liposome interaction of talin and talin-vinculin complexes: a kinetic, thermodynamic and lipid labeling study. *Biochemistry*, 31(33):7665–71, aug 1992.

[115] Camilla L. Oxley, Nicholas J. Anthis, Edward D. Lowe, Ioannis Vakonakis, Iain D. Campbell, and Kate L. Wegener. An integrin phosphorylation switch: the effect of beta3 integrin tail phosphorylation on Dok1 and talin binding. *Journal of Biological Chemistry*, 283(9):5420–6, feb 2008.

[116] Hannu Larjava, Edward F Plow, and Chuanyue Wu. Kindlins: essential regulators of integrin signalling and cellmatrix adhesion. *EMBO reports*, 9(12):1203–1208, dec 2008.

[117] Edward F Plow, Jun Qin, and Tatiana Byzova. Kindling the flame of integrin activation and function with kindlins. *Current Opinion in Hematology*, 16(5):323–328, sep 2009.

[118] Feng Ye and Brian G Petrich. Kindlin: helper, co-activator, or booster of talin in integrin activation? *Current opinion in hematology*, 18(5):356–60, sep 2011.

[119] Bryan N. Kahner, Hisashi Kato, Asoka Banno, Mark H. Ginsberg, Sanford J. Shattil, and Feng Ye. Kindlins, integrin activation and the regulation of talin recruitment to αIIbβ3. *PLoS one*, 7(3):e34056, jan 2012.

[120] Benjamin T. Goult, Mohamed Bouaouina, David S. Harburger, Neil Bate, Bipin Patel, Nicholas J. Anthis, Iain D. Campbell, David A. Calderwood, Igor L. Barsukov, Gordon C. Roberts, and David R. Critchley. The structure of the N-terminus of kindlin-1: A domain important for αIIbβ3 integrin activation. *Journal of Molecular Biology*, 394(5):944–956, dec 2009.

[121] H. Dhanuja Perera, Yan-Qing Ma, Jun Yang, Jamila Hirbawi, Edward F. Plow, and Jun Qin. Membrane binding of the N-terminal ubiquitin-like domain of kindlin-2 is crucial for its regulation of integrin activation. *Structure*, 19(11):1664–1671, nov 2011.

[122] Jianmin Liu, Koichi Fukuda, Zhen Xu, Y.-Q. Ma, Jamila Hirbawi, Xian Mao, Chuanyue Wu, Edward F. Plow, and Jun Qin. Structural basis of phosphoinositide binding to kindlin-2 protein pleckstrin homology domain in regulating integrin activation. *Journal of Biological Chemistry*, 286(50):43334–43342, dec 2011.

[123] Yan Liu, Yun Zhu, Sheng Ye, and Rongguang Zhang. Crystal structure of kindlin-2 PH domain reveals a conformational transition for its membrane anchoring and regulation of integrin activation. *Protein & cell*, 3(6):434–40, jun 2012.

[124] Luke a Yates, Craig N Lumb, Nina N Brahme, Ruta Zalyte, Louise E Bird, Luigi De Colibus, Raymond J Owens, David a Calderwood, Mark S P Sansom, and Robert J C Gilbert. Structural and sunctional characterization of the kindlin-1 pleckstrin homology domain. *Journal of Biological Chemistry*, 287(52):43246–43261, dec 2012.

[125] Luke A. Yates, Anna K. Füzéry, Roman Bonet, Iain D. Campbell, and Robert J C Gilbert. Biophysical analysis of Kindlin-3 reveals an elongated conformation and maps integrin binding to the membrane-distal β-subunit NPXY motif. *The Journal of biological chemistry*, 287(45):37715–31, nov 2012.

[126] Eloi Montanez, Siegfried Ussar, Martina Schifferer, M. Bosl, Roy Zent, Markus Moser, and R. Fassler. Kindlin-2 controls bidirectional signaling of integrins. *Genes & Development*, 22(10):1325–1330, may 2008.

[127] Markus Moser, Bernhard Nieswandt, Siegfried Ussar, Miroslava Pozgajova, and Reinhard Fässler. Kindlin-3 is essential for integrin activation and platelet aggregation. *Nature Medicine*, 14(3):325–330, mar 2008.

[128] Siegfried Ussar, Markus Moser, Moritz Widmaier, Emanuel Rognoni, Christian Harrer, Orsolya Genzel-Boroviczeny, and Reinhard Fässler. Loss of Kindlin-1 causes skin atrophy and lethal neonatal intestinal epithelial dysfunction. *PLoS Genetics*, 4(12):e1000289, dec 2008.

[129] Taco W. Kuijpers, E. van de Vijver, M. A J Weterman, M. de Boer, A. T J Tool, T. K. van den Berg, Markus Moser, Marja E. Jakobs, Karl Seeger, O. Sanal, S. Unal, M. Cetin, Dirk Roos, Arthur J. Verhoeven, and Frank Baas. LAD-1/variant syndrome is caused by mutations in FERMT3. *Blood*, 113(19):4740–4746, may 2009.

[130] Nikolay L Malinin, Li Zhang, Jeongsuk Choi, Alieta Ciocea, Olga Razorenova, Yan-Qing Ma, Eugene A Podrez, Michael Tosi, Donald P Lennon, Arnold I Caplan, Susan B Shurin, Edward F Plow, and Tatiana V Byzova. A point mutation in KINDLIN3 ablates activation of three integrin subfamilies in humans. *Nature Medicine*, 15(3):313–318, mar 2009.

[131] Eugenia Manevich-Mendelson, Sara W. Feigelson, Ronit Pasvolsky, Memet Aker, Valentin Grabovsky, Ziv Shulman, Sara Sebnem Kilic, Maria Alessandra Rosenthal-Allieri, Shifra Ben-Dor, Adi Mory, Alain Bernard, Markus Moser, Amos Etzioni, and Ronen Alon. Loss of Kindlin-3 in LAD-III eliminates LFA-1 but not VLA-4 adhesiveness developed under shear flow conditions. *Blood*, 114(11):2344–2353, sep 2009.

[132] Lena Svensson, Kimberley Howarth, Alison McDowall, Irene Patzak, Rachel Evans, Siegfried Ussar, Markus Moser, Ayse Metin, Mike Fried, Ian Tomlinson, and Nancy Hogg. Leukocyte adhesion deficiency-III is caused by mutations in KINDLIN3 affecting integrin activation. *Nature Medicine*, 15(3):306–312, mar 2009.

[133] Markus Moser, Kyle R Legate, Roy Zent, and Reinhard Fässler. The tail of integrins, talin, and kindlins. *Science (New York, N.Y.)*, 324(5929):895–9, may 2009.

[134] Craig T. Lefort, Jan Rossaint, Markus Moser, Brian G. Petrich, Alexander Zarbock, Susan J. Monkley, David R. Critchley, Mark H. Ginsberg, R. Fassler, and Klaus Ley.

Distinct roles for talin-1 and kindlin-3 in LFA-1 extension and affinity regulation. *Blood*, 119(18):4275–4282, may 2012.

[135] Mohamed Bouaouina, Benjamin T. Goult, Clotilde Huet-Calderwood, Neil Bate, Nina N. Brahme, Igor L. Barsukov, David R. Critchley, and David A. Calderwood. A conserved lipid-binding loop in the kindlin FERM F1 domain is required for kindlin-mediated αIIbβ3 integrin coactivation. *The Journal of biological chemistry*, 287(10):6979–90, mar 2012.

[136] David A. Calderwood, Anna Huttenlocher, William B. Kiosses, David M. Rose, Darren D. Woodside, Martin A. Schwartz, and Mark H. Ginsberg. Increased filamin binding to beta-integrin cytoplasmic domains inhibits cell migration. *Nature cell biology*, 3(12):1060–8, dec 2001.

[137] Mitali Das, Sujay Subbayya Ithychanda, Jun Qin, and Edward F. Plow. Migfilin and filamin as regulators of integrin activation in endothelial cells and neutrophils. *PLoS ONE*, 6(10):e26355, oct 2011.

[138] Sujay Subbayya Ithychanda, Mitali Das, Y.-Q. Ma, Keyang Ding, Xiaoxia Wang, Sudhiranjan Gupta, Chuanyue Wu, Edward F. Plow, and Jun Qin. Migfilin, a molecular switch in regulation of integrin activation. *Journal of Biological Chemistry*, 284(7):4713–4722, feb 2009.

[139] Yatish Lad, Pengju Jiang, Salla Ruskamo, David S. Harburger, J. Ylanne, Iain D. Campbell, and David A. Calderwood. Structural basis of the migfilin-filamin interaction and competition with integrin tails. *Journal of Biological Chemistry*, 283(50):35154–35163, dec 2008.

[140] Susanna M Nurmi, Carl G Gahmberg, and Susanna C Fagerholm. 14-3-3 proteins bind both filamin and alphaLbeta2 integrin in activated T cells. *Annals of the New York Academy of Sciences*, 1090(1):318–25, dec 2006.

[141] Heikki Takala, Elisa Nurminen, Susanna M. Nurmi, Maria Aatonen, Tomas Strandin, Maarit Takatalo, Tiila Kiema, Carl G. Gahmberg, Jari Ylänne, and Susanna C. Fagerholm. Beta2 integrin phosphorylation on Thr758 acts as a molecular switch to regulate 14-3-3 and filamin binding. *Blood*, 112(5):1853–62, sep 2008.

[142] Jeroen Pouwels, Jonna Nevo, Teijo Pellinen, Jari Ylänne, and Johanna Ivaska. Negative regulators of integrin activity. *Journal of cell science*, 125(Pt 14):3271–80, jul 2012.

[143] Pere Roca-Cusachs, Armando del Rio, Eileen Puklin-Faucher, Nils C. Gauthier, Nicolas Biais, and Michael P. Sheetz. Integrin-dependent force transmission to the extracellular matrix by -actinin triggers adhesion maturation. *Proceedings of the National Academy of Sciences*, 110(15):E1361–E1370, apr 2013.

[144] Seiji Tadokoro, Tsuyoshi Nakazawa, Tsuyoshi Kamae, Kazunobu Kiyomizu, Hirokazu Kashiwagi, Shigenori Honda, Yuzuru Kanakura, and Yoshiaki Tomiyama. A potential role for α-actinin in inside-out αIIbβ3 signaling. *Blood*, 117(1):250–8, jan 2011.

[145] Juha K. Rantala, Jeroen Pouwels, Teijo Pellinen, Stefan Veltel, Petra Laasola, Elina Mattila, Christopher S. Potter, Ted Duffy, John P. Sundberg, Olli Kallioniemi, Janet a. Askari, Martin J. Humphries, Maddy Parsons, Marko Salmi, and Johanna Ivaska. SHARPIN is an endogenous inhibitor of β1-integrin activation. *Nature Cell Biology*, 13(11):1315–1324, sep 2011.

[146] Boris Ratnikov, Celeste Ptak, Jaewon Han, Jeffrey Shabanowitz, Donald F Hunt, and Mark H Ginsberg. Talin phosphorylation sites mapped by mass spectrometry. *Journal of cell science*, 118(Pt 21):4921–3, nov 2005.

[147] David W. Litchfield and Eric H. Ball. Phosphorylation of the cytoskeletal protein talin by protein kinase C. *Biochemical and Biophysical Research Communications*, 134(3):1276–1283, feb 1986.

[148] Mary C. Beckerle. The adhesion plaque protein, talin, is phosphorylated in vivo in chicken embryo fibroblasts exposed to a tumor-promoting phorbol ester. *Cell regulation*, 1(2):227–36, jan 1990.

[149] Kohei Murata, Masato Sakon, Jun-ichi Kambayashi, Masaki Okuyama, Toshiharu Hase, and Takesada Mori. Platelet talin is phosphorylated by calyculin A. *Journal of Cellular Biochemistry*, 57(1):120–126, jan 1995.

[150] Cai Huang, Zenon Rajfur, Nima Yousefi, Zaozao Chen, Ken Jacobson, and Mark H. Ginsberg. Talin phosphorylation by Cdk5 regulates Smurf1-mediated talin head ubiquitylation and cell migration. *Nature Cell Biology*, 11(5):624–630, may 2009.

[151] Maria E. Bertagnolli, Sarah J. Locke, Mary E. Hensler, Paul F. Bray, and Mary C. Beckerle. Talin distribution and phosphorylation in thrombin-activated platelets. *Journal of cell science*, 106 (Pt 4:1189–99, dec 1993.

[152] Christopher E. Turner, Ffredrick M. Pavalko, and Keith. Burridge. The role of phosphorylation and limited proteolytic cleavage of talin and vinculin in the disruption of focal adhesion integrity. *The Journal of biological chemistry*, 264(20):11938–44, jul 1989.

[153] Adam Orłowski, Sampo Kukkurainen, Annika Pöyry, Sami Rissanen, Ilpo Vattulainen, Vesa P. Hytönen, and Tomasz Róg. PIP2 and Talin Join Forces to Activate Integrin. *The Journal of Physical Chemistry B*, 2015.

[154] Frédéric Saltel, Eva Mortier, Vesa P Hytönen, Marie-Claude Jacquier, Pascale Zimmermann, Viola Vogel, Wei Liu, and Bernhard Wehrle-Haller. New PI(4,5)P2- and membrane proximal integrin-binding motifs in the talin head control beta3-integrin clustering. *The Journal of cell biology*, 187(5):715–31, nov 2009.

[155] Doris M. Haverstick and Michael Glaser. Visualization of Ca2+-induced phospholipid domains. *Proceedings of the National Academy of Sciences of the United States of America*, 84(13):4475–9, jul 1987.

[156] Doris M. Haverstick and Michael Glaser. Visualization of domain formation in the inner and outer leaflets of a phospholipid bilayer. *The Journal of cell biology*, 106(6):1885–92, jun 1988.

[157] Timothy H. Bayburt, Yelena V. Grinkova, and Stephen G. Sligar. Self-assembly of discoidal phospholipid bilayer nanoparticles with membrane scaffold proteins. *Nano Letters*, 2(8):853–856, aug 2002.

[158] Ilia G. Denisov, Yelena V. Grinkova, Anne A. Lazarides, and Sephen G. Sligar. Directed self-assembly of monodisperse phospholipid bilayer Nanodiscs with controlled size. *Journal of the American Chemical Society*, 126(11):3477–87, mar 2004.

[159] Yelena V. Grinkova, Ilia G. Denisov, and Stephen G. Sligar. Engineering extended membrane scaffold proteins for self-assembly of soluble nanoscale lipid bilayers. *Protein engineering, design & selection : PEDS*, 23(11):843–8, nov 2010.

[160] Natanya R. Civjan, Timothy H. Bayburt, Mary A. Schuler, and Stephen G. Sligar. Direct solubilization of heterologously expressed membrane proteins by incorporation into nanoscale lipid bilayers. *BioTechniques*, 35(3):556–60, 562–3, sep 2003.

[161] Bradley J. Baas, Ilia G. Denisov, and Stephen G. Sligar. Homotropic cooperativity of monomeric cytochrome P450 3A4 in a nanoscale native bilayer environment. *Archives of biochemistry and biophysics*, 430(2):218–28, oct 2004.

[162] Timothy H. Bayburt, Yelena V. Grinkova, and Stephen G. Sligar. Assembly of single bacteriorhodopsin trimers in bilayer nanodiscs. *Archives of Biochemistry and Biophysics*, 450(2):215–222, jun 2006.

[163] Li-Zhi Mi, Michael J. Grey, Noritaka Nishida, Thomas Walz, Chafen Lu, and Timothy A. Springer. Functional and structural stability of the epidermal growth factor receptor in detergent micelles and phospholipid nanodiscs. *Biochemistry*, 47(39):10314–23, sep 2008.

[164] Timothy H. Bayburt, Sergey A. Vishnivetskiy, Mark A. McLean, Takefumi Morizumi, Chih-Chin Huang, John J G Tesmer, Oliver P. Ernst, Stephen G. Sligar, and Vsevolod V. Gurevich. Monomeric rhodopsin is sufficient for normal rhodopsin kinase (GRK1) phosphorylation and arrestin-1 binding. *The Journal of biological chemistry*, 286(2):1420–8, jan 2011.

[165] Aditi Das and Stephen G. Sligar. Modulation of the cytochrome P450 reductase redox potential by the phospholipid bilayer. *Biochemistry*, 48(51):12104–12112, dec 2009.

[166] Sayaka Inagaki, Rodolfo Ghirlando, Jim F. White, Jelena Gvozdenovic-Jeremic, John K. Northup, and Reinhard Grisshammer. Modulation of the interaction between neurotensin receptor NTS1 and Gq protein by lipid. *Journal of Molecular Biology*, 417(1-2):95–111, mar 2012.

[167] Jonas Borch, Federico Torta, Stephen G. Sligar, and Peter Roepstorff. Nanodiscs for immobilization of lipid bilayers and membrane receptors: kinetic analysis of cholera toxin binding to a glycolipid receptor. *Analytical Chemistry*, 80(16):6245–6252, aug 2008.

[168] Antreas C. Kalli, Iain D. Campbell, and Mark S. P. Sansom. Conformational changes in talin on binding to anionic phospholipid membranes facilitate signaling by integrin transmembrane helices. *PLoS Computational Biology*, 9(10):e1003316, oct 2013.

[169] Von Th. Forster. Zweischenmolekulare Energiewanderung und Fluoreszenz. *Annalen der Physik*, 6(2):55–75, 1948.

[170] Joseph R. Lakowicz. *Principles of fluorescence spectroscopy*. Springer US, Boston, MA, 2006.

[171] L Stryer and R P Haugland. Energy transfer: a spectroscopic ruler. *Proceedings of the National Academy of Sciences of the United States of America*, 58(2):719–26, aug 1967.

[172] Samuel H. Sternberg, Benjamin LaFrance, Matias Kaplan, and Jennifer A. Doudna. Conformational control of DNA target cleavage by CRISPRCas9. *Nature*, 527(7576):110–113, oct 2015.

[173] Sarah F Martin, Michael H Tatham, Ronald T Hay, and Ifor D W Samuel. Quantitative analysis of multi-protein interactions using FRET: application to the SUMO pathway. *Protein science : a publication of the Protein Society*, 17(4):777–84, 2008.

[174] Anne K Kenworthy. Imaging protein-protein interactions using fluorescence resonance energy transfer microscopy. *Methods*, 24(3):289–296, jul 2001.

[175] Lus M.S. Loura, Aleksandre Fedorov, and Manuel Prieto. Partition of membrane probes in a gel/fluid two-component lipid system: a fluorescence resonance energy transfer study. *Biochimica et Biophysica Acta (BBA) - Biomembranes*, 1467(1):101–112, jul 2000.

[176] Jiyao Wang, Alok Gambhir, Gyöngyi Hangyás-Mihályné, Diana Murray, Urszula Golebiewska, and Stuart McLaughlin. Lateral sequestration of phosphatidylinositol 4,5-bisphosphate by the basic effector domain of myristoylated alanine-rich C kinase substrate is due to nonspecific electrostatic interactions. *The Journal of biological chemistry*, 277(37):34401–12, sep 2002.

[177] Fritz Jahnig. Thermodynamics and kinetics of protein incorporation into membranes. *Proceedings of the National Academy of Sciences*, 80(12):3691–3695, jun 1983.

[178] Russel E. Jacobs and Stephen H. White. The nature of the hydrophobic binding of small peptides at the bilayer interface: implications for the insertion of transbilayer helices. *Biochemistry*, 28:3421–3437, 1989.

[179] C Dietrich, Wolfgang H. Goldmann, Erich Sackmann, and Gerhard Isenberg. Interaction of NBD-talin with lipid monolayers. *FEBS Letters*, 324(1):37–40, jun 1993.

[180] Markus Tempel, Wolfgang H. Goldmann, Gerhard Isenberg, and Erich Sackmann. Interaction of the 47-kDa talin fragment and the 32-kDa vinculin fragment with acidic phospholipids: a computer analysis. *Biophysical Journal*, 69(1):228–241, jul 1995.

[181] Anna Seelig, Xiaochun L. Blatter, Adrian Frentzel, and Gerhard Isenberg. Phospholipid binding of synthetic talin peptides provides evidence for an intrinsic membrane anchor of talin. *Journal of Biological Chemistry*, 275(24):17954–17961, 2000.

[182] Liang Tong, Abraham M. de Vos, Michael V. Milburn, and Sung Hou Kim. Crystal structures at 2.2 Å resolution of the catalytic domains of normal ras protein and an oncogenic mutant complexed with GDP. *Journal of Molecular Biology*, 217(3):503–516, 1991.

[183] David W. Banner, Allan D'Arcy, Christiana Chene, Fritz K. Winkler, Arabinda Guha, William H. Konigsberg, Yale Nemerson, and Daniel Kirchhofer. The crystal structure of the complex of blood coagulation factor VIIa with soluble tissue factor, 1996.

[184] Jacky Chi Ki Ngo, Mingdong Huang, David A. Roth, Barbara C. Furie, and Bruce Furie. Crystal structure of human factor VIII: implications for the formation of the factor IXa-factor VIIIa complex. *Structure*, 16(4):597–606, 2008.

[185] Iman van den Bout and Nullin Divecha. PIP5K-driven PtdIns(4,5)P2 synthesis: regulation and cellular functions. *Journal of cell science*, 122(Pt 21):3837–50, nov 2009.

[186] Stuart McLaughlin, Jiyao Wang, Alok Gambhir, and Diana Murray. PIP 2 and proteins: Interactions, organization, and information flow. *Annual Review of Biophysics and Biomolecular Structure*, 31(1):151–175, jun 2002.

[187] D Raucher, T Stauffer, W Chen, K Shen, S Guo, J D York, M P Sheetz, and T Meyer. Phosphatidylinositol 4,5-bisphosphate functions as a second messenger that regulates cytoskeleton-plasma membrane adhesion. *Cell*, 100(2):221–228, jan 2000.

[188] Jing Zhou, Agnieszka Bronowska, Johanne Le Coq, Daniel Lietha, and Frauke Gräter. Allosteric regulation of focal adhesion kinase by PIP2 and ATP. *Biophysical Journal*, 108(3):698–705, 2015.

[189] Guillermina M Goñi, Carolina Epifano, Jasminka Boskovic, Marta Camacho-Artacho, Jing Zhou, Agnieszka Bronowska, M Teresa Martín, Michael J. Eck, Leonor Kremer, Frauke Gräter, Francesco Luigi Gervasio, Mirna Perez-Moreno, and Daniel Lietha. Phosphatidylinositol 4,5-bisphosphate triggers activation of focal adhesion kinase by inducing clustering and conformational changes. *Proceedings of the National Academy of Sciences of the United States of America*, 111(31):E3177–86, aug 2014.

[190] Prerna N Domadia, Yan-Feng Li, Anirban Bhunia, Harini Mohanram, Suet-Mien Tan, and Surajit Bhattacharjya. Functional and structural characterization of the talin F0F1 domain. *Biochemical and biophysical research communications*, 391(1):159–65, jan 2010.

[191] Andrew J. Leitz, Timothy H. Bayburt, Alexander N. Barnakov, Barry a. Springer, and Stephen G. Sligar. Functional reconstitution of β2-adrenergic receptors utilizing self-assembling Nanodisc technology. *BioTechniques*, 40(5):601–612, 2006.

[192] T Boldog, S Grimme, M Li, S G Sligar, and G L Hazelbauer. Nanodiscs separate chemoreceptor oligomeric states and reveal their signaling properties. *Proceedings of the National Academy of Sciences*, 103(31):11509–11514, 2006.